

Probabilistic analysis of the robustness of earthquake resistant steel structures

Master Thesis
Jannie Jessen Nielsen
Faculty of Engineering, Science and Medicine
Aalborg University, 2009

Master Thesis

Probabilistic analysis of the robustness of
earthquake resistant steel structures

Author

Jannie Jessen Nielsen

Supervisors

John Dalsgaard Sørensen
Poul Henning Kirkegaard

Number printed: 4

Number of pages: 115

Completed: June 10th

CD is enclosed

Faculty of Engineering, Science and Medicine
Department of Civil Engineering
Sohngaardsholmsvej 57
DK-9000 Aalborg

Preface

This master thesis serves as documentation of the authors Master of Science degree in Civil Engineering and it has been prepared at the Faculty of Engineering, Science and Medicine at Aalborg University.

The title is *Probabilistic analysis of the robustness of earthquake resistant steel structures*, and it is a short candidate project prepared in the period February 2nd – June 10th 2009. Basis knowledge about earthquake design was gained during an internship at Ramboll Aalborg at the 3th semester of the candidate program, and additional knowledge has been gained through literature study.

A CD with MATLAB programs, finite element models and this thesis in pdf-format is enclosed.

Acknowledgements

The undersigned would like to acknowledge Ramboll Aalborg for putting a computer with Robot [Robobat 2008] license for disposal.

June 10th 2009 Jannie Jessen Nielsen

Abstract

The aim of this project was to investigate whether structures designed for earthquake loads were robust too. Two steel structures with ten stories and five bays in each direction and with eccentric and concentric braces in the facades respectively have been analyzed using pushover analyzes. The performance for a given ground acceleration have been found using a response spectrum reduced due to the ductile behavior found in the pushover analysis with the method from ATC-40.

The robustness has been assessed using a deterministic, probabilistic and risk based approach, where intact and damaged structures were analyzed. In the deterministic assessment the robustness was analyzed in relation to static and seismic horizontal loads, and the influence of ductility and hardening of the material was investigated. In the probabilistic assessment aleatoric and epistemic uncertainties were taken into account in the estimation of the annual probability of failure due to earthquakes, and two different robustness indices were calculated, one based on the probability of failure and one based on the reliability index. Finally a risk based approach was used where both direct and indirect consequences were taken into account.

The analyzes have shown that the damaged structures will often have a behavior that is different from that of the original structure, because the yielding mechanisms does not work the way they are designed to when members are missing. Thus the global ductile behavior for damaged structures was found to have great importance for the earthquake related robustness, and the structural configuration was especially important for the performance. This means that structures designed for seismic actions will not necessarily be robust towards seismic loads, as this depends on the structural configuration.

Resume

Formålet med dette projekt var at undersøge om konstruktioner dimensioneret for seismiske laster også er robuste. To stålkonstruktioner med hver ti etager og fem sektioner i hver retning og med hhv. excentriske og koncentriske afstivere er blevet analyseret vha. pushoveranalyser. Opførslen ved en givet grundacceleration er beregnet vha. et responspektrum reduceret afhængigt af duktiliteten fundet med pushoveranalysen med metoden fra ATC-40.

Robustheden er blevet vurderet med hhv. en deterministisk, probabilistisk og risikobaseret tilgang, hvor intakte og skadede konstruktioner blev analyseret. Med den deterministiske tilgang blev robustheden analyseret i relation til både statisk og seismisk horisontal last, og påvirkningen af duktilitet og hærkning af materialet blev undersøgt. Med den probabilistiske tilgang blev der taget hensyn til aleatoriske og epistemiske usikkerheder i beregningen af den årlige svigtsandsynlighed pga. jordskælv, og to forskellige robusthedsindekser blev beregnet, ét baseret på svigtsandsynligheden og ét baseret på sikkerhedsindekset. Endelig blev der brugt en risikobaseret tilgang, hvor der blev taget højde for både direkte og indirekte konsekvenser.

Analyserne viste, at skadede konstruktioner ofte vil have en opførsel som er forskellig fra den intakte konstruktion, idet de energidissiperende mekanismer ikke virker på den måde de er dimensioneret til, når nogle konstruktionsselementer mangler. Derfor havde den globale duktile opførsel af skadede konstruktioner stor indflydelse på den jordskælvsrelaterede robusthed, og den strukturelle konfiguration var særligt vigtig for opførslen. Dette betyder, at konstruktioner der er dimensioneret for seismiske påvirkninger ikke nødvendigvis er robuste ift. seismiske laster, da det afhænger af den strukturelle konfiguration.

Contents

1	Introduction	11
1.1	Performance based seismic design	11
1.1.1	Response of structures	12
1.2	Robustness	16
1.2.1	Strategies to ensure robustness	18
1.2.2	Methods to assess robustness	21
1.3	Robustness in seismic design	24
1.4	Aim of the project	26
1.4.1	Methods	26
1.4.2	Contents	26
2	Structural seismic analyzes	29
2.1	Structures	29
2.1.1	Lateral load resisting systems	31
2.1.2	Seismic demands	31
2.2	Nonlinear modeling of the structures	33
2.2.1	Structural systems	33
2.2.2	Nonlinear hinges	34
2.2.3	Modeling of eccentrically braced frame	35
2.2.4	Modeling of concentrically braced frame	39
2.3	Performance of structures	41
2.3.1	Eccentrically braced frame	41
2.3.2	Concentrically braced frame	44
2.4	Summary	47
3	Assessment of robustness	49
3.1	Structural configuration	49
3.1.1	Redundancy and ductility	49
3.1.2	Isolation by compartmentalization	50
3.1.3	Design of key elements	51
3.2	Behavior of damaged systems	51
3.2.1	Eccentrically braced frame	52
3.2.2	Concentrically braced frame	55
3.3	Deterministic assessment of robustness	56

3.3.1	Load type	56
3.3.2	Results	58
3.4	Other materials	64
3.4.1	Analyzes	65
3.5	Summary	69
4	Probabilistic seismic analysis	71
4.1	Uncertainties in seismic risk assessment	71
4.2	Procedure for seismic risk assessment	72
4.2.1	Capacity	73
4.2.2	Demand	74
4.3	Probabilistic seismic analyzes of the structures	76
4.3.1	Capacity of the structure	76
4.3.2	Seismic demand	76
4.3.3	Limit state probability	79
4.3.4	Sensitivity analysis	80
4.4	Probabilistic assessment of robustness	82
4.4.1	Eccentrically braced frame	82
4.4.2	Centrally braced frame	83
4.5	Comparison	84
4.6	Summary	86
5	Risk analysis	87
5.1	Analyzes	89
5.1.1	Robustness index	92
5.2	Summary	93
6	Summary	95
6.1	Conclusion	97
	Bibliography	99
A	Time history analysis in Robot	105
A.1	Time history of linear SDOF system	105
A.2	Time history of nonlinear SDOF system	108
A.3	Conclusion on tests	108
B	Nonlinear static performance based analysis	109
B.1	Capacity curve	109
B.2	Performance point	110
B.2.1	Hysteretic damping	111
C	Programs	115

Chapter 1

Introduction

During the last decade there has been increased focus on the subject robustness. This is caused by collapses such as Ronan Point (1968), World Trade Center (2001), Siemens Arena in Ballerup (2003), and The Bad Reichenhall Ice-Arena Collapse (2006). In Eurocode 0 the following robustness requirement can be found: "*A structure shall be designed and executed in such a way that it will not be damaged by events such as: explosion, impact, and the consequences of human errors, to an extent disproportionate to the original cause.*"[EN 1990:2002 2002]. Lots of research has been done within the area, and different definitions and methods to assess robustness have been proposed (eg [Starossek & Wolff 2005] [Canasius, Sørensen & Baker 2007] [Baker, Schubert & Faber 2008]). In this project the robustness of structures designed for seismic loads is considered when the structures are exposed to seismic loads. This chapter introduces the two main topics for the project, seismic design and robustness.

1.1 Performance based seismic design

The load from an earthquake is an inertia load, caused by the accelerations of the masses in the structure. Due to the equal displacement theory proposed by [Newmark & Hall 1982] the displacements of a yielding structure will be the same as those of an elastic structure. When a structure yields during an earthquake energy is dissipated in the yielding regions by hysteresis processes, and the accelerations of the structure and thus the inertial load will be decreased compared to an elastic structure. The term *seismic demand* is often used for an earthquake load.

Modern seismic codes use the concept of performance based design, where

different allowable damage levels (limit states) are set for different return periods of the earthquakes, with the objective to control the loss due to earthquakes [Bommer & Pinho 2006]. The damage of the structure is found to be related to the maximum inter-story drift angle (ISDA) during an earthquake [Ellingwood 2001]. Therefore the starting point for performance based seismic design is the allowable ISDA, even though most present codes use force based methods of analysis [Bazeos 2009].

The limit states can be defined as: [Ellingwood & Kinali 2009]

- Immediate Occupancy (IO):
Onset of inelastic behavior
- Structural Damage (SD):
Global lateral stiffness drops to half of initial value
- Collapse Prevention (CP):
Onset of instability

For each limit state the corresponding ISDA can be found for a given structure.

The design criteria for a seismic limit state is that the capacity has to exceed the seismic demand. The capacity is a property of the structure, whereas the demand is a property of the earthquake, but is changed due to the ductility of the structure. There exist several different methods to design earthquake resistant structures, and in the following some of the methods are outlined.

1.1.1 Response of structures

The dynamic response of a structure is dependent on the mass, stiffness, damping and load. For a viscously damped multi degree of freedom (MDOF) system the governing equation is:

$$\mathbf{M}\ddot{\mathbf{x}}(\mathbf{t}) + \mathbf{C}\dot{\mathbf{x}}(\mathbf{t}) + \mathbf{K}(\mathbf{x})\mathbf{x}(\mathbf{t}) = \mathbf{F}(\mathbf{t}) \quad (1.1)$$

where \mathbf{M} is the mass matrix, \mathbf{C} is the damping matrix, \mathbf{K} is the stiffness matrix, \mathbf{x} is the node displacement vector, and \mathbf{F} is the load vector. For an earthquake load \mathbf{F} is time dependent, and if the analysis is nonlinear, \mathbf{K} is dependent on \mathbf{x} .

The performance of a structure is best evaluated using nonlinear methods. The most precise analysis can be utilized with nonlinear time history analyzes of a spatial model with several bidirectional earthquake records

as input motions. This analysis precisely takes the ductility into account, and it tells where the structure is damaged, thus it gives a good estimate of the performance of the entire structure during an earthquake. [Wen & Song 2003]

Response spectrum analysis

The nonlinear time history analysis has the disadvantage that various time consuming analyzes has to be run in order to use this design method. A much faster analysis can be performed, if a linear analysis is made, and the nonlinearity is taken into account by reducing the seismic demand with a behavior factor. Instead of making a time history analysis, the MDOF system can be decoupled to a number of single degree of freedom (SDOF) systems, and a response spectrum can be used.

A response spectrum uses that for a linear SDOF system the peak response acceleration to a given time history of an earthquake load can be found to be dependent on the natural period of vibrations of the system. If there is a large amount of energy in the time history near the natural period of the structure, the response is large. A response spectrum takes advantage of this as it gives the peak spectral acceleration as function of the natural period of vibrations of the structure for a specific damping level. The process of making a response spectrum from a specific time history is shown in figure 1.1.

For an elastic MDOF system a modal analysis can be utilized, which results in the natural vibration periods, mode shapes, and mass participation percentages for the structure. For each natural period the peak spectral acceleration, reduced due to the ductility, is found and applied to the masses corresponding to the the mode shapes and mass participation percentages. At last the total response is found by combining the responses of each mode. Many codes eg [*EN 1998-1:2004* 2004] allows the use of this method for earthquake analyzes.

The main flaw of this method is related to the way, ductility is taken into account. The reduction factor is set due to the type of structural system, the deformations are calculated with large uncertainty, and the analysis tells nothing about the size and location of the structural damage. This can be done with the static pushover analysis that has become a frequently used tool for seismic design [Poursha, Khoshnoudian & Moghadam 2009].

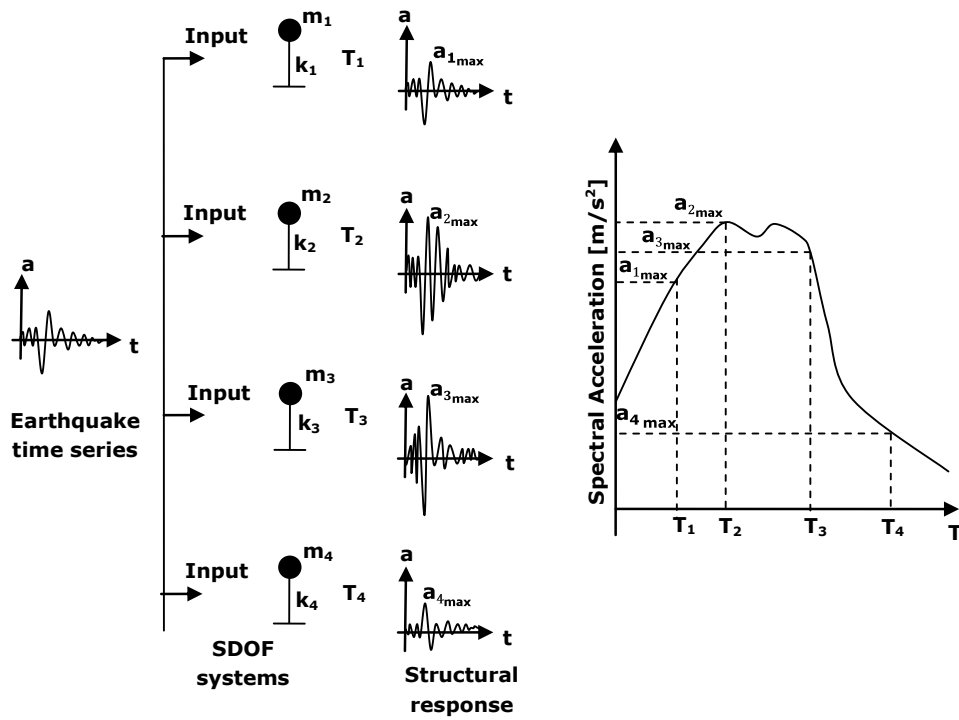


Figure 1.1: Calculation of a response spectrum based on an earthquake acceleration time series. This is used as input for SDOF systems with different natural vibration periods, and a time series of the structural response is calculated for each SDOF system. The maximum response is determined for each, and the values are plotted as function of the natural vibration periods.

Pushover analysis

The pushover analysis is a static nonlinear analysis, where the post yield behavior of the structure is investigated. A lateral force, distributed due to the masses and the mode shape with largest mass participation, is applied and increased until collapse is reached. The corresponding deformations are found for each load step. The total lateral force is plotted as function of the roof displacement to form the capacity curve, as shown in figure 1.2.

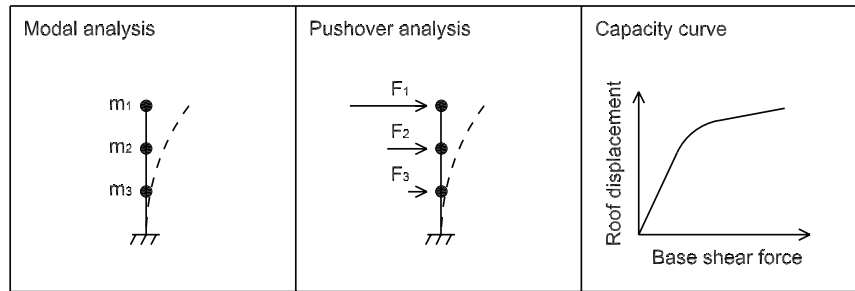


Figure 1.2: Use of pushover analysis to make the capacity curve.

This curve can be converted to a capacity spectrum corresponding to a SDOF system where the spectral acceleration is plotted as function of the spectral displacement. The seismic demand is controlled by the elastic response spectrum that can be plotted in this diagram as well, as shown in figure 1.3.

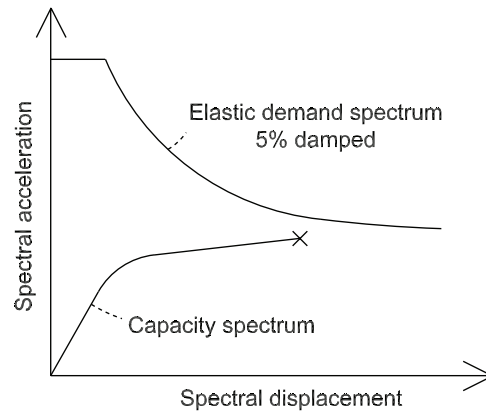


Figure 1.3: Capacity spectrum and elastic demand spectrum.

Due to the hysteretic damping, estimated on basis of the shape of the capacity spectrum, the elastic response spectrum is reduced. The intersection between the reduced response spectrum and the capacity spectrum is the performance point, and gives an estimate on the displacement and the damage of the structure for a given elastic response spectrum. The method is

explained further in appendix B.

This method is limited to structures where only one mode shape contributes significantly to the response, but several extended methods have been proposed, where more modes are taken into account [Poursha et al. 2009].

1.2 Robustness

An accident in 1968 was the triggering event that led to awareness on the topic of robustness. A gas explosion happened in a kitchen in a corner apartment at 18th floor in the 22 story Ronan Point apartment tower. A woman in the kitchen survived the explosion, but some of the outer precast concrete walls blew out due to bad connectivity, and the local damage resulted in progressive collapse of the corner bays in the entire height of the building, cf. figure 1.4, and four other persons died. The accident itself was relatively small, even though some walls got knocked out, since the woman standing next to it survived. But the indirect consequences were huge, and thus the local damage and the escalated damage are clearly disproportionate. [Nair 2006]

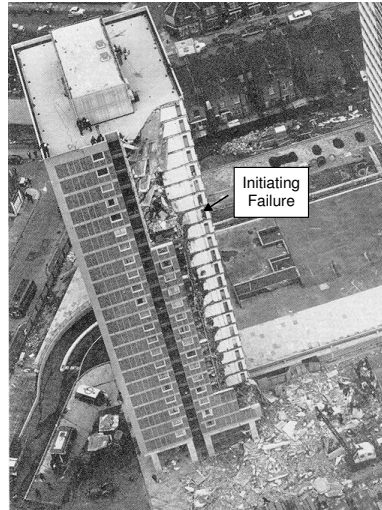


Figure 1.4: Progressive collapse of Ronan Point. [Ellingwood, Smilowitz & Dusenberry 2007]

An inquiry found that the building was designed and built according to the codes of the time, but the codes did not include design for accidents with low probability of occurrence [Ellingwood, Smilowitz & Dusenberry 2007]. From a pure probabilistic point of view there is no reason to include most accidental loads, since the annual probability of occurrence is very small.

The consequences, however, can be very huge *if* an accident happens anyway. This can be included in the design by examining the *risk*, R , defined basically as:

$$R = P_f C \quad (1.2)$$

where P_f is the probability of failure and C are the consequences with an appropriate measure.

Another flaw of the design procedures in the building codes is that the safety of structures is examined on element level instead of system level, thus the total safety of the structure is not directly investigated. If more elements work together in a series system, the safety of the building can be significantly less than the safety for each element. [Starossek & Wolff 2005]

The most correct way to assess the safety of a building is to perform a full risk analysis. The procedure is described in [EN 1991-1-7:2006 2006, Annex B] and an overview of the procedure of performing a risk analysis is shown in figure 1.5.

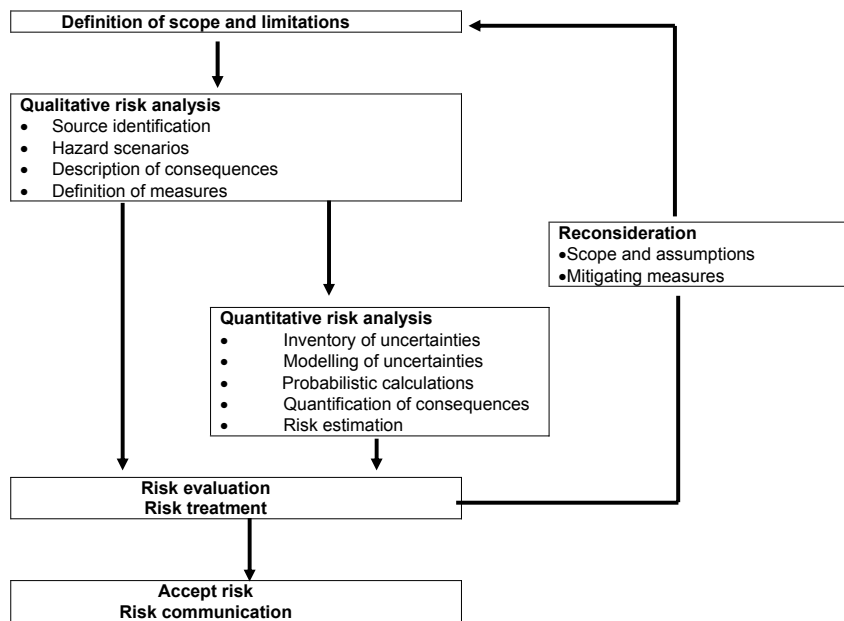


Figure 1.5: Overview of the risk analysis. [EN 1991-1-7:2006 2006]

However the completion of a full risk analysis on structure level is a very time demanding task with many unknown parameters, and is not a possibility for a standard design routine. Still it is wanted to avoid disproportionate collapses such as Ronan Point, and instead of the full risk analysis, modern codes have robustness requirements that should be fulfilled on top of the design on element level.

1.2.1 Strategies to ensure robustness

In the Eurocodes such robustness requirements can be found in two documents, [EN 1990:2002 2002] and [EN 1991-1-7:2006 2006]. The first requires that *"A structure shall be designed and executed in such a way that it will not be damaged by events such as: explosion, impact, and the consequences of human errors, to an extent disproportionate to the original cause."*[EN 1990:2002 2002].

Robustness is meant to avoid failures caused by:

- Errors in the design
- Error during construction
- Lack of maintenance
- Unforeseeable events

The first three are most often caused by human errors, whereas the last point is accidental loads. [Munch-Andersen 2009]

Accidental loads

In [EN 1991-1-7:2006 2006] different strategies for designing for accidental design situations are listed.

In general there are strategies within two categories, design for identified actions and limiting extent of local damage. For identified accidents the strategies fall into three categories:

- Ensure the robustness by making the structure ductile, redundant, and/or design elements that are important for the stability of the structure, as key elements cf. figure 1.6a.
- Protect the elements from the accidental loads by barriers cf. figure 1.6b.
- Design the elements to resist the accidental loads.

For unidentified actions ductility, redundancy, and the design of key elements are enhanced as well.

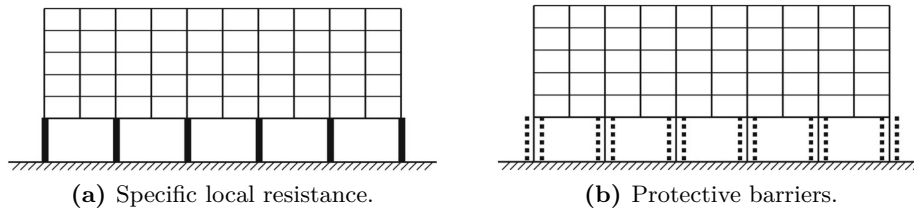


Figure 1.6: Strategies to survive accidental loads. [Starossek & Wolff 2005]

Loss of structural element scenario

These demands can also be found in the *NIST* document *Best Practise for Reducing the Potential for Progressive Collapse in Buildings* [Ellingwood, Celik & Kinali 2007]. To avoid progressive collapses in an event with a loss of a structural element the structure should have the following properties: (cite from [Vrouwenvelder & Sørensen 2009])

Redundancy: Incorporation of redundant load paths in the vertical load carrying system.

Ties: Using an integrated system of ties in three directions along the principal lines of structural framing.

Ductility: Structural members and member connections have to maintain their strength through large deformations (deflections and rotations) so the load redistribution(s) may take place.

Adequate shear strength: As shear is considered as a brittle failure, structural elements in vulnerable locations should be designed to withstand shear load in excess of that associated with the ultimate bending moment in the event of loss of an element.

Capacity for resisting load reversals: The primary structural elements (columns, girders, roof beams, and lateral load resisting system) and secondary structural elements (floor beams and slabs) should be designed to resist reversals in load direction at vulnerable locations.

Connections (connection strength): Connections should be designed in such way that it will allow uniform and smooth load redistribution during local collapse.

Key elements: Exterior columns and walls should be capable of spanning two or more stories without bucking, columns should be designed to withstand blast pressure etc.

Alternate load path(s): After the basic design of structure is done, a review of the strength and ductility of key structural elements is required to determine whether the structure is able to "bridge" over the initial damage.

Key elements are elements that are important for the overall stability of the structure, and thereby corresponds to elements in a series system. According to the Danish National Annex for Eurocode 0, [*EN 1990 DK NA:2007* 2007], the partial factor on key elements should be increased with a factor 1.2. This value corresponds to the factor the strength of elements in a series system should be increased, to obtain the same safety as equivalent elements in a parallel system [Sørensen & Christensen 2006].

In many cases, however, it is better to ensure the robustness by choosing a redundant structure. A redundant structure is characterized by being statically indeterminate. Like a parallel system the structure is able to provide alternate load paths, if the structure is damaged. Ductility is a property of the material to allow large strains. In general a ductile structure is more redundant than a brittle, as the elements retain its strength at large strains, at thereby allows the structure to activate the alternate load paths.

Isolation by compartmentalization

Another strategy to prevent progressive collapse is *isolation by compartmentalization*. Here the idea is to allow local damage to happen with the purpose that the remaining structure is not overloaded.

The Bad Reichenhall Ice-Arena collapse in 2006 is an example where this strategy might have helped. The collapse happened a winter day, where the roof was covered by snow. The load caused a timber beam to collapse, and as the purlins were strong and stiff, a progressive collapse caused the entire roof to collapse. An investigation found that the snow load did not exceed the design load, but design errors and unforeseen degradation of the strength of the glue due to the use of a new technology, had caused the beams to be significantly weaker than expected. The redundancy of the structure was the reason that the design errors caused a total collapse and not just a limited collapse. [Dietsch 2009]

In the case of the partial collapse of the Charles de Gaulle Airport Terminal in 2004, there were limited interconnections between the bays, and only one bay collapsed cf. figure 1.7. The collapse was caused by poor workmanship and design errors, and increased redundancy might have resulted in a progressive collapse of more bays. [Starossek & Wolff 2005]



Figure 1.7: Partial collapse of the Charles de Gaulle Airport Terminal, Paris.

The two collapses have in common that they were mainly caused by human errors and that the errors were not just located in one point, but distributed through the entire structure. For such errors it seems that if a little part of the structure fails due to the error, the rest of the structure will have the same error, and redundancy will increase the probability of a progressive collapse instead of a limited failure. Redundancy will more often work efficiently against failures caused by accidental events, as the accidental loads are often located at a smaller point, and the rest of the structure will have a reserve strength. [Munch-Andersen 2009]

Further there seems to be a tendency that the isolation by compartmentalization strategy works best for structures with a large horizontal extend like bridges and arenas, so that the collapse of one bay will not result in a horizontal progressive collapse, resulting in the collapse of other bays. On the other hand redundancy is better at preventing vertical progressive collapse, and increased redundancy of Ronan Point would probably have prevented the progressive collapse [Nair 2006].

1.2.2 Methods to assess robustness

Recently a lot of research has been done within the area of robustness, and as a result many different proposals have been given in how to quantify robustness. In the following some of the definitions are presented. Robustness can be assessed using three different approaches:

- Deterministic approach
- Probabilistic approach
- Risk based approach

Deterministic

For offshore structures a robustness measure can be obtained using the reserve strength ratio (RSR) defined as:

$$RSR = \frac{R_C}{S_C} \quad (1.3)$$

where R_C is the base shear capacity and S_C is the design load. [Straub & Faber 2005]

The redundancy (robustness) can be evaluated using the residual influence factor (RIF):

$$RIF_i = \frac{RSR_{F_i}}{RSR_{intact}} \quad (1.4)$$

Where RSR_{intact} and RSR_{F_i} is the reserve strength ratio for an intact structure and a structure where element i is damaged respectively.

If the design load is equal for the intact and damaged structure, the RIF can be rewritten to:

$$RIF_i = \frac{R_{C(F_i)}}{R_{C(intact)}} \quad (1.5)$$

Thus the redundancy can be evaluated as the fraction between the capacity of the damaged and the intact structure. If the intact and damaged structures have same capacity the value is one, if the damaged structure has no capacity it is zero.

For a lateral load the base shear capacities can be found by performing a static pushover analysis.

Probabilistic

In a probabilistic formulation the total probability of collapse $P(C)$ can be written as:

$$P(C) = \sum_i \sum_j P(C|E_i \cap D_j)P(D_j|E_i)P(E_i) \quad (1.6)$$

where E_i is the i 'th exposure and D_j is the j 'th damage type, $P(E_i)$ is the probability of the exposure, $P(D_j|E_i)$ is the probability of damage given the exposure, and $P(C|E_i \cap D_j)$ is the probability of collapse given the exposure and damage. Thus the robustness can be increased by decreasing one of the factors. [Sørensen & Christensen 2006]

For unidentified accidental loads the probability of the exposure, $P(E_i)$, is in general very small and can be very hard to assess, and the probability

of damage given the exposure, $P(D_j|E_i)$, is hard to assess too. Regardless of the accidental load the robustness can then be increased by decreasing the probability of collapse given the exposure and damage, $P(C|E_i \cap D_j)$. This corresponds to investigating the ability of the structure to resist load in a damaged state using the the alternate load path method. [Ellingwood, Smilowitz & Dusenberry 2007]

A probabilistic redundancy index, β_R , was proposed by [Frangopol & Curley 1987]:

$$\beta_R = \frac{\beta_{intact}}{\beta_{intact} - \beta_{damaged}} \quad (1.7)$$

where β_{intact} is the reliability index of the intact structure and $\beta_{damaged}$ is the reliability index of the damaged structure. If the reliability index is unchanged for the damaged structure it is infinite, and if there is no capacity of the damaged structure it is one.

The probability of failure and the reliability index is related through the following expression:

$$P(C) = \Phi(-\beta) \quad (1.8)$$

A vulnerability index was proposed by [Lind 1995] as:

$$V = \frac{P(R_d, S)}{P(R_0, S)} \quad (1.9)$$

where $P(R_d, S)$ is the probability of failure for a damaged structure, and $P(R_0, S)$ is the probability of failure for the intact structure. The reciprocal of this is the damage tolerance factor:

$$T_d = \frac{P(R_0, S)}{P(R_d, S)} \quad (1.10)$$

which is also a measure of the robustness of the structure. This measure is one if the failure probability is equal for the damaged and undamaged structure, and zero if the failure probability of the damaged structure is infinite. Hereby this measure can be compared with the deterministic *RIF* value.

Risk analysis

A risk analysis is the most complete way to assess the safety of a structure. In a risk analysis there are three influencing factors; hazard, consequences and context. The hazard could be an earthquake, the consequences could be economic losses and losses of lives caused by a collapse. The context

is important too, as individuals and eg a government have different views upon acceptable risk. Acceptable risk in structural engineering is a relative term, and must be calibrated against other risks in the society. Further the cost for decreasing the risk, or gain for increasing the risk will influence the choice. The acceptable risk is orders of magnitude larger for risks taken voluntary than those taken by society. Risk can be measured in different terms, and in building codes the main objective is to protect human lives and to minimize considerable societal consequences (economic and environmental). [Ellingwood, Smilowitz & Dusenberry 2007]

The total risk can be found as:

$$R = R_{dir} + R_{indir} = \sum_i \sum_j C_{dir,ij} P(D_j|E_i) P(E_i) + \sum_i \sum_j \sum_k C_{indir,ijk} P(S_k|D_j) P(D_j|E_i) P(E_i) \quad (1.11)$$

where $C_{dir,ij}$ consequence of damage D_j due to exposure E_i and $C_{indir,ijk}$ is the consequence of comprehensive damages S_k given local damage D_j due to exposure E_i [Vrouwenvelder & Sørensen 2009].

One way to increase the robustness is to minimize the indirect risk, given by the second term in equation 1.11. With that in mind the risk based robustness index was proposed by [Baker et al. 2008]:

$$I_{Rob} = \frac{R_{dir}}{R_{dir} + R_{indir}} \quad (1.12)$$

where R_{dir} is the direct risk associated to local damage, and R_{indir} is indirect risk associated to comprehensive damage. It is one for a robust structure with no indirect risk and zero for a structure that is not robust at all.

However, the risk can also be reduced by reducing the first term in equation 1.11, and this means that the risk based robustness index will not always be consistent with a full risk analysis. [Vrouwenvelder & Sørensen 2009]

1.3 Robustness in seismic design

As the previous sections might have illustrated, seismic resistant structures are in general born with some attributes that ensures some robustness of the structures. This is due to requirements in seismic codes and the methods used for the seismic design.

The influence of different factors, normally considered as contributing to the redundancy of structures was investigated by [Wen & Song 2003]. They

evaluated the factors by calculating the column drift ratio for different lateral systems using nonlinear time history analyzes with earthquake records as input. Because of the large uncertainty in seismic excitation and structural resistance the redundancy was measured in terms of the probability of exceeding a limit state measured in terms of story drift. They found that the structural configuration was very important for the redundancy, and that the number of shear walls did not have a great importance for the redundancy, thus it is not crucial for the seismic behavior how many times indeterminate a structure is.

The resistance against progressive collapse for seismically designed braced steel frames was investigated by [Khandelwal, El-Tawil & Sadek 2009]. The dynamic response was found when columns and adjoining braces were instantaneously removed. The brace system, able to resist seismic loads, was also found to be capable of preventing progressive collapse. Only the non-braced corner columns were sensitive, thus the structural configuration was found very important for the progressive collapse resistance.

In general seismic resistant structures are designed to act inelastic during severe earthquakes, which requires that the proportion between columns and beams is set due to the concept of capacity design. For a moment resistant structure this is ensured by the concept of strong column/weak beam, meaning that plastic hinges will be developed in the beams and not in the columns, so that many hinges have to be developed before the structure fails. Thus the structure is designed to fail in less fatal failure modes first, what gives an increase in the redundancy.

It is also a demand that the materials in a seismic resistant structure act ductile, so that the structure retains its strength at large deformation, else the structure cannot benefit from the formation of the hinges. This was also pointed out by [Bertero & Bertero 1999] as redundancy cannot be quantified alone in terms of over strength, since it is highly important that sufficient rotation capacity is available. This is an important feature for a redundant structure, but the demands are even more crucial for a seismic resistant structure. Not only shall it provide ductile behavior against a static load, but it also has to be able to survive hysteretic cycles in and out the plastic area without losing its strength. This sets requirements for the connections and for use of stiffeners, so that buckling of the web will not prevent the cycles.

1.4 Aim of the project

Since seismic resistant structures are in general ductile and redundant, one might assume that they are also robust. The aim of this project is to analyze the robustness of seismically designed steel structures, and thereby seek to investigate it. The robustness will be quantified through different measures, and in addition the influence of the ductility of the material is investigated.

The analyzes of the robustness will be performed in connection with seismic loads. The studied case is seismic resistant steel structures that are damaged eg by an impact or because of design or execution errors. It is investigated how these damaged structures will perform during an earthquake compared to the intact structure. The behavior towards vertical loads is not included in the analysis.

1.4.1 Methods

The seismic behavior is best evaluated using time history analyzes with bidirectional earthquake records as input for inelastic spatial models [Wen & Song 2003]. It has been chosen to use the finite element program Robot by Robobat [Robobat 2008] for the structural analyzes in this project. Simple analyzes have been made in Robot to investigate, whether the build in opportunity to make time history analyzes could be used to make nonlinear analyzes where the supports were subjected to an acceleration time history. As explained in appendix A this could not be done with reliable results, and the options were to find another program or to make simpler analyzes. The latter was chosen because of limited time.

Instead nonlinear static pushover analyzes are used. To minimize the time consumption the analyzes are performed for plane structures, and thus the spatial effects are not taken into account.

The robustness is evaluated using a deterministic, probabilistic, and risk based approach. For the probabilistic analyzes first order reliability methods (FORM) are used.

1.4.2 Contents

Two seismically designed braced steel structures are chosen for case studies for this project. At first the nonlinear modeling of the structures is evaluated, and the seismic behavior is analyzed for both structures.

The overall robustness of the structures is discussed, and it is assessed for horizontal loads only, both for seismic loads and static loads. It is assessed using deterministic, probabilistic and risk based approaches. The robustness is evaluated on basis of the difference between the intact structure and a damaged structure. For the analysis of the damaged structure a limited part of the structure is removed, that is, a column and adjoining braces.

Further the influence of the material is investigated by making similar analyzes for structures where the ductility and hardening is changed.

Chapter 2

Structural seismic analyzes

In this chapter the seismic behavior of two steel structures are investigated.

2.1 Structures

The prototype structures chosen for this analysis were originally design by The National Institute of Standards and Technology (NIST), and have been used for progressive collapse studies by [Khandelwal et al. 2009]. Both structures have ten stories and five bays in each direction. They are steel structures with a lateral load resisting system consisting of braced frames in the facades and concrete slaps are distributing the loads to the facades.

The structures are designed for seismic actions corresponding to Seattle, Washington with high seismic activity and Atlanta, Georgia with less seismic activity respectively. The structure designed for high seismic activity is an eccentrically braced frame (EBF), whereas the other is a special concentrically braced frame (SCBF), and both structures can be seen in figure 2.1.

All sections are taken from the American AISC Shapes Database. The braces are made of Hollow Steel Sections (HSS), and the other members are I-sections from the W-series. A500-46 steel ($F_y = 317$ MPa) is used for the braces and A992-50 ($F_y = 345$ MPa) is used for the other sections.

The loads on the slabs are listed in table 2.1. The live load is reduced based on [ASCE 7-05 2005, Sec. 4.8.1]. Each facade gets the seismic load from half of the building.

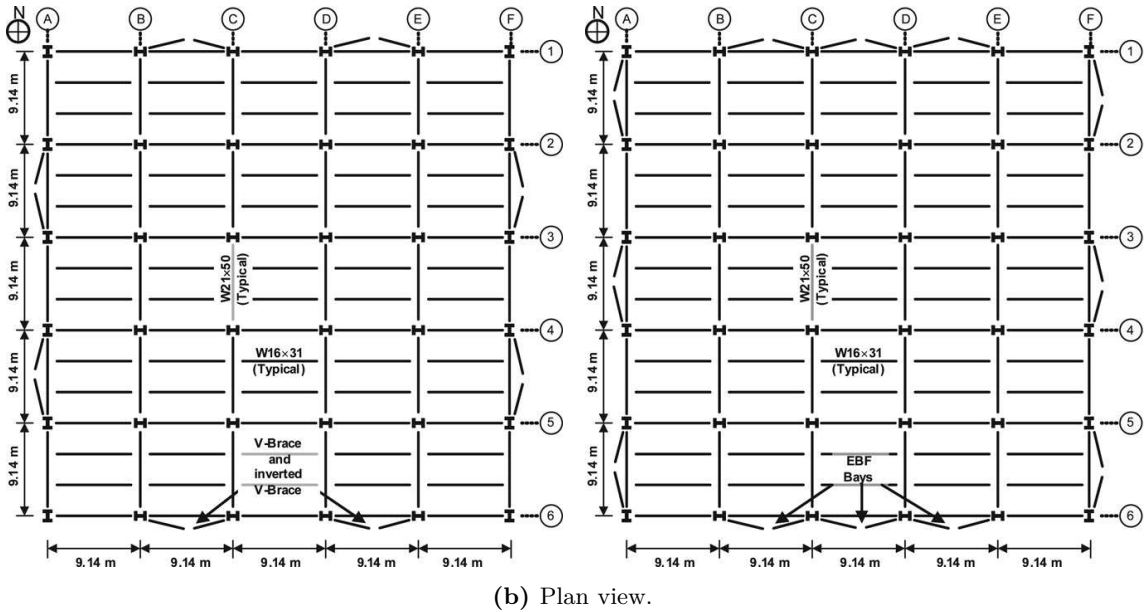
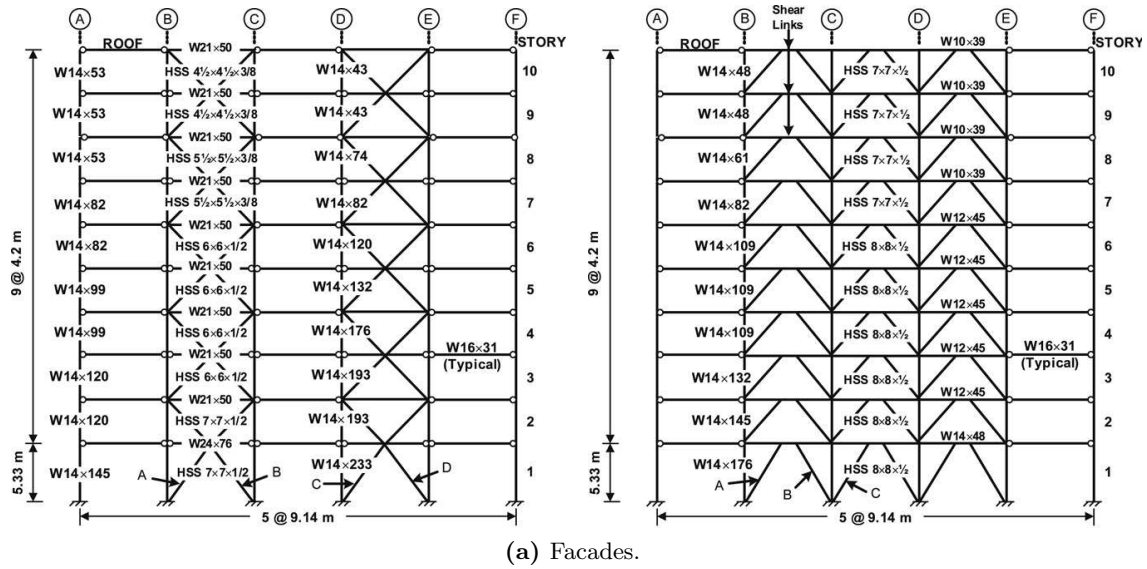


Figure 2.1: Facades and plan view of the two structures. [Khandelwal et al. 2009]

	Typical floors	Roof
Self-weight of slabs	2202 N/m ²	2202 N/m ²
Super-imposed dead load	1436 N/m ²	479 N/m ²
Live load	4788 N/m ²	958 N/m ²

Table 2.1: Loads on the slabs.

2.1.1 Lateral load resisting systems

In the facades of the structures there are gravity bays and braced bays. The braced bays function as lateral load resistant system, whereas the connections in the gravity bays are shear connections, only able to transfer a small moment. The supports for the columns are fixed, and the structures are designed using the principle of capacity design with *strong column/weak beam*. The connections are designed to be stronger than the adjoining beams and braces, so that plastic hinges will not be formed in the connections. [Khandelwal et al. 2009]

In the EBF the links (the part of the beams between the braces) are designed to yield during severe earthquakes, and they are designed as shear links according to [EN 1998-1:2004 2004]. The rest of the structure is designed to remain elastic during the design earthquake. In the SCBF the inelastic deformations primarily comes from yielding of the tension braces and inelastic buckling of the compression braces. Both inelastic mechanisms are shown in figure 2.2.

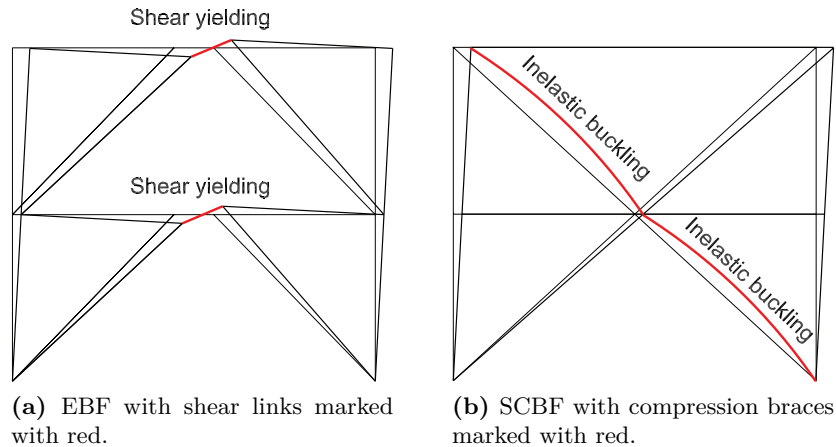


Figure 2.2: Inelastic mechanisms for the two bracing systems.

2.1.2 Seismic demands

Seattle is in a zone with high seismic activity, with a horizontal peak ground acceleration $a_g = 60\%$ of g with 2% probability of occurrence in 50 years, whereas Atlanta has only $a_g = 10\%$ of g in 50 years. The horizontal peak accelerations are found at the national seismic hazard map published by U.S. Geological Survey [USGS 2008], and a map with the locations of the cities is shown in figure 2.3.

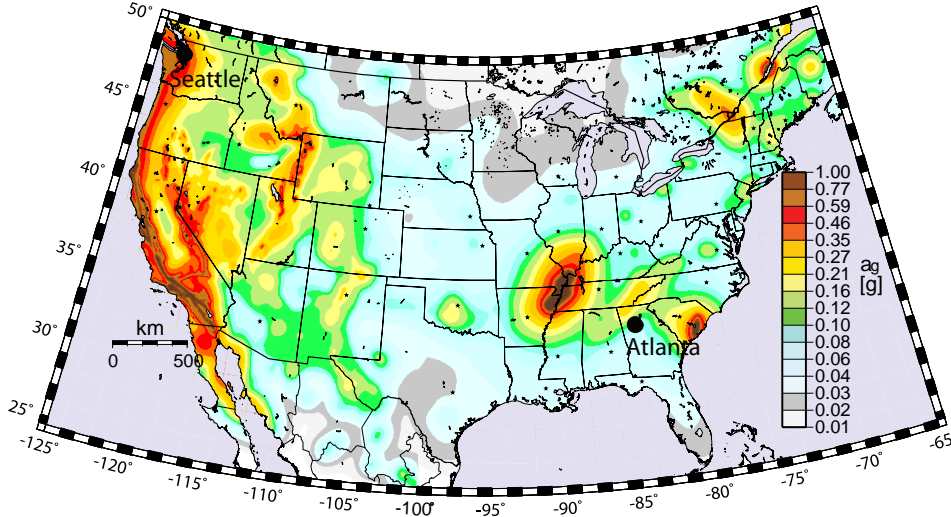


Figure 2.3: Seismic hazard map with 2% probability of occurrence in 50 years. [USGS 2008]

A general response spectrum is used to represent the seismic demand in seismic codes as [EN 1998-1:2004 2004] and [ATC-40 1996]. Robot uses the response spectrum from [ATC-40 1996], and generally seen it is like the one from [EN 1998-1:2004 2004] with a part with constant acceleration and a part with constant velocity, as shown in figure 2.4, where the peak ground acceleration is C_A . If the period T_S is equal to 0.4, as it is for a near source spectrum in [EN 1998-1:2004 2004] on hard rock, C_V is equal to $C_A/2.5$. In [EN 1998-1:2004 2004] the response spectrum has a last part with constant displacement for large periods.

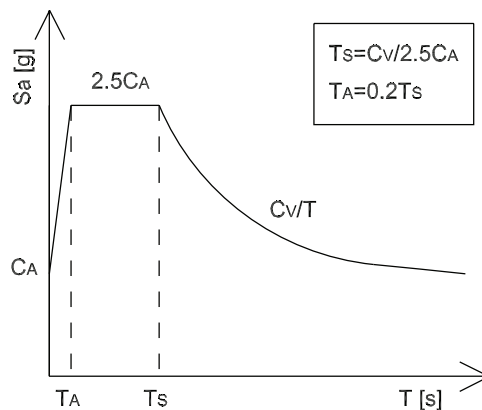


Figure 2.4: General response spectrum from [ATC-40 1996].

2.2 Nonlinear modeling of the structures

For a nonlinear pushover analysis the correct stiffness and nonlinear behavior of the structure have to be modeled.

The output of the pushover analysis is the capacity curve, where the total horizontal reaction is plotted as function of the roof displacement. In the beginning the structure will respond elastic, and the capacity curve will be linear. At some point the structure will begin to yield, resulting in a smaller slope, and at last the structure will collapse, and the bearing capacity will decrease to zero.

In order to calculate the full pushover curve all elements should be assigned correct nonlinear material behavior, and geometrical nonlinearity at large deformations ($P - \Delta$ effects) should be taken into account as well. Further connections and panel zones should be modeled explicitly in order to get accurate results. However, the software has limitations that sets an upper bound for the accuracy of the model.

In Robot softening of the material and damage of the structure can only take place in nonlinear hinges defined by the user. The hinges should be placed, where the structure is allowed to be damaged, and the rest of the structure should remain elastic.

2.2.1 Structural systems

In the model for the static pushover analysis it should be considered how to model the connections. Figure 2.1b shows the modeled sections, where the beam-column connections in the gravity bays of both structures are simple shear connections. In reality the shear connection will have a limited ability to transfer a moment, because it is not perfectly pinned, and because compression forces can be transferred through the concrete slabs. The structural systems and loads are explained in section 2.1.

All other connections in the EBF are momentstiff. For the momentstiff connections nonlinear hinges has to be placed wherever the stresses leaves the elastic range during the analysis. Further shear hinges has to be placed in the shear links to allow plastic deformations.

The braces are connected with moment stiff connections to ensure that compression hinges in the SCBF will form three plastic hinges in the brace when buckling. It is chosen to model the resulting behavior to compression cf. [Khandelwal et al. 2009, Fig. 8], thus the braces can be modeled in a simpler way.

2.2.2 Nonlinear hinges

In Robot there can only be defined one hinge in each node, thus if two beams meets a column in the same point, there can only be defined a hinge in one of them. To overcome this problem it may be necessary to place the hinge a bit away from the intersection point. For tension/compression bars, however this is not an option, since hinges can only be defined at the ends.

The force-displacement (or moment-rotation) curve for the hinges can either be defined directly for each hinge, or it can be defined relative to the limit force and limit displacement, corresponding to first yield of the element. The limit force and deformation is then calculated by Robot for each hinge according to the specific cross section, material, and length using formulas presented in [FEMA 273 1997]. The hinge has the general shape with the points A to E as shown in figure 2.5 that is representative for a typical ductile behavior.

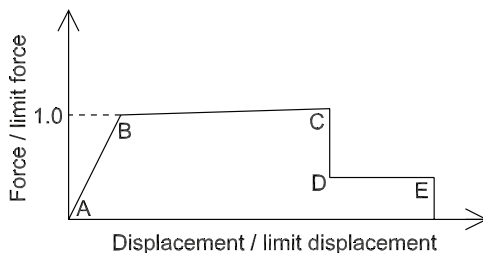


Figure 2.5: General relative force-displacement curve for hinges.

At first the behavior is elastic until point B, then the sections starts to yield, and the behavior is plastic with hardening until the point C, where buckling starts in the parts with compression or shear. This causes the strength to drops to a residual value until it breaks at the point E, where the strength drops to zero. In reality it will not be instantaneous drops, but can be modeled in this way. Tests in Robot have shown that even though the deformation at point E is defined, the strength does not drop to zero when that deformation is reached in a pushover analysis. Instead it remains at the residual value, which should not be possible.

When defining the location of the hinges in Robot, care should be taken that the hinges are defined compatible with the way that Robot calculate the limit values. If the hinges are placed at the end of the elements, the entire length is used. But if it is placed in an element, the length is the distance from one end to the hinge. Which end it is calculated from depends on the direction of the element and how it was selected.

In Robot there are three types of predefined hinges, for moment, shear-, and normal force, defined according to [FEMA 273 1997]. For all three

types of hinges the force-displacement curve is linear from origo until the point where yielding begins, where the values are the limit displacement and the limit force. This limit displacement, however, corresponds to the elastic displacement, which takes place in the length of the element already. If the predefined hinges are used directly, the elastic deformation of the elements with hinges will be twice the size of those of a structure without hinges, which is clearly wrong. Instead the hinges should be infinitely stiff until the limit force is reached, so that the only contribution is the plastic deformation. To be able to find a numerical solution it is necessary to have some slope though.

On basis of [*FEMA 273* 1997] and the explained errors in the predefined hinges, the moment hinge is defined corresponding to a moment resistant connection. The shear hinge is defined corresponding to a shear link and takes the deformation from the rotation due to the moment into account. Both the moment and shear hinge is equal for positive and negative forces, and has a steep curve until the limit force/moment is reached, then hardening until buckling happens and causes the force to drop to the residual value, where it decreases linearly until the point, where there is no capacity left. The normal hinge for the braces has different behavior in tension and compression, and is defined on basis of [*FEMA 273* 1997], but altered to reflect the braces in the specific structure according to [Khandelwal et al. 2009] in compression. In tension the curve looks like the shear hinge, but in compression the maximum force is the buckling load, and after this point is reached the force decreases while the brace buckles inelastically.

The three hinge types can be seen in figure 2.6. All hinges are supplied with a slope of 100, on the elastic part of the curve, where it should be infinitely stiff. This results in a displacement that is 1% of the limit value when the plastic deformations begins.

2.2.3 Modeling of eccentrically braced frame

Investigations has been made to examine the sensitivity of the model to changes, as the model is not totally accurate. The reference is model 1 that can be seen in figure 2.7, and has the following configuration:

- Shear connections: released
- Supports: moment hinge
- Braces: tension/compression bars
- Beam-column connections in braced bays: moment hinge

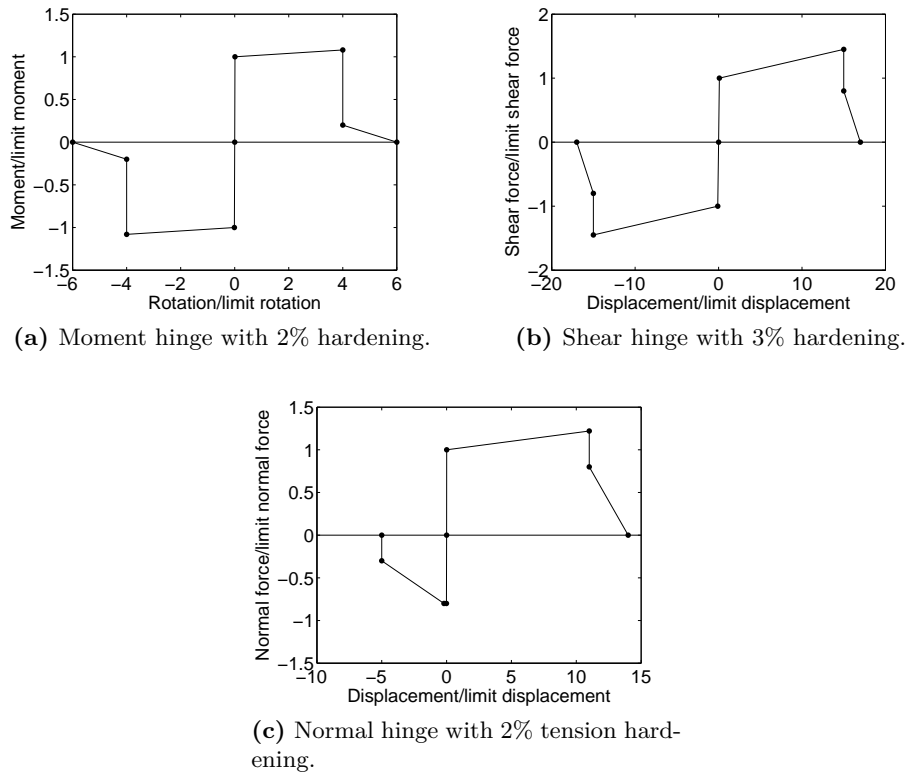


Figure 2.6: Force-displacement relationships for the hinges.

- Shear links: shear links in left side of the link

The hinges in the beam-column connection in the center bay is moved $1/100$ of the length of the beam towards the center, because two hinges cannot be placed in the same point.

The moment and shear hinges are not modeled totally stiff until the limit rotation is reached because of convergence difficulties, and models are made to examine the effect of this. This is done by replacing moment hinges with stiff connections. The shear hinges are not removed, because the nonlinear behavior primarily takes place in those, instead it is made 10 times less stiff, to examine the influence of the stiffness.

In reality the braces are connected with stiff connections, but because the nonlinear compression behavior is taken into account with the shape of the hinge, the brace can be modeled as a tension/compression bar or a bar that is released in the ends instead. The influence of the way it is modeled is examined.

The shear connections will not be totally released, and the influence of this is examined by making the connection stiff.

The other models are also shown in figure 2.7, and are described one by one in the following:

Model 2 The supports are moment stiff without hinges.

Model 3 The braces are not tension/compression bars but are released in the ends.

Model 4 The braces are not tension/compression bars and are momentstiff.

Model 5 The beam-column connections in the braced bays are modeled stiff without hinges.

Model 6 The shear connections are modeled stiff instead of released.

Model 7 The shear hinge has a slope of 10 in the elastic range instead of 100.

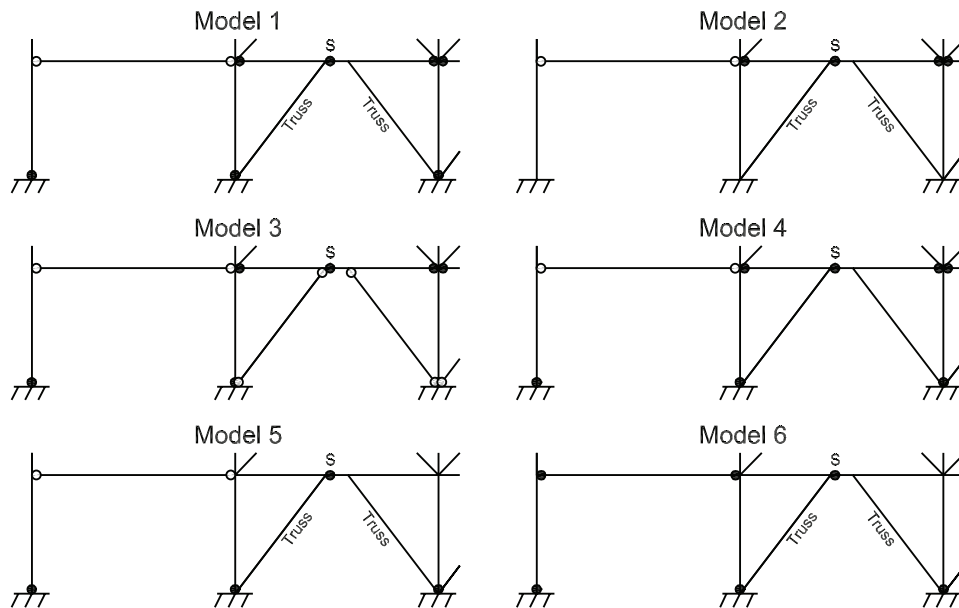


Figure 2.7: Representative extracts of the models of the EBF structure. Circles are released and filled circles are nonlinear hinges. An S next to a hinge means shear hinge, and all other hinges are moment hinges. Truss means tension/compression bar.

The pushover curves for the models are shown in figure 2.8. It can be seen that the curves are very close to each other, as only model 4 and 6 stands out a little. The curves stops at the points, where the solution does not

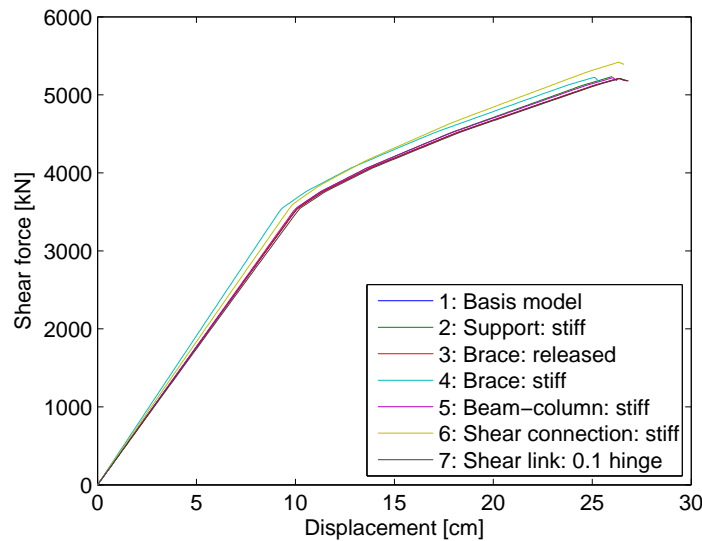


Figure 2.8: Capacity curves for the model test of the EBF structure.

converge, thus equilibrium cannot be fulfilled at larger deformations, and the structure becomes unstable.

Model 2 and 5 shows that the used moment hinges are sufficient stiff to give results near a totally stiff connection in the elastic area. The use of hinges are preferred because it ensures correct behavior in the plastic area.

Model 7 is equal to model 1 but with a 10 times less stiff hinge. The figure shows that this has almost no influence thus the shear hinge does not contribute significantly to the elastic deformation of the structure.

The influence of the braces is examined in model 3 and 4 and the moment stiff model gives noticeable increased global stiffness in the elastic range. If this were to be taken into account it would be necessary with moment hinges in the ends to ensure correct behavior outside the elastic range.

Stiff connections instead of simple shear connections in the gravity bays gives an increased global stiffness, especially within the plastic range of the curve. The reality will be somewhere between the two cases, and the difference between the outer bounds are so small that the use of simple connections are fine.

The conclusion in the analysis is that the stating model gives a good approximation, and the result is not very sensitive to the inaccuracies of the model. The analyzes are performed for an intact structure. For analyzes of the damaged structure it might be necessary to define additional hinges.

2.2.4 Modeling of concentrically braced frame

For the SCBF it is assumed that the modeling of the shear connections and supports has the same influence as for the EBF. Here investigations has been made to examine the influence of the modeling of the beams in the braced bays.

The reference is model 1 that can be seen in figure 2.9. The model has the following configuration:

- Shear connections: released
- Supports: moment hinge
- Braces: released with normal hinge
- Stiff beam-column connections in braced bays: moment hinge
- Beam where braces meet: released and with moment hinges at the center

The braces are not made as tension/compression bars because it is only possible to define hinges in the ends of tension/compression bars, and since two hinges cannot be located in the same point, the brace configuration makes it impossible unless eccentricities are introduced.

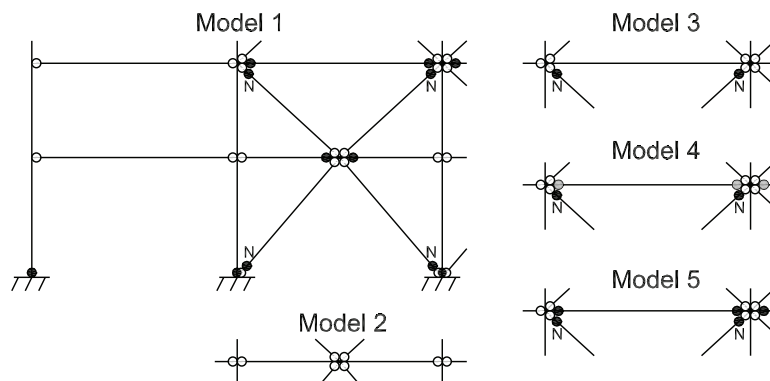


Figure 2.9: Representative extracts of the models of the SCBF structure. Circles are released and filled circles are nonlinear hinges. An N next to a hinge means normal hinge, and all other hinges are moment hinges. Grey hinges are less stiff moment hinges.

Extracts of the other models are also shown in figure 2.9 and diverges from the reference model in the following ways:

Model 2 There is no hinges in the center of the beams where the braces meets.

Model 3 The stiff beam-column connections are modeled stiff without hinges.

Model 4 The stiff beam-column connections are modeled with hinges that have a slope in the elastic range of 1.

Model 5 The stiff beam-column connections are modeled as released.

The pushover curves for the models are shown in figure 2.10. Until the point of maximum force the curves are almost coincidental. After this point model 1 to 3 stops because equilibrium apparently cannot be fulfilled. In model 4 and 5 it manages to reestablish equilibrium after the failure of the first braces, and collapse occurs at larger deformations. There is no obvious reason, why equilibrium cannot be found in model 1 to 3, and this might be due to limitations in the program.

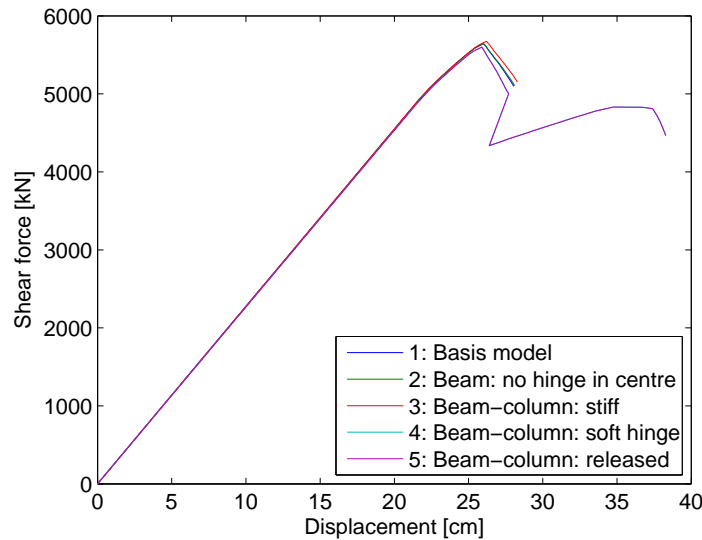


Figure 2.10: Capacity curves for the model test of the SCBF structure.

2.3 Performance of structures

In this section the performance of the structures at the earthquake with 2% probability of occurrence in 50 years is found, and the nonlinear behavior is investigated. Forces and deformations originating from the lateral force is investigated, but the influence of the vertical load from self and live load is not taken into account due to limitations in the program.

2.3.1 Eccentrically braced frame

For the EBF structure the horizontal peak ground acceleration with a probability of 2% of being exceeded in 50 year is $a_g = 60\%$ of g . If the type 1 response spectrum in Eurocode 8 is used and rock ground is assumed, the corresponding elastic response spectrum can be calculated. On basis of the capacity curve and the modal analysis results the capacity spectrum can be found for the corresponding SDOF system. On this basis the current design spectrum and performance point can be found for the given ground acceleration, as explained in appendix B. The found spectra are showed in figure 2.11. Since the performance point can be found for the current peak ground acceleration, the structure is found not to collapse at that seismic demand.

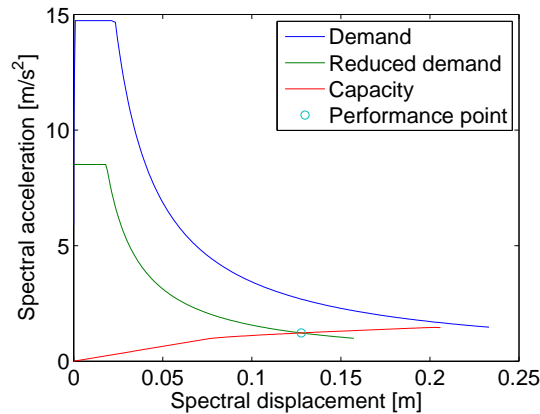


Figure 2.11: Capacity spectrum, demand spectrum and reduced demand spectrum for the performance point corresponding to $a_g = 0.6g$. The performance point is found at a roof deformation of 16.6 cm and a base shear force of 4356 kN.

For the eccentrically braced frame the nonlinear behavior primarily takes place in the shear hinges, and the rest of the forces do not redistribute significantly, because the calculations stop at the point where the first hinge breaks. This happens because all hinges in one story breaks at the same

time, and thus the stiffness of the story decreases so much that an equilibrium state cannot be found. The deformations of the structure and the force and deformation in the hinge with the largest stresses can be seen in figure 2.12. It can be seen in figure 2.12b that large deformations have occurred in the hinges in the bottom stories.

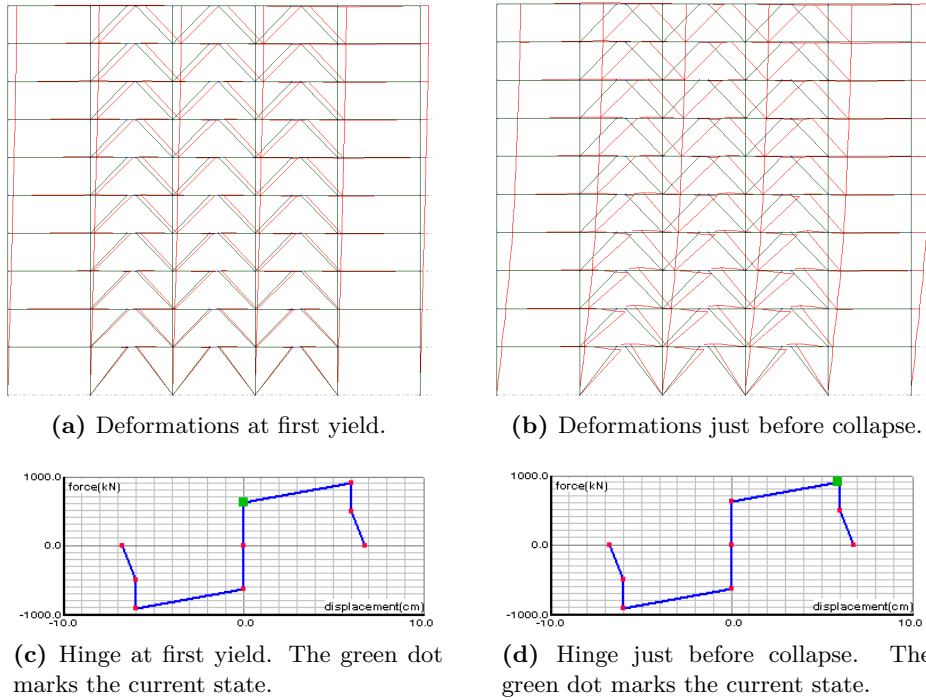


Figure 2.12: Deformations of the EBF structure and the force in the hinge with largest force located in story two.

The forces in the structure at the capacity point for the design earthquake are shown in figure 2.13.

Figure 2.13c shows that there is a large moment in the right pin in all beams in gravity bays, even though this moment should be zero. An analysis has been performed, where each of these beams were divided into 20 beams, and the analysis was performed again, giving the results displayed in figure 2.14a. This gives more plausible results, and the difference is there because Robot can only handle linear force curves within each element in the pushover analysis. The capacity curve for the structures are compared in figure 2.14b. It can be seen that they are coincident, and therefore the analysis with lesser elements gives sufficient results for the analyzes.

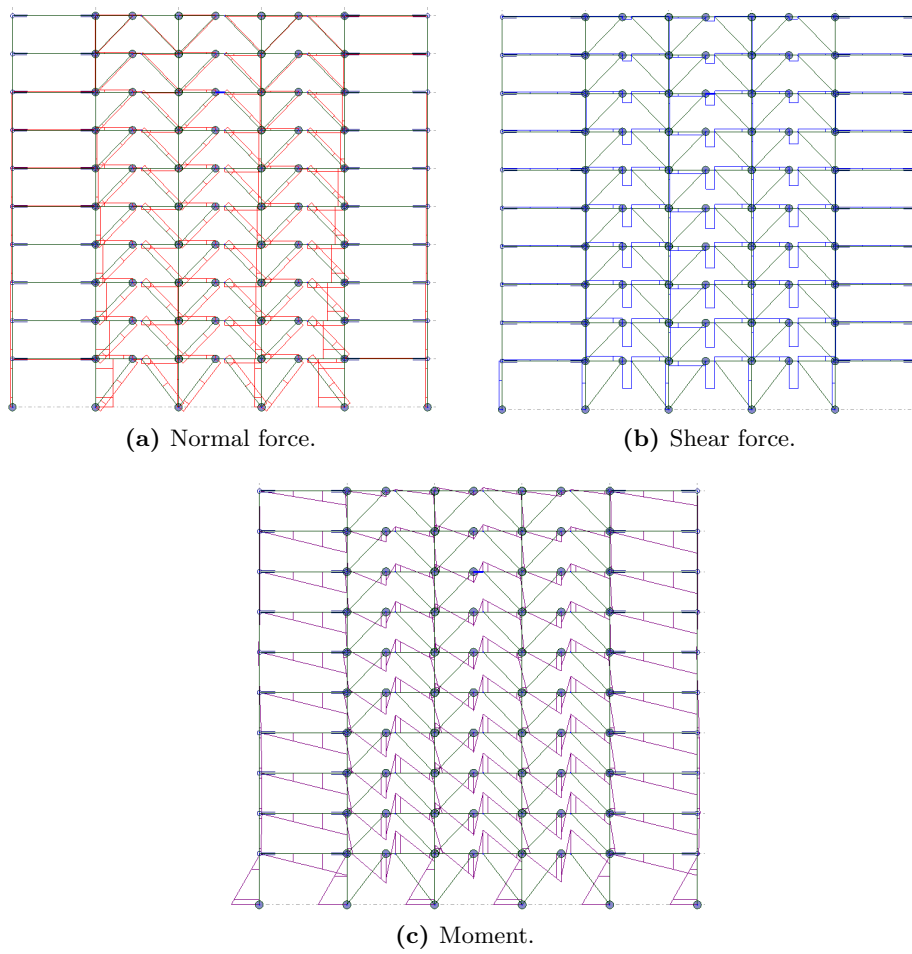


Figure 2.13: Section forces in the EBF structure at the performance point.

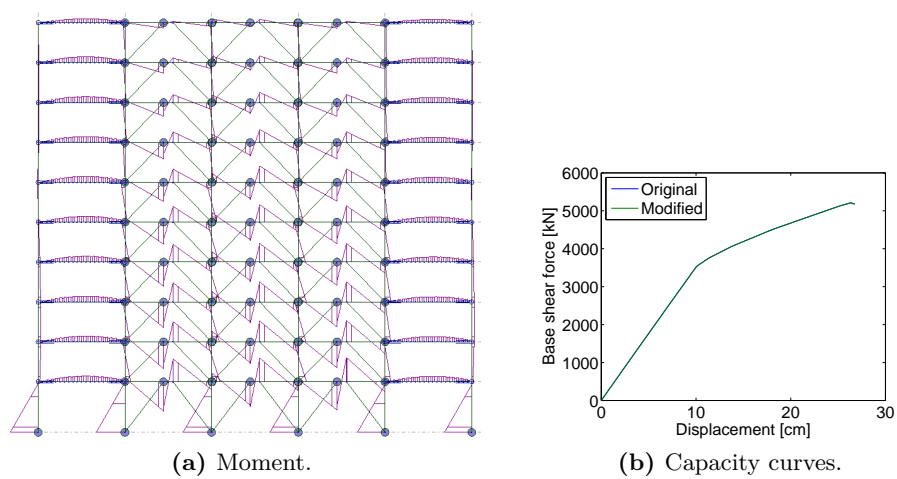


Figure 2.14: Moment curve for the modified model, and capacity curve for the two models.

2.3.2 Concentrically braced frame

For the SCBF structure the peak ground acceleration with a probability of 2% of being exceeded in 50 year is $a_g = 10\%$ of g . The same procedure as for the EBF structure is used, and the found spectra are showed in figure 2.15. The figure shows that the seismic demand is very small compared to the capacity of the structure.

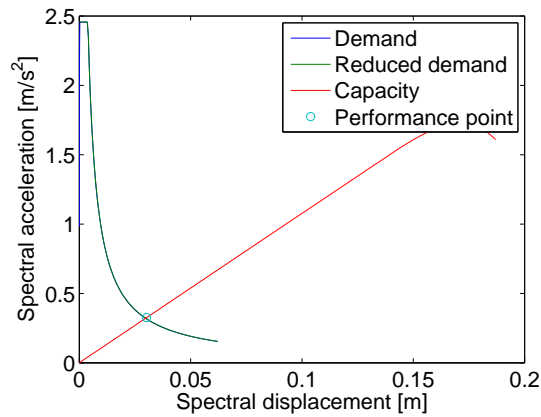


Figure 2.15: Capacity spectrum, demand spectrum and reduced demand spectrum for the performance point corresponding to $a_g = 0.1g$. The performance point is found at a roof deformation of 4.53 cm and a base shear force of 1032 kN.

For the concentrically braced frame the nonlinear behavior primarily takes place in the diagonals as tension with hardening and inelastic bending in compression. The deformations in the structure and the force in the compression and tension hinge with largest forces are displayed in figure 2.16 for the point of first yield and the point just before collapse. The hinges with the largest loads are located in 3rd and 4rd story, which can be seen from figure 2.16b, as the largest horizontal deflection occurs in these stories.

Figure 2.17 shows the maximum stresses in the structure at the point of first yield and just before collapse. At first yield it can be seen that the stresses are distributed rather smooth throughout the structure. At the point just before collapse it can be seen from figure 2.17b that two of the compression braces now transfer a smaller load, caused by strength degradation, as shown in figure 2.16d. This causes the tension hinges in the same stories to obtain a larger stress, which happens at large deformations, as the yield stress is reached cf. figure 2.16f. The different forces in the compression and tension braces causes the columns and beams to get an increased bending force cf. figure 2.17d and 2.17f.

In figure 2.17e and 2.17f it can be seen that there is a mistake in the moment curve as was the case with the EBF model, and the reason is the same.

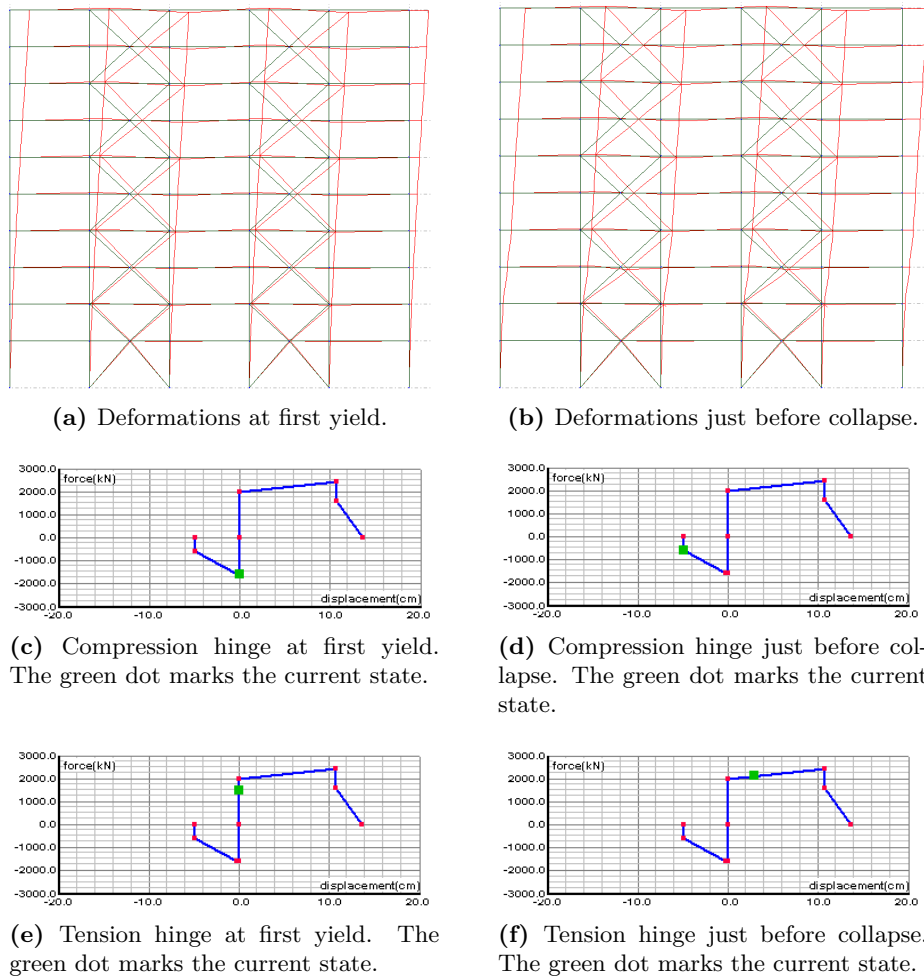


Figure 2.16: Deformations of the SCBF structure and the force in the compression and tension hinges with largest forces located in story three to four.

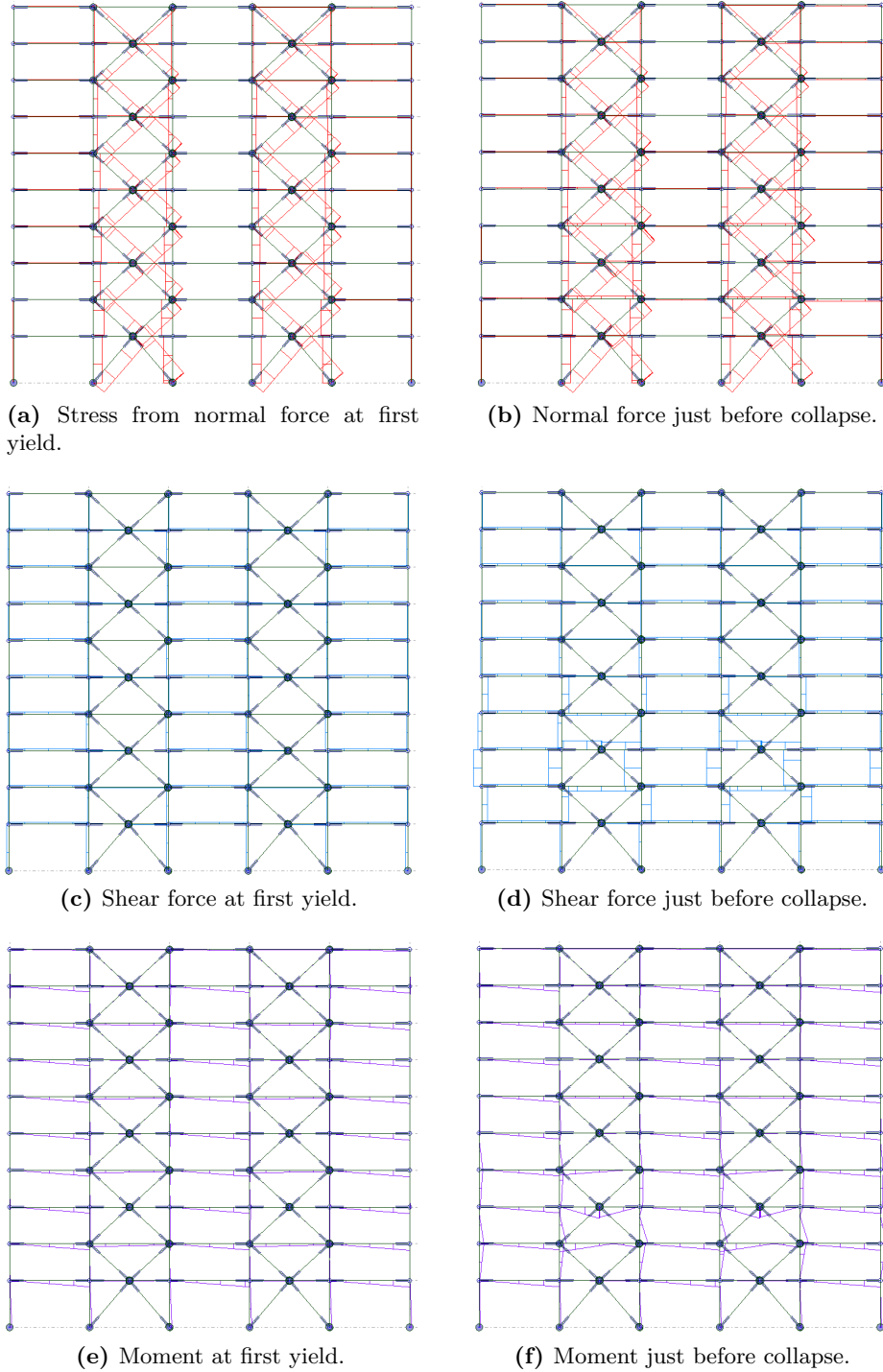


Figure 2.17: Section forces in the SCBF structure.

2.4 Summary

Two structures have been chosen for this analysis, an EBF located in Seattle and a SCBF located in Atlanta. A plane finite element model of each has been made, and nonlinear hinges have been placed to ensure the correct nonlinear behavior. More different models have been made to investigate the sensitivity of the pushover curve towards minor changes in the models.

The EBF was found to have a ductile behavior and it collapses at the point, where all shear hinges in one story fail. For the SCBF equilibrium could not be found after the failure of the first compression braces except for two of the alternate models, where the moment connections were less stiff. This indicates that it might be due to limitations in the program that the structure does not retain some strength after the failure of the first compression hinges.

The performance of structures was found for earthquakes with 2% probability of occurrence in 50 years for the respective locations. Both structures were found to have sufficient capacity using the performance based method in [ATC-40 1996], and the SCBF had a capacity much higher than necessary for the given earthquake.

Chapter 3

Assessment of robustness

In this chapter the robustness of the structures is evaluated through a qualitative discussion and through deterministic analyzes.

3.1 Structural configuration

In section 1.2.1 different strategies to ensure the robustness were discussed. The robustness of the structures is evaluated through a discussion of the three different strategies:

- Redundancy and ductility
- Isolation by compartmentalization
- Design of key elements

3.1.1 Redundancy and ductility

Redundancy and ductility are two properties of a structure that is able to provide alternate load paths if damaged. The structures, cf. section 2.1, are made of steel that is a highly ductile material, and are able to absorb large deformations without breaking. The braced bays of the structures are several times statically undetermined, and thus it might be able to provide alternate load paths if damaged.

The progressive collapse behavior of the structures was studied by [Khandelwal et al. 2009], and they found the structures capable of providing alternate load

paths in most cases. For the SCBF structure they found that the Achilles heel was the corner columns. This is quite obvious because they are not hold by any brace, and all beam-column connections are shear connections. If the column in the lower story is damaged or removed, only the concrete slabs that will work as cantilevers, and the very limited moment capacity of the shear connections can help the corner bays from collapsing.

The same is the case for the interior columns, where there are no braces either. But because the slabs are supported in the entire perimeter by the intact columns, they will be able to hold a larger load because this will give a smaller moment and due to the membrane forces in the slab.

An alternative system, where at least one braced bay was placed next to all outer columns, would eliminate the problem with the corner columns. Alternatively the robustness might be increased by making moment resistant connections instead of shear connections. This will increase the number of alternate load paths and increase the stiffness of the structure. But it might not be a good system, since it might require larger beams and it will increase the loading of the columns.

3.1.2 Isolation by compartmentalization

Isolation by compartmentalization is a strategy that allows a partial collapse of the structure with the aim of avoiding a complete collapse. If "removal of column"-scenarios are examined it might be necessary to allow a bay to collapse in the entire height of the building, if that strategy is to be used. It might be relevant in connection with the corner columns that are not supported by braces. Due to this strategy, the corner bay should be allowed to break like in the case of Ronan Point, to save the remaining structure. But failure of the corner bays in the entire height of the structure will still be disproportionate, when the local damage is only one column, and it is not an acceptable damage.

In addition the strategy will not help much if the resistance against horizontal loads is investigated. The seismic load will be a little bit smaller, since the mass is smaller, but unless a larger part of the structure is allowed to collapse, the influence will be infinitesimal. Further it will be hard to implement in this type of structure, without a general weakening of the structure.

3.1.3 Design of key elements

If the structure contains key elements the partial factor on these can be increased with a factor 1.2 to increase the overall safety of the structure. For the current structures it might be relevant to regard the corner columns that are not next to a braced bay in any direction, as key elements. Since the columns in general are designed with respect to the principle of strong column-weak beam (capacity design) they might already be oversized for their design loads.

3.2 Behavior of damaged systems

The robustness can be evaluated on basis of the capacity of the intact system versus the capacity of a damaged structure, where a limited part of the structure is removed (eg a column and adjoining braces). In this project only the resistance against horizontal load is evaluated, as the resistance against vertical load was studied by [Khandelwal et al. 2009]. The capacity against horizontal load is found through a pushover analysis, and the vertical load is not taken into account in the analysis because of limitations in the program.

In this analysis different scenarios are investigated, where a column and adjoining braces in the lower story is removed, and the capacity is found. The considered facades has six columns, and thus six different damage scenarios are possible. The corner columns in the SCBF, however, are key elements as they are placed next to gravity bays, and removal of those columns would result in an instable model, where the gravity bay is movable, and where the capacity of the rest of the model would not be changed significantly. For the EBF the corner columns are hold by braces in the other direction, but since the model is plane it would not make sense to remove them in this analysis. Further the structures are symmetric, and only two basically different scenarios are possible. Those are referred to as *Damage1* and *Damage2*, and can be seen in figure 3.1.

Three different limit states for the structure as system are investigated, with definitions from [Ellingwood & Kinali 2009]:

- Immediate Occupancy (IO):
Onset of inelastic behavior
- Structural Damage (SD):
Global lateral stiffness drops to half of initial value

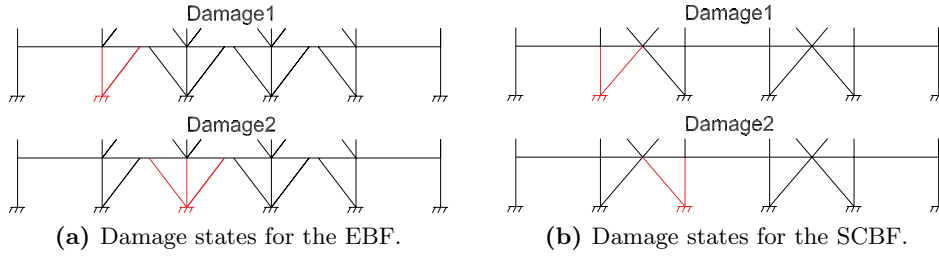


Figure 3.1: Damage states. Members marked with red are removed in the relevant damage state.

- Collapse Prevention (CP):
Onset of instability

The IO limit state is the point, where the first hinge leaves the elastic range, the SD limit state is the point where the slope drops to half of the initial slope, and the CP limit state is set to the point with maximum base shear force if the structure does not come to a stable equilibrium path again after strength degradation.

3.2.1 Eccentrically braced frame

The capacity curves for the EBF are shown in figure 3.2 for both the intact structure and the for the two damage states, and the three limit states are marked with dots. Both damage states have a collapse load smaller than for the intact structure, and the maximum load is almost equal for the two damage states. But the maximum deflection is significantly larger for damage state 1 than 2, and where the initial stiffness of damage state 1 is closer to that of the intact structure, it is significantly smaller for damage state 2, causing a larger natural period, as shown in table 3.1. The intermediate damage state, SD, is for the intact structure and damage state 1 close to the IO limit state, because the stiffness of the structure decreases significantly just after first yield. But for damage state 2 the SD limit state is located just before collapse.

	T [s]
Intact	1.73
Damage1	2.23
Damage2	1.96

Table 3.1: Elastic natural periods for the EBF found using modal analyzes.

The deflections just before collapse for the two damage states for the EBF can be seen in figure 3.3, and the section forces can be seen in figure 3.4. In

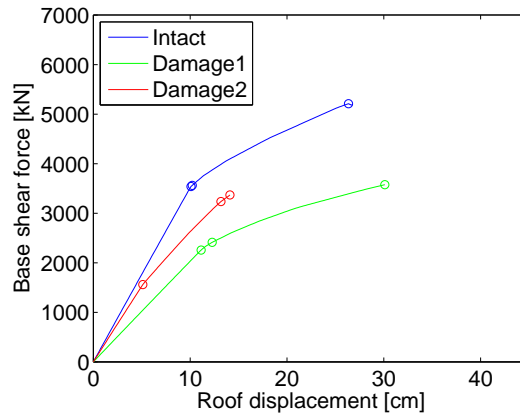


Figure 3.2: Capacity curves for the EBF. The dots mark the three limit states, IO, SD and CP.

damage state 1 only one shear link is affected, as only one brace is removed, whereas two shear links are affected in damage state 2 where two braces are removed. In damage state 1 the two unaffected braced bays make a joint system, and the damaged bay follows the deformations without helping significantly to transmit the forces. In damage state 2 the only undamaged shear link has a significantly larger force than the shear links in the other stories. In the other stories the shear links in each story have forces close to each other, and the two damaged bays work together in a system. Since all bays still contribute to the stiffness of the structure it is stiffer than in damage state 1. In damage state 1 the deformations are distributed quite even to the stories, but in damage state 2 a large part of the total horizontal deformation takes place in story 1.

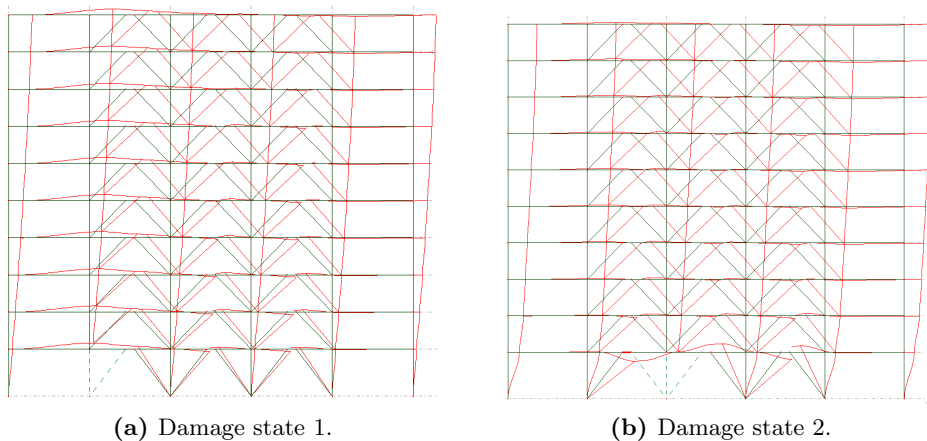


Figure 3.3: Deflections just before collapse for the damage states for the EBF.

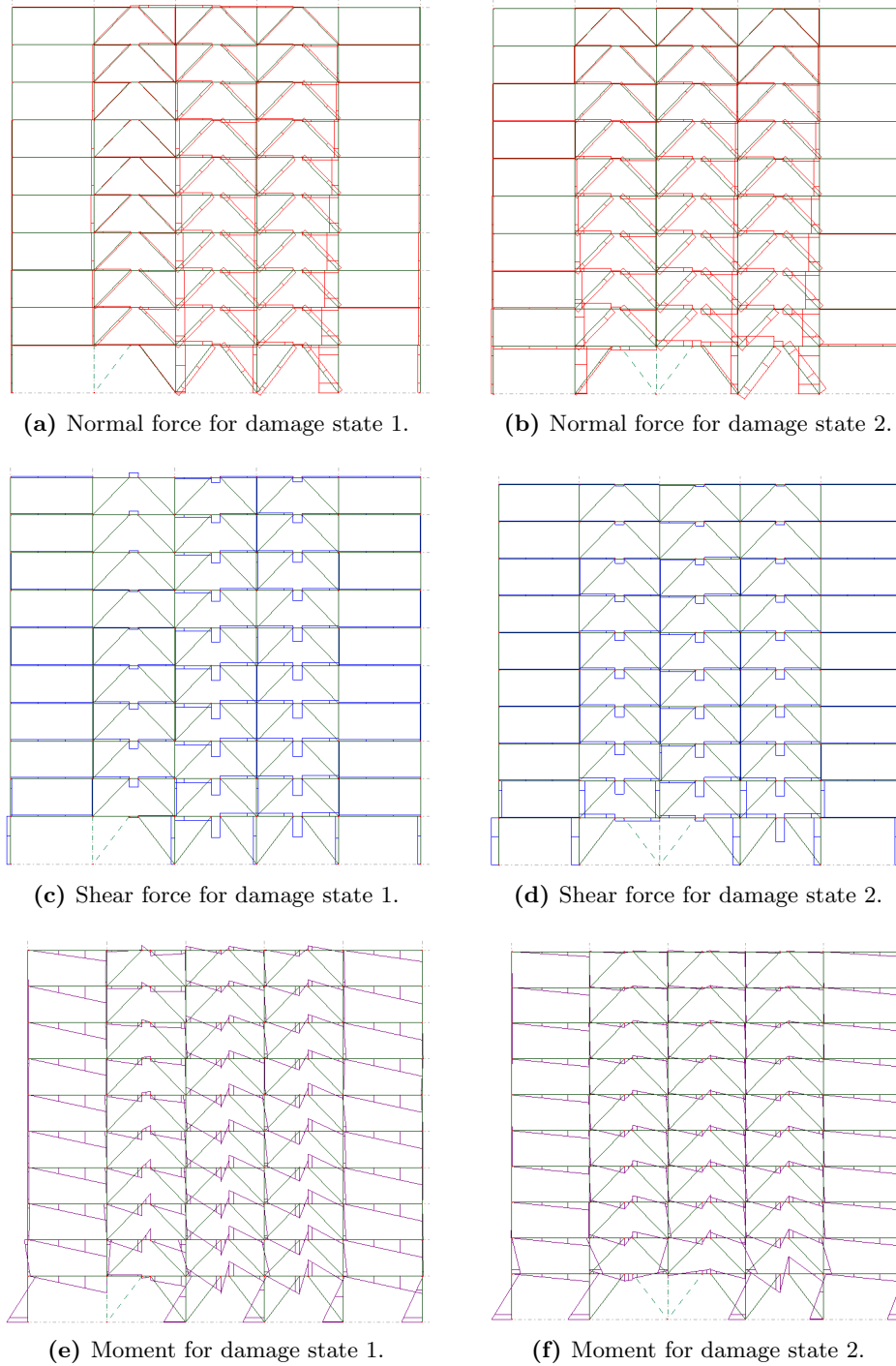


Figure 3.4: Section forces just before collapse for the damage states for the EBF.

3.2.2 Concentrically braced frame

The capacity curves for the SCBF are shown in figure 3.5 for both the intact structure and the for the two damage states, and the limit states are marked with dots. The curves for the two damage states are very alike, and they have a smaller maximum force, but a larger maximum displacement. They are less stiff than the intact structure, yielding larger natural periods, as it can be seen in table 3.2. The distance between the IO and SD limits are almost equal for the structures, but where the CP limit is obtained just after the SD limit for the intact structure, there is a long ductile path with very small slope for the damage states until the CP limit.

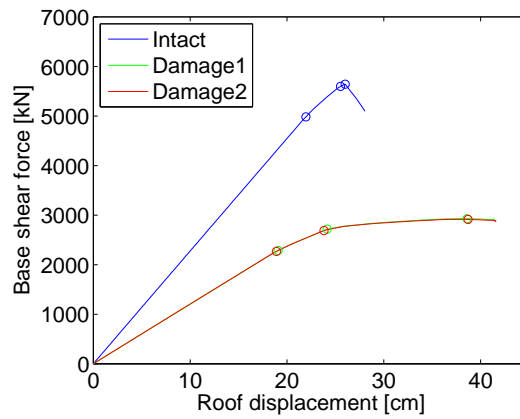


Figure 3.5: Capacity curves for the SCBF. The dots mark the three limit states, IO, SD and CP.

	T [s]
Intact	1.96
Damage1	2.74
Damage2	2.73

Table 3.2: Elastic natural periods for the SCBF using modal analysis.

The deflections just before collapse for the two damage states for the SCBF can be seen in figure 3.6, and the section forces can be seen in figure 3.7. The forces in the damaged bay are very small, except for the shear force and moment in story 1.

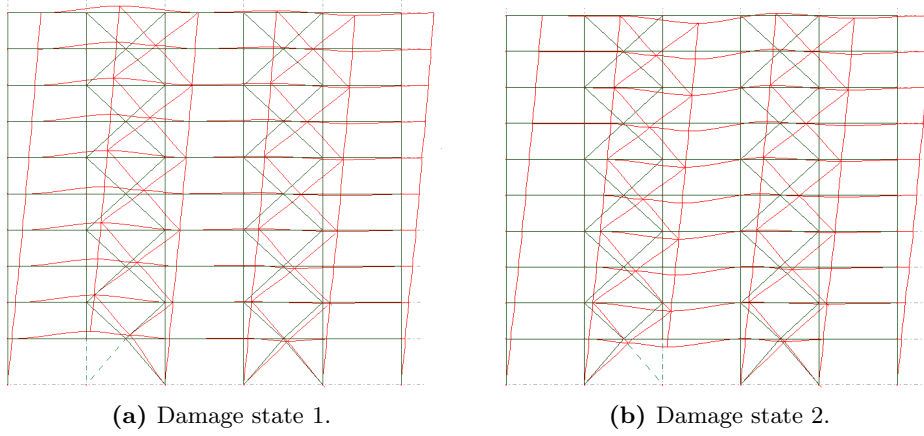


Figure 3.6: Deflections just before collapse for the damage states for the SCBF.

3.3 Deterministic assessment of robustness

The *RIF* value used in the offshore industry can be considered as a measure for the robustness of a structure cf. section 1.2.2, and can be found for the i 'th damage state as:

$$RIF_i = \frac{R_{C(F_i)}}{R_{C(intact)}} \quad (3.1)$$

where $R_{C(F_i)}$ and $R_{C(intact)}$ is the capacity against horizontal load of the damaged and intact structure respectively. The way the capacity should be measured, depends on the load type.

3.3.1 Load type

If a static load type is considered, only the force is interesting. Ductility ensures that local strength degradations does not happen at first yield, but only the maximum force has an influence on the capacity. For a seismic load however, it is different.

In the spirit of performance based design the capacity against seismic loads should not be measured in terms of force, but in terms of peak ground acceleration. For two capacity curves with the same maximum force, as shown in figure 3.8, the maximum structural peak acceleration capacity will be the same. But if the maximum displacement is larger for one of them, the fraction between the energy dissipated by hysteresis and the strain energy is larger too, and thus the hysteretic damping will be larger. Further the design spectrum for the performance point at the end of the capacity curve with the larger displacement will lay over the other. Both factors will

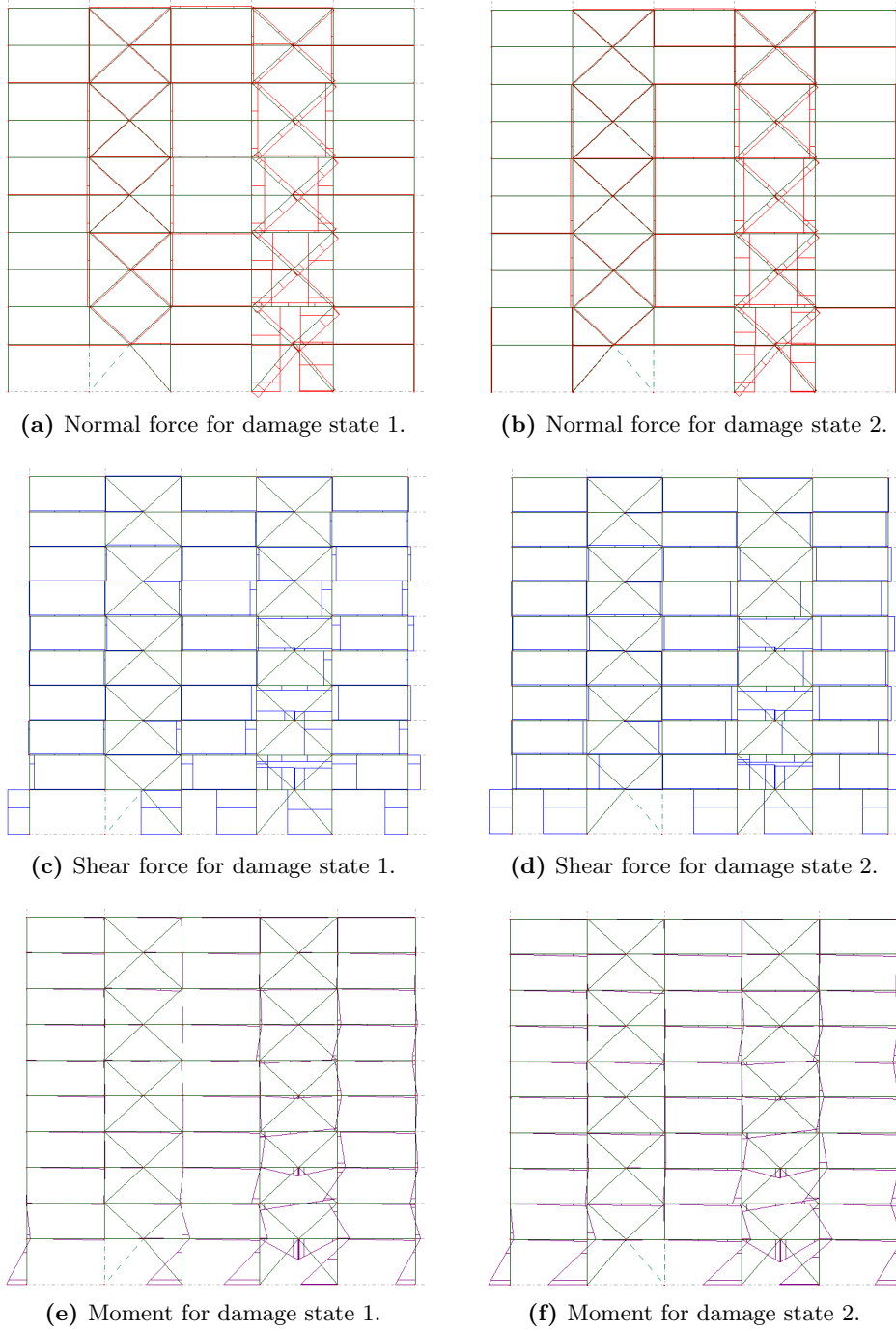


Figure 3.7: Section forces just before collapse for the damage states for the SCBF.

increase the corresponding peak ground acceleration in the case of the more ductile structure. See appendix B for more explanation about the nonlinear performance based design procedure.

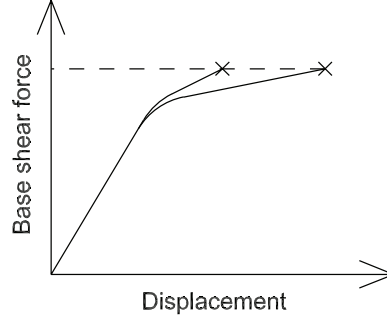


Figure 3.8: Capacity curves for structures with same maximum load but different hysteretic damping.

For a static load the deterministic robustness index, $RIF(Q)_i$, connected with the i 'th damage state can be found as:

$$RIF(Q)_i = \frac{Q_{C(damage,i)}}{Q_{C(intact)}} \quad (3.2)$$

where Q_C is the static horizontal load necessary to cause collapse.

For a seismic load the deterministic robustness index, $RIF(a_g)_i$, connected with the i 'th damage state can be found as:

$$RIF(a_g)_i = \frac{a_{g,C(damage,i)}}{a_{g,C(intact)}} \quad (3.3)$$

where $a_{g,C}$ is the horizontal peak ground acceleration necessary to cause collapse.

3.3.2 Results

In this section the results for the analyzes are presented.

Eccentrically braced frame

The peak ground acceleration, necessary to cause collapse, can be found with the method described in appendix B. But instead of knowing a_g and finding the performance point through an iterative process, the performance point is set from the start to be the point of collapse. Then the collapse a_g can be found as the value, where the belonging demand spectrum reduced due

to hysteretic damping, goes through the performance point. The capacity spectra, performance point/collapse point, and reduced demand spectra for the intact and damaged structures are shown in figure 3.9.

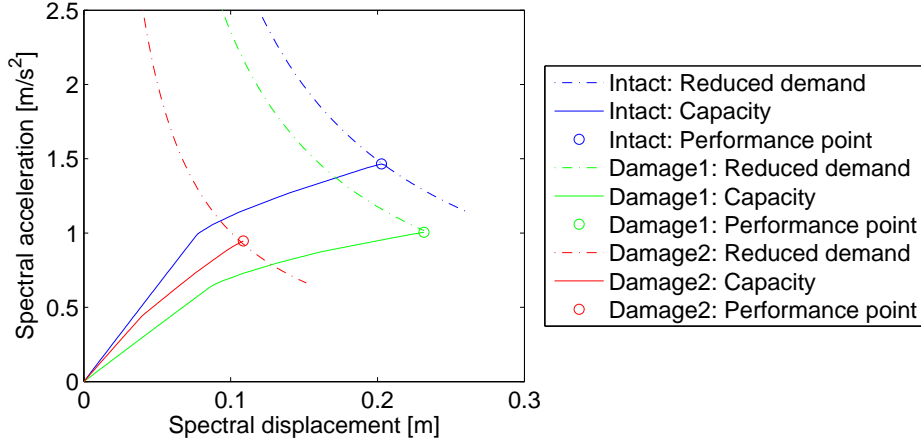


Figure 3.9: Capacity spectra, reduced demand spectra and performance points for the EBF.

The total effective damping (cf. appendix B), the spectral reduction factor for the part of the demand curve with constant velocity, SR_V , and the collapse peak ground acceleration, $a_{g,C}$ for each case are shown in table 3.3.¹ The table shows the effect of the difference in ductility for damage state 1 and 2. The effective damping are smaller for damage state 2 and therefore the spectral reduction factor is closer to one, thus the elastic spectrum is closer to the reduced spectrum. In addition the reduced demand spectrum through the collapse point for damage state 2 is over the one for damage state 1. Together these things means that the capacity for damage state 1, in terms of ground acceleration, is almost twice the size of damage state 2, even though the capacity, in terms of force, is almost equal.

If more limit states are to be investigated, and for use in probabilistic analyzes, it is not enough to determine the single value of a_g that causes collapse. Instead each limit state can be represented as the value of the maximum inter story drift angle (ISDA). This value can be calculated directly from the node deflections at the limit state, found during the pushover analysis.

For a specific structure there can be found approximately to be the following relationship between the maximum ISDA and the spectral acceleration at

¹The values in table 3.3 and figure 3.9 are calculated with estimated values, calibrated against the results from Robot in one point, because it has not been possible to get the needed values out of Robot. Therefore the RIF values calculated on basis of these values will not accurately give the results in table 3.4, as the latter is found using Robot directly. The same counts for the SCBF.

	β_{eff} %	SR_V -	$a_{g,C}$ g
Intact	24.3	0.61	0.92
Damage1	23.0	0.62	0.80
Damage2	12.5	0.77	0.42

Table 3.3: Effective damping, β_{eff} , spectral reductions factor for the part of the demand spectrum with constant velocity, SR_V , and collapse peak ground acceleration, $a_{g,C}$, for EBF.

the vibration period of a structure, $S_a(T)$:

$$ISDA = b \cdot S_a(T)^a \quad (3.4)$$

where a and b are regression constants [Ellingwood & Kinali 2009].

When the demand is expressed by a response spectrum, the same relationship will count for ISDA and a_g , since a_g and $S_a(T)$ are proportional for a constant value of T . Thus the relationship will not be the same for the intact and damaged structure, but for each damage state the relationship can be found. For the capacity curve for the intact structure the performance points and the belonging ISDA has been found for different values of a_g , as shown in figure 3.10. The solid black line is the regression line for all the performance points, and it can be seen that it does not fit very well at the last part of the curve, thus the estimated collapse value of a_g is larger than the value that seems to be right. For a regression line through the last two points only (the red line) the estimated collapse value seems to be better.

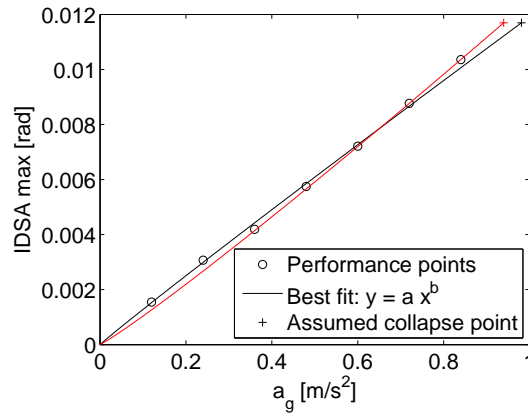


Figure 3.10: IDSA- a_g relationship for the found performance points and the assumed collapse performance point for best fit through all point (black), and through the last two points (red) for the EBF.

The same counts for the two damage states, and for a collapse analysis it will give a more accurate result to use only the last points to estimate the

collapse value of a_g . Using only the last two points the limit values of a_g have been found for all limit states, and are showed in figure 3.11 together with the force Q in the different limit states. It can be seen that the ratio between the intact and the different damage states are very different for the SD limit state compared to the other. This is caused by the difference in location of the SD point on the capacity curves cf. figure 3.2, and this measure does not tell much for the damaged structures. For the IO and CP limit state the difference between the two damage states is significantly larger for a_g than for Q .

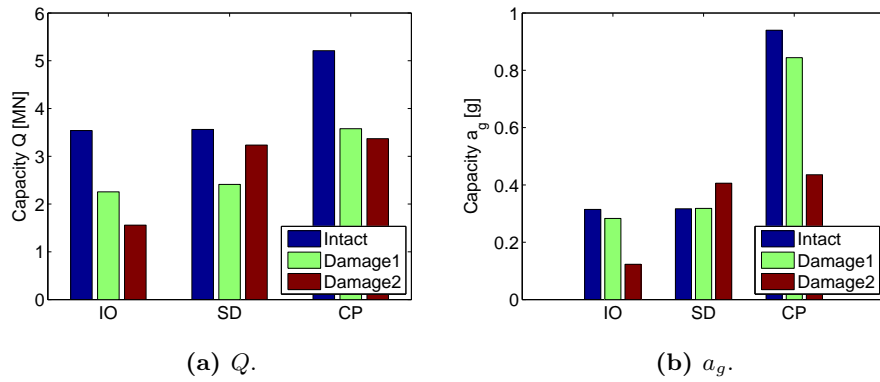


Figure 3.11: Capacity for the different limit states for EBF.

In table 3.4 the RIF values based on the collapse force and based on the calculation of the belonging peak ground acceleration are shown for both damage states. The $RIF(a_g)$ values are higher than one for the SD limit, but this limit is connected to the global change in stiffness, and does not tell much for the damaged structures, where the initial stiffness is less.

	$RIF(Q)$		$RIF(a_g)$	
	Damage1	Damage2	Damage1	Damage2
IO	0.64	0.44	0.90	0.39
SD	0.68	0.91	1.00	1.28
CP	0.69	0.65	0.90	0.46

Table 3.4: RIF values for EBF.

To investigate the influence of the number of points taken into account in the ISDA- a_g relationship, cf. figure 3.10, the value of $RIF(a_g)$ has been found for different numbers of points for the IO and CP limit state, and are displayed in figure 3.12.

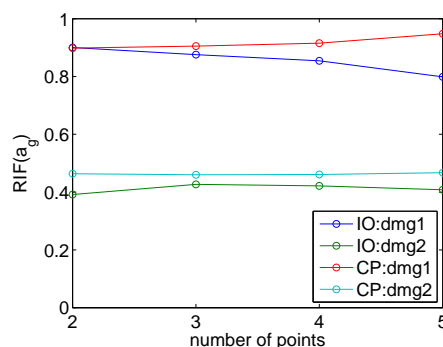


Figure 3.12: Sensitivity of $RIF(a_g)$ towards number of points taken into account in the ISDA- a_g relationship for the EBF.

Concentrically braced frame

The capacity spectra, reduced demand spectra and performance points for the SCBF, are shown in figure 3.13. The reduced demand spectra for the two damage states are below the one for the intact structure, but the ductility for the damaged structures is larger, and thus the effective damping is much larger, as it can be seen in table 3.5. This results in a spectral reduction factor farther from one, and the value of a_g corresponding to collapse is actually larger than the one of an intact structure. This indicates that the damaged structure has a higher capacity towards seismic loads than the intact structure, because the behavior is more ductile. This is probably due to the smaller initial global stiffness, which makes a redistribution of the forces possible. It should be noted for the intact structure that the point defined as collapse might not be the correct point. A model that was moderately changed, cf. figure 2.10, was able to find a new equilibrium path, and this might be possible for this intact structure as well, even though Robot could not find equilibrium. In addition the vertical loads are not taken into account, and this might give a change in the result.

	β_{eff} %	SR_V	$a_{g,C}$ g
Intact	7.6	0.90	0.638
Damage1	25.6	0.59	0.840
Damage2	26.0	0.59	0.843

Table 3.5: Effective damping, β_{eff} , spectral reductions factor for the part of the demand spectrum with constant velocity, SR_V , and collapse peak ground acceleration, $a_{g,C}$, for SCBF.

Using same method as for the EBF the limit values of a_g have been found for all limit states, and are showed in figure 3.14 together with the force

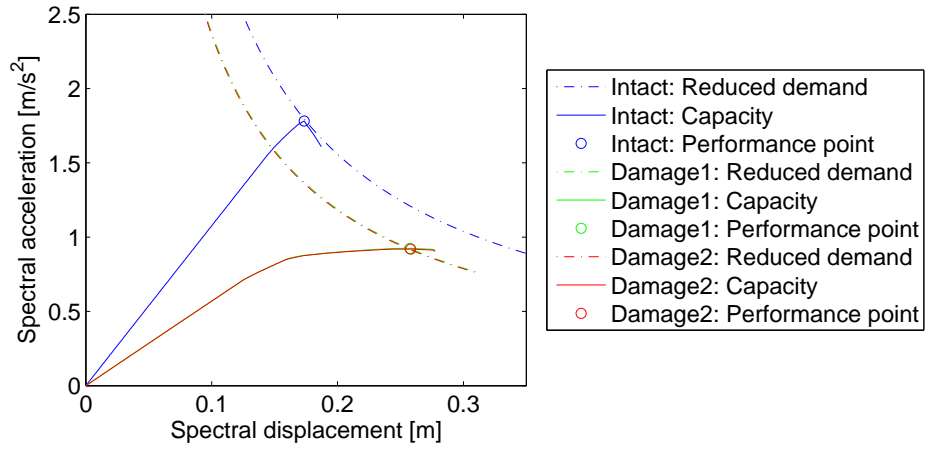


Figure 3.13: Capacity spectra, reduced demand spectra and performance points for the SCBF.

Q in the different limit states. It shows that the damaged structures only performs better in the CP limit state under seismic load. Else the intact structure performs better.

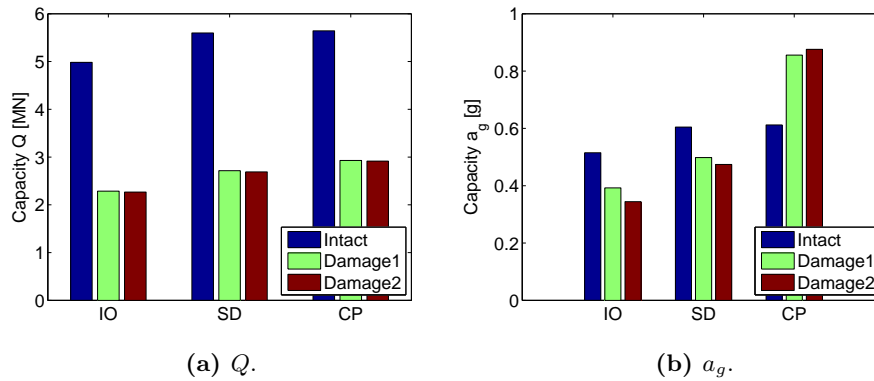


Figure 3.14: Capacity for the different limit states for SCBF.

The RIF values for all limit states are shown in table 3.6. For static loads the RIF value will always be less than one, but this analysis indicates that this is not always the case for seismic loads, as the found capacity in the CP limit is larger for the damaged structures.

The RIF values has been calculated with only the two last points in the ISDA- a_g relationship. The influence on the results of the number of points taken into account is shown in figure 3.15.

	$RIF(Q)$		$RIF(a_g)$	
	Damage1	Damage2	Damage1	Damage2
IO	0.46	0.46	0.76	0.67
SD	0.48	0.48	0.82	0.78
CP	0.52	0.52	1.40	1.43

Table 3.6: RIF values for SCBF.

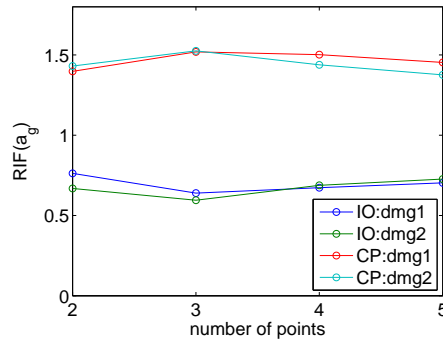


Figure 3.15: Sensitivity towards number of points taken into account in the ISDA- a_g relationship for the SCBF.

3.4 Other materials

Steel is known to be a highly ductile material, and it gives a redundant structure. If a material with another force-displacement relationship is used for the structure, it would be noticeable from the capacity curve in the following way:

- A changed Young's Modulus would both change the initial slope of the curve and the post yield slope.
- A changed yield stress would change the height of the elastic part of the curve.
- A changed hardening would change the post yield slope of the curve.
- A changed ductility would change the length of the post yield part of the curve.

The influence of the hardening and ductility are shown in figure 3.16.

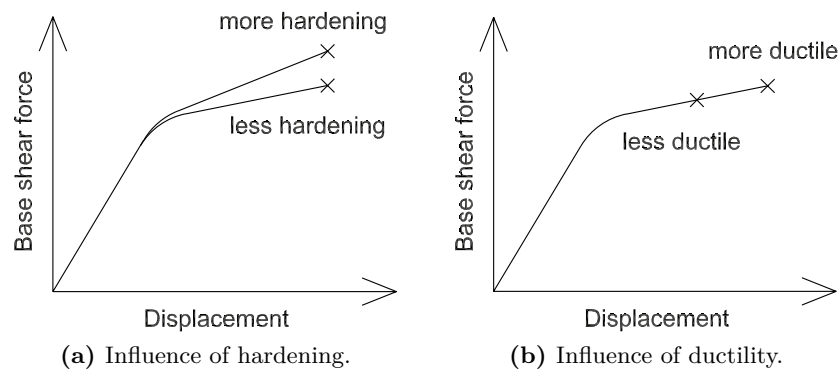


Figure 3.16: Capacity curves.

3.4.1 Analyzes

To investigate the influence of the material properties, ductility and hardening, analyzes has been made where the plastic hinges were changed. Four different configurations have been used:

- Original
- Half as ductile as original
- Hardening-% twice as big as original
- Hardening-% twice as big as original and half as ductile as original

These chances does not reflect specific other materials, but reflects general differences there can be for different materials. The starting point was construction steel that is a homogenous and isotrope material with high ductility. But for other steel types, eg high strength steel used in cables for suspension bridges, the ductility is less, and thus the behavior is more brittle.

Concrete is an anisotrope material, which has a low strength in tension, where the behavior is brittle, and a ductile hardening behavior in compression. In a reinforced beam the ductility is ensured by the ductile behavior of the reinforcement. The magnitude of the ductility depends on class of the used reinforcement. Timber is anisotrope as well and has a brittle behavior in tension and ductile with softening in compression. Often the connections are made of steel which gives a ductile behavior.

Eccentrically braced frame

In figure 3.17 the capacity curves for the EBF is shown, and collapse point is marked with a dot. The curves are as expected with equal curves in the elastic area, then the curves with more hardening is steeper than the other, and the less ductile curves stops before the other.

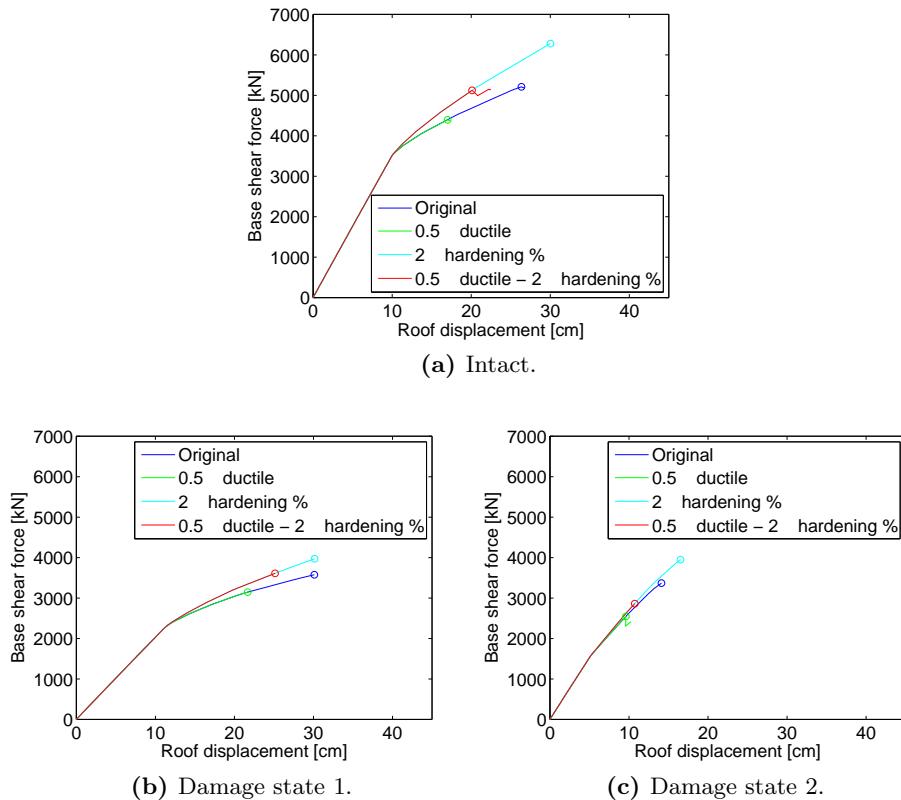


Figure 3.17: Capacity curves for changed material properties for EBF.

The capacities for the CP limit states are found in the same way as in section 3.3.2, both in terms of Q and a_g , and are shown in figure 3.18. The CP limit is most interesting as this limit is connected to the total capacity, and is the limit that is most changed by the shift in material. In general the capacities for models with more hardening is larger than the corresponding with less hardening, and larger ductility also gives larger capacities.

The RIF values are shown in table 3.7 for the different materials. Here it can be seen that the models with less ductility have a larger RIF value in most cases. This is not an expected result as ductility is considered as a factor that normally increases the robustness.

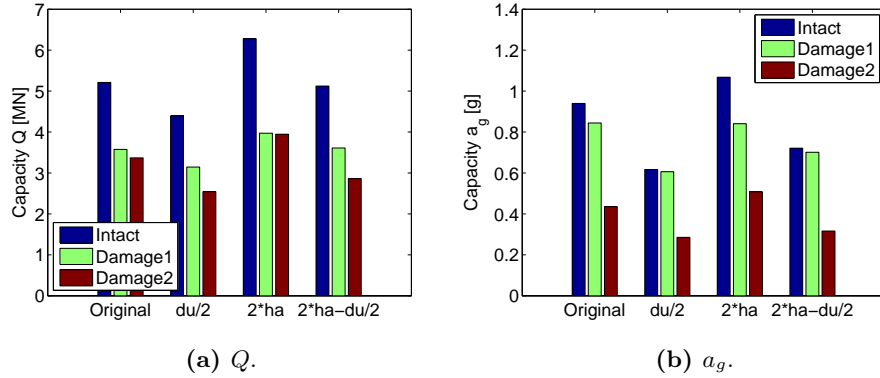


Figure 3.18: Capacity for the different materials for CP limit state for EBF.

	$RIF(Q)$		$RIF(a_g)$	
	Damage1	Damage2	Damage1	Damage2
Original	0.69	0.65	0.90	0.46
0.5×ductile	0.72	0.58	0.98	0.46
2×hardening-%	0.63	0.63	0.79	0.48
2×hardening-% - 0.5×ductile	0.70	0.56	0.97	0.44

Table 3.7: RIF values for other materials for the EBF.

Concentrically braced frame

The capacity curves for the SCBF are shown in figure 3.19, and the collapse points are marked with a dot. For the intact structure the points are rather close, but for the damaged structures the original material gives a significantly more overall ductile behavior than the others. For the intact structure the less ductile material gives a new equilibrium path, after the maximum force is reached, but the maximum point is considered as collapse.

The capacities for the structures is shown in figure 3.20 for the different materials. It shows that it is only for the model with original material properties that the damaged structures have a significantly larger a_g value. For the other materials the capacities in terms of a_g is rather close.

The RIF values are shown in table 3.8. For the SCBF less ductility gives a smaller RIF value, and more hardening in general, also gives a smaller RIF value.

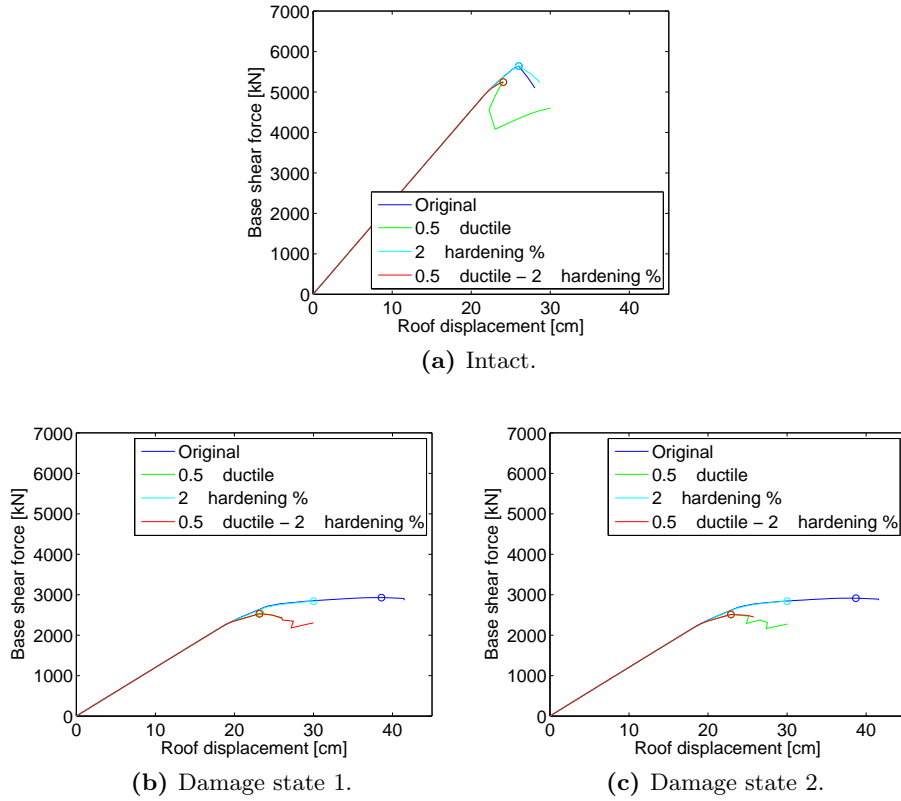


Figure 3.19: Capacity curves for changed material properties for SCBF.

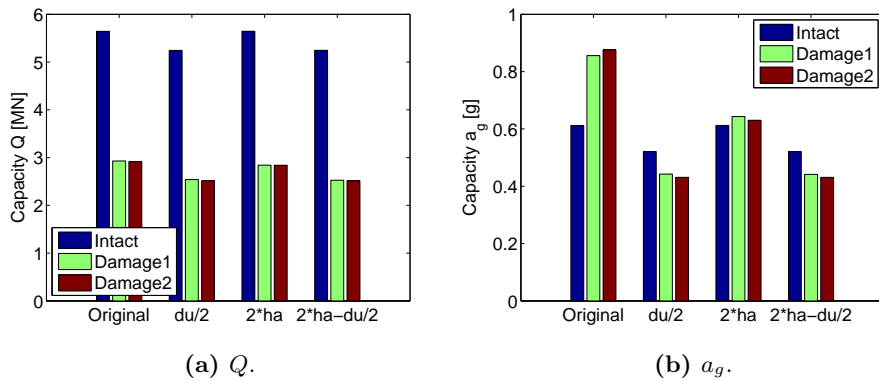


Figure 3.20: Capacity for the different materials for SCBF.

	$RIF(Q)$		$RIF(a_g)$	
	Damage1	Damage2	Damage1	Damage2
Original	0.52	0.52	1.40	1.43
0.5×ductile	0.48	0.48	0.85	0.83
2×hardening-%	0.50	0.50	1.05	1.03
2×hardening-% - 0.5×ductile	0.48	0.48	0.85	0.83

Table 3.8: RIF values for other materials for the SCBF.

3.5 Summary

In the deterministic assessment of the robustness three different limit states were investigated for static and seismic horizontal load, and the influence of ductility and hardening was investigated for the collapse limit. For each of the two structures two different damage states were investigated. The corner columns are either key elements (SCBF) or hold by braces in the other direction (EBF), and in both cases it would not make sense to investigate cases, where they were removed.

The intermediate limit state, SD, was found to give very different results for the intact and damaged structures for the EBF, because the stiffness degradation happened at different places. But because the deformations were not equally distributed throughout the structure in the damaged states, the used definition with the point where the global lateral stiffness drops to half of the original value is not very good, when damaged structures are investigated.

Because of the different structural configurations for the EBF and SCBF structure, the behavior of the damaged structures compared to the intact were different for the two cases. For both structures the maximum base shear force for the two damaged structures were close to each other, and significant smaller than for the intact structure. But where the maximum deflection was significantly different for the damage states for the EBF, it was almost equal for the SCBF, where it was significantly larger than the deflection of the intact structure.

The size of the deformation is very important when the resistance against seismic loads is investigated. For the EBF structure it gave a big difference between the two damage states, and for the SCBF structure it gave an unexpected result, as the damaged structures were found able to resist a larger peak ground acceleration than the intact. This is caused by a more ductile behavior of the damaged structure due to the smaller initial global stiffness, with the results that a redistribution of the forces is possible. But this result might also be caused by limitations in the program, as the vertical loads are

not taken into account, and the intact structure might still have additional capacity left at the point defined as collapse. The use of more complicated analysis methods might give another result, and also the use of a spatial model instead of a plane model would make it possible to take torsional effects into account. But in principle it is possible for a damaged structure to act more ductile, and thereby perform better during an earthquake, yielding a *RIF* value of more than one.

The ductility is a parameter that is normally considered as important for the robustness when the alternate load path strategy is used. The analyzes with different ductility and hardening showed that the structures with more ductile behavior were in fact able to resist a larger force and ground acceleration than those with smaller ductility. But when the *RIF* value is calculated a more ductile behavior both makes the intact and damaged structures perform better, and in fact it was found to increase the capacity more for the intact than for the damaged structures, yielding that more ductility gives a smaller *RIF* value, with the used definition. This means that if earthquake resistant structures are designed taking the actual ductility into account, a structure with less ductile behavior would have a higher seismic resistance in a damaged case.

In general increased hardening was found to give larger capacities, except for damaged states for the SCBF. Here the hardening seems to restrict the deformations, giving less ductile behavior, and thus a smaller capacity in terms of peak ground acceleration.

Chapter 4

Probabilistic seismic analysis

In probabilistic analyzes uncertainties are taken into account and the probability of exceeding a limit state as defined in section 3.3 can be found. These values can be used in a probabilistic assessment of the robustness.

4.1 Uncertainties in seismic risk assessment

The uncertainties can be divided into two groups, aleatoric and epistemic. The aleatoric uncertainties are caused by natural variation (inherent uncertainty) and cannot be reduced. They can be quantified with statistical analyzes when the available data is sufficient. The epistemic uncertainties are caused by limited knowledge and inaccurate computational models, and are set with larger uncertainty. Epistemic uncertainties can be reduced by better models and analysis methods.

For a seismic analysis there will be aleatoric uncertainties related to the capacity of the structure and the load from the earthquake, illustrated as the upper level in figure 4.1. The epistemic uncertainties lies in the shift from the upper level (real) to the lower level (model). In a seismic analysis there will be uncertainties related to the subjects listed below.

- Aleatoric
 - Material properties: Strength, stiffness
 - Seismic load: Intensity, spectrum
 - Local effects: Effect of local soil conditions

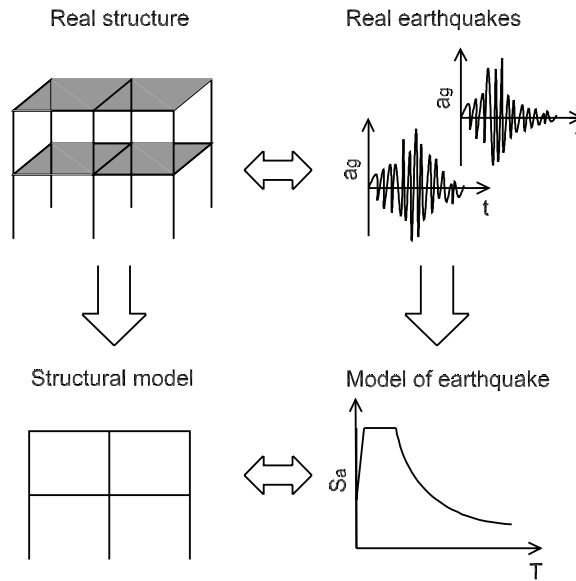


Figure 4.1: Uncertainties in seismic risk assessment.

- Epistemic
 - Model of structure: Connections, panel zones, inelastic behavior, plane vs. spatial, mass distribution
 - Analysis of structural model: Time history analysis (dynamic) vs. static analysis with equal effective damping
 - Model of earthquake: Time history \rightarrow general response spectrum
 - Failure functions: Definition of limit states

4.2 Procedure for seismic risk assessment

A procedure for assessing the annual probability of exceeding a limit state was proposed by [Ellingwood & Kinali 2009].

The limit state probability, P_{LS} , in seismic risk assessment is defined as:

$$P_{LS} = \sum_x P[S_a = x] \cdot P[LS|S_a = x] \quad (4.1)$$

where S_a is the intensity measured in terms of the peak spectral acceleration at the period of the structure, $P[S_a = x]$ is the probability that the intensity of the seismic demand is x , and $P[LS|S_a = x]$ is the probability of exceeding a defined limit state given that $S_a = x$. In this way the problem is divided into two quantities, the first dependent on the seismic demand and the second dependent on the capacity of the structure. [Ellingwood & Kinali 2009]

4.2.1 Capacity

The failure function can be written as:

$$g = M_R - X \quad (4.2)$$

where M_R is the capacity in terms of S_a and X is the seismic demand (load) in terms of S_a . If both are considered as lognormal distributed stochastic variables the failure function can equivalently be expressed as:

$$g = \ln(M_R) - \ln(X) \quad (4.3)$$

Using the definition of the reliability index, β , the probability of exceeding a given limit state can for a specific S_a be calculated as:

$$P[\text{LS}|S_a = x] = \Phi(-\beta) = \Phi\left(-\frac{\ln(m_R) - \ln(x)}{\sigma_R}\right) = \Phi\left(\frac{\ln(x/m_R)}{\sigma_R}\right) \quad (4.4)$$

where m_R and σ_R is the median value and the logarithmic standard deviation of the capacity respectively, and x is the given demand.

As described in section 3.3.2 the limit states can be expressed as limit values of ISDA, and thus the capacity in terms of S_a can be transmitted into a capacity in terms of ISDA. This can be done using the relationship:

$$m_c = a \cdot m_R^b \quad (4.5)$$

where m_c is the capacity in terms of ISDA and a and b are regression constants. In [Ellingwood & Kinali 2009] this relationship was found using time history analyzes with a range of different earthquake records as input. As it can be seen in figure 4.2 there are uncertainty connected with this model, as the found points are not located at a perfect curve, and the logarithmic standard deviation connected with the relationship is called $\sigma_{D|S_a}$ (drift (ISDA) given S_a). In [Ellingwood & Kinali 2009] this is referred to as aleatoric uncertainty, because it is caused by the structures different behavior towards the natural difference in earthquakes. But it is also connected to the model giving the relationship between the ISDA and S_a , which is an argument that it should be counted as epistemic uncertainty, but in [Ellingwood & Kinali 2009] it is assumed that the deviance from the curve is caused by aleatoric uncertainty alone. The epistemic uncertainty connected to the model and the time history analyzes is called σ_{RU} .

Insertion of equation 4.5 into 4.4 gives the following expression for the probability of exceeding a given limit state given $S_a = x$.

$$P[\text{LS}|S_a = x] = \Phi\left(\frac{\ln(ax^b/m_c)}{\sigma_R}\right) \quad (4.6)$$

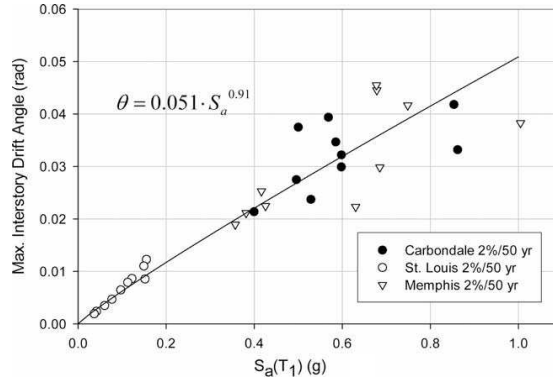


Figure 4.2: An example of the relationship between ISDA and S_a for an analysis with time history analyzes with different earthquake records as input. [Ellingwood & Kinali 2009].

The logarithmic standard deviation σ_R reflects all the aleatoric uncertainties connected to the capacity expressed in ISDA, and is found as:

$$\sigma_R = \sqrt{\sigma_c^2 + \sigma_{D|S_a}^2} \quad (4.7)$$

where σ_c that is the uncertainty in capacity in S_a , and $\sigma_{D|S_a}$ is the uncertainty in the relationship between the capacity in terms of S_a and ISDA. One might notice that the epistemic uncertainty (model uncertainty) for the capacity is not taken into account in this expression.

4.2.2 Demand

The seismic demands are described by seismic hazard curves, in terms of an acceleration, and the mean annual probability of exceeding it. Hazard curves for the entire US is mapped by U.S. Geological Survey (USGS), and in general the curves can be described as:

$$P[S_a = x] = 1 - \exp\left(-(x/u)^{-k}\right) \quad (4.8)$$

where u is a scale parameter and k is a shape parameter. This expression gives convex curve in a logarithmic representation. When the annual probability of exceeding a limit state is calculated using equation 4.1, only a small range of S_a contributes significantly to the integral.

The hazard curve can then be approximated with the following Taylor polynomial that gives a straight line in a logarithmic representation:

$$P[S_a = x] = k_0 \cdot x^{-k} \quad (4.9)$$

where $k_0 = u^k$ is a scale parameter.

After insertion of equation 4.4 and 4.9 into equation 4.1 and performing the integration one may obtain the expression [Cornell, Jalayer, Hamburger & Foutch 2002]:

$$P_{LS} = k_0 m_R^{-k} \cdot \exp[(k\sigma_R)^2/2] \quad (4.10)$$

where m_R can be found from equation 4.5.

Equation 4.10 still only takes the aleatoric uncertainties in connection with the capacity into account and the result is a point estimate of the probability of exceeding a limit state. The formulation can be extended to take the epistemic uncertainties into account as well. This is done by replacing the values k_0 and m_R with random variables K_0 and M_R modeled by lognormal distributions with medians k_0 and m_R and logarithmic standard deviations σ_{HU} and σ_{RU} .

Thus the annual probability of exceeding a limit state can be found as:

$$P_{LS} = \int_0^\infty \int_0^\infty k_0 m_R^{-k} \cdot \exp[(k\sigma_R)^2/2] f_{k_0}(k_0) f_{m_R}(m_R) dk_0 dm_R \quad (4.11)$$

The uncertainties taken into account in this expression are:

- Aleatoric
 - Uncertainty associated with the representation of the capacity in terms of ISDA limits: σ_c
 - Natural deviation between a given spectral acceleration and the resulting ISDA: $\sigma_{D|S_a}$
- Epistemic
 - Model uncertainty for the structural model: σ_{RU}
 - Model uncertainty for the seismic hazard curves: σ_{HU}

The two aleatoric uncertainties are connected with the interaction between the left and right side in figure 4.1, and the two epistemic uncertainties are connected to the shift from upper to the lower level. As explained earlier the division between the two types of uncertainty can be discussed.

The aleatoric uncertainty in strength and stiffness is small compared to the other uncertainties, and does not affect the results significantly, thus it is neglected. [Ellingwood & Kinali 2009]

4.3 Probabilistic seismic analyzes of the structures

The method explained above is used in the following to assess the annual probability of exceeding a limit state for the specific structures.

4.3.1 Capacity of the structure

If the relationship between S_a and ISDA was found using nonlinear time history analyzes with a range of different earthquakes, the value of $\sigma_{D|S_a}$ could be set to the logarithmic standard deviation connected to the deviation between the regression function and found performance points. But in this analysis this connection is found using a nonlinear pushover analysis and response spectra with different peak ground accelerations, thus the found deviation will not reflect the aleatoric uncertainty connected with the different behavior of a structure for earthquakes with different time history and spectra. In [Ellingwood & Kinali 2009] the values are in the range 0.19-0.26, and in this analysis it is set to 0.25.

The values of σ_c can be set to 0.25 for the IO and SD limit states and 0.15 for the CP limit state [Kinali 2007].

With these values the fragility curves can be found using equation 4.6 for the EBF and SCBF structure, in both intact and damaged states. There is used the same values of a and b as found in section 3.3.2, and the fragility curves can be seen in figure 4.3. The structural peak acceleration is used as abscissa, but the ground acceleration could be used as well.

4.3.2 Seismic demand

The seismic hazard curves corresponding to the locations of Seattle and Atlanta are displayed in figure 4.4 for the peak acceleration of a structural period of 1 s. The current structures both has periods larger than one, and the curves for the actual periods can be found using the response spectrum cf. section 2.1.2.

Especially for Atlanta it can be seen that the curve tends to be flat at large values of S_a , which makes the approximation in equation 4.9 good. For Seattle the curve is more convex, and the approximation will only be accurate for a limited range of S_a values. The important range is the range that contribute significantly to the total probability of exceeding a limit state given by equation 4.1. Figure 4.5 shows the annual probability of exceeding

4.3. PROBABILISTIC SEISMIC ANALYZES OF THE STRUCTURES77

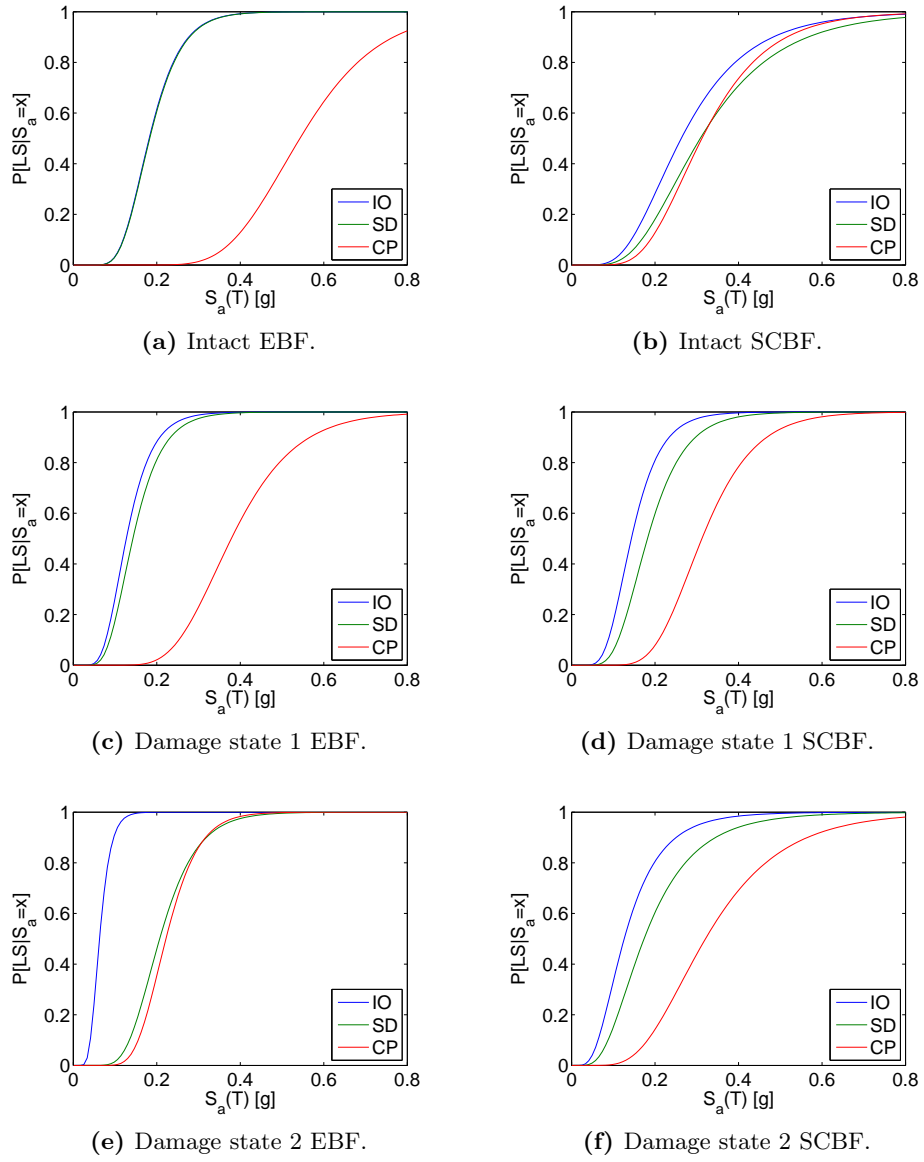


Figure 4.3: Fragility curves.

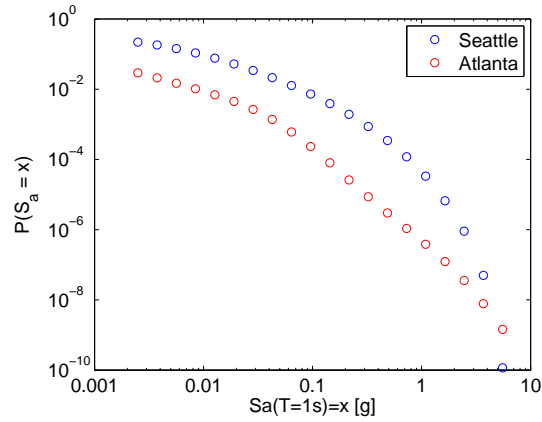


Figure 4.4: Seismic hazard curves for the locations for $T = 1$ s.

a limit state, calculated at the points from figure 4.4, modified to the actual period of the EBF structure.

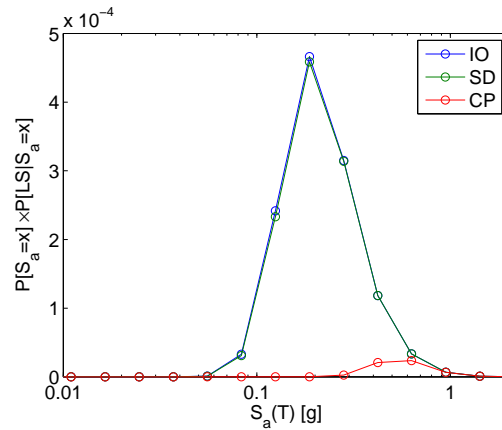


Figure 4.5: Contribution for different values of S_a to the annual probability of exceeding a limit state for EBF.

Figure 4.5 shows that the approximation has to be most accurate in the range $0.1 \text{ s} < S_a < 1 \text{ s}$. In figure 4.6 the hazard curves are shown for the periods of the structures, and the approximations are shown. The values of k_0 and k are shown in table 4.1.

	k	k_0
EBF	2.9046	$9.0357 \cdot 10^{-6}$
SCBF	2.5499	$8.6320 \cdot 10^{-8}$

Table 4.1: Seismic hazard factors for the periods of the structures.

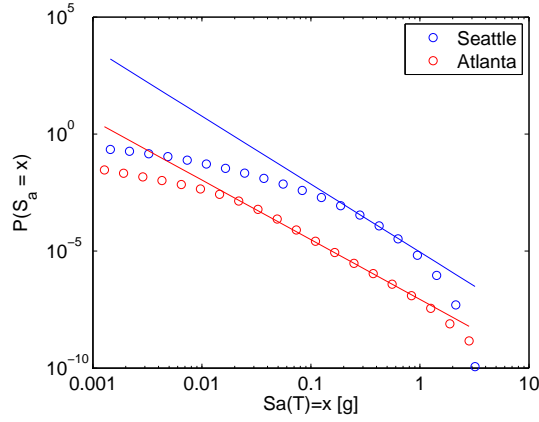


Figure 4.6: Seismic hazard curves for the locations for the periods of the intact structures and approximations with the form $P[S_a = x] = k_0 \cdot x^{-k}$.

4.3.3 Limit state probability

The logarithmic standard deviation of K_0 , σ_{HU} , is approximately 0.50 for the Central and Eastern U.S. (CEUS)[Ellingwood & Kinali 2009].

The value of σ_{RU} depends on the accuracy of the model of the structure. For the time history analyzes used in [Ellingwood & Kinali 2009] with refinements (e.g. panel zone modeling, connection fracture, brace buckling and $P - \Delta$ effects) the value was approximated to 0.20. The analyzes used in this project are static pushover analyzes, where eg the vertical load is not taken into account and plastic behavior occurs only in hinges, and the value will be larger, and is estimated to 0.30.

With those values the frequency distributions of K_0 and M_R for the EBF are as shown in figure 4.7.

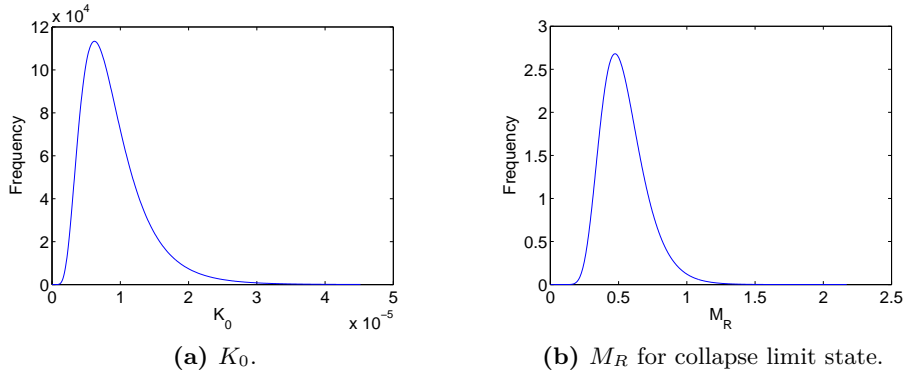


Figure 4.7: Frequency distributions.

With discrete distributions of K_0 and M_R the value of P_{LS} are found for each combination of the two using equation 4.10. The belonging frequencies are found as the product of the actual frequency for each cf. figure 4.7. The mean annual probability of exceeding a limit state, P_{LS} , can be found directly by numerical integration or Monte Carlo Simulation.

Alternatively a histogram can be made by defining a number of intervals for P_{LS} , and finding the frequency for each by numerical summation of the frequency of the occurrences in each interval and at last setting the norm to unity. Using an appropriate number of intervals and points in K_0 and M_R , a smooth curve is obtained for the frequency distribution of P_{LS} . Figure 4.8 shows such curves for the EBF for the IO and CP limits. The mean of the curves can be found, and gives the mean annual probability of exceeding a given limit state, P_{LS} .

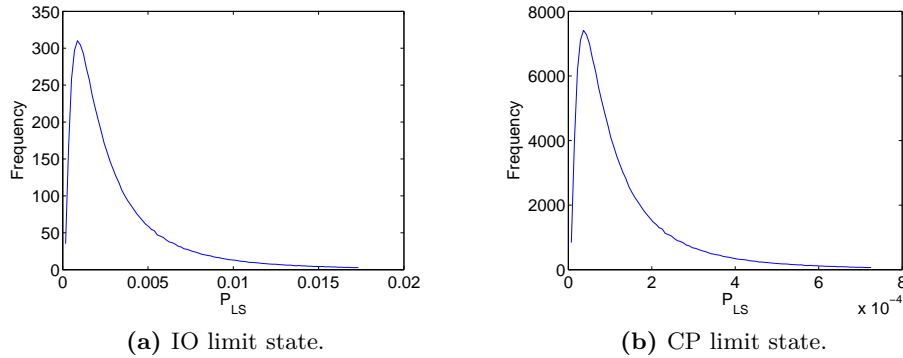


Figure 4.8: Frequency distributions for the annual probability of exceeding a limit state for EBF.

4.3.4 Sensitivity analysis

The logarithmic standard deviations σ_R , σ_{HU} , and σ_{RU} are set with uncertainty, and the number of points used in the ISDA- S_a relationship will have an influence on the result too. To assess the possible error connected with these uncertainties, a sensitivity analysis has been made. The mean annual probability of exceeding a limit state, P_{LS} , has been found for different combinations, where one of the values is changed and the rest is held constant. In figure 4.9 curves are shown, where the values of P_{LS} are divided with a reference value.

For the analysis with different numbers of points taken into account, the deviation is different for the different limit states and damage states, and it is shown for the IO and CP limit state for both the EBF and SCBF for the intact and damaged structures. The scaled value of P_{LS} for different values

4.3. PROBABILISTIC SEISMIC ANALYZES OF THE STRUCTURES81

of the logarithmic standard deviations are not dependent on the damage and limit state, thus it is shown for the EBF and SCBF structure.

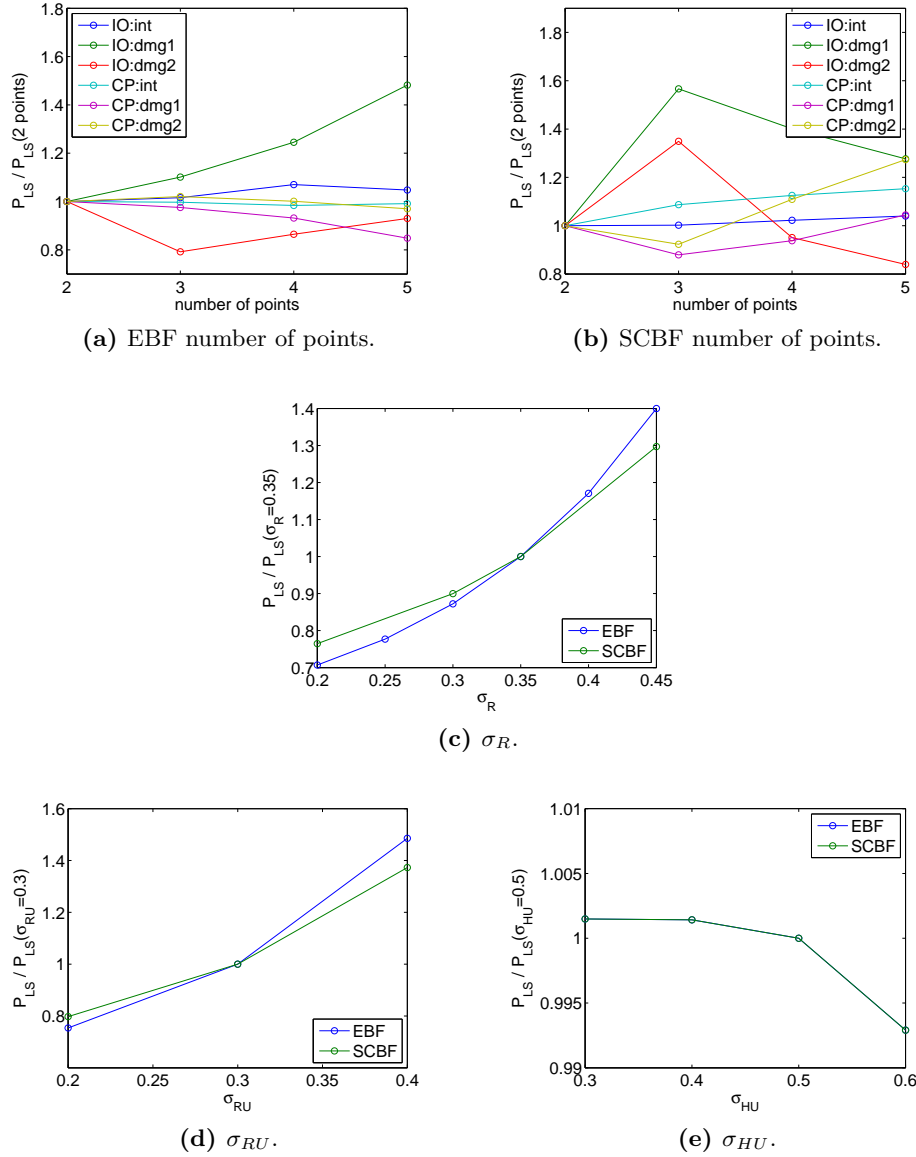


Figure 4.9: Sensitivity analyzes for P_{LS} scaled to one for the set value.

It can be seen that the value of P_{LS} is highly dependent on the the number of points taken into account in the ISDA- a_g relationship. Especially for the damaged structures in the IO limit state the deviation is more than 50%.

The change of P_{LS} in percent for different values of σ_R is not affected by the limit and damage state, because only the value of the shape factor, k ,

influences this cf. equation 4.11. The same counts for σ_{RU} , and for σ_{HU} the change in percent is independent of what structure it is, because P_{LS} is directly proportional to K_0 . Both the value of σ_R and σ_{RU} have large influence on the value of P_{LS} , but σ_{HU} has almost no influence because of the linear relationship.

4.4 Probabilistic assessment of robustness

In section 3.3 the robustness was evaluated using deterministic methods of analysis. With the failure probabilities found as described in section 4.3, the robustness can be evaluated on a probabilistic basis.

The probabilistic redundancy index, β_R , was proposed by [Frangopol & Curley 1987]:

$$\beta_R = \frac{\beta_{intact}}{\beta_{intact} - \beta_{damaged}} \quad (4.12)$$

where β_{intact} is the reliability index of the intact structure and $\beta_{damaged}$ is the reliability index of the damaged structure. If the reliability index is unchanged for the damaged structure it is infinite, and if there is no capacity of the damaged structure, it is equal to one.

The damage tolerance factor proposed by [Lind 1995] is given by:

$$T_d = \frac{P(R_0, S)}{P(R_d, S)} \quad (4.13)$$

which is also a measure of the robustness of the structure. This measure is one if the failure probability is equal for the damaged and undamaged structure, and zero if the failure probability of the damaged structure is infinite. Hereby this measure can be compared with the deterministic *RIF* value.

4.4.1 Eccentrically braced frame

The mean annual probabilities of exceeding a limit state, and the reliability indices corresponding to the different limit and damage states are shown in table 4.2 and 4.3. On basis of these values the redundancy index, β_R , and the damage tolerance factor, T_d , have been calculated, and are shown in table 4.4.

Again the values from the SD limit does not tell anything, because of the difference in stiffness and the defined limit point. The two measures are not

	IO	SD	CP
Intact	0.356	0.349	0.0126
Damage1	0.483	0.345	0.0172
Damage2	5.401	0.170	0.1171

Table 4.2: Annual probability of exceeding a limit state, P_{LS} , for EBF in 10^{-2} .

	IO	SD	CP
Intact	2.691	2.698	3.660
Damage1	2.588	2.702	3.580
Damage2	1.607	2.930	3.043

Table 4.3: Reliability index, β , for each limit state for EBF.

β_R	IO	SD	CP
Damage1	26.056	-649.835	45.488
Damage2	2.483	-11.646	5.930
T_d	IO	SD	CP
Damage1	0.737	1.013	0.733
Damage2	0.066	2.056	0.108

Table 4.4: Redundancy indices and damage tolerance factors for each limit state for EBF.

compatible, as the values for damage state 1 in the IO and CP limits are very close for T_d , while the β_R value is significantly higher for the CP limit than the IO limit.

4.4.2 Concentrically braced frame

As for the EBF the mean annual probabilities of exceeding a limit state, and the reliability indices corresponding to the different limit and damage states are shown in table 4.5 and 4.6. One basis of these values the redundancy index, β_R , and the damage tolerance factor, T_d , has been calculated, and are shown in table 4.7.

	IO	SD	CP
Intact	0.587	0.390	0.332
Damage1	1.174	0.639	0.141
Damage2	1.640	0.725	0.133

Table 4.5: Annual probability of exceeding a limit state for SCBF in 10^{-5} .

For the IO limit the T_d values are in a range, where the structure does not seem to be rather robust, but the β_R values are high, corresponding to a

	IO	SD	CP
Intact	4.382	4.470	4.505
Damage1	4.229	4.364	4.683
Damage2	4.153	4.336	4.695

Table 4.6: Reliability index for each limit state for SCBF.

β_R	IO	SD	CP
Damage1	28.564	41.944	-25.285
Damage2	19.107	33.294	-23.683
T_d	IO	SD	CP
Damage1	0.500	0.611	2.350
Damage2	0.358	0.538	2.492

Table 4.7: Redundancy indices and damage tolerance factors for each limit state for SCBF.

robust structure. This large value reflects that the probabilities of exceeding the limit state in general are very small, giving a large reliability index. For the SD limit the β_R values are negative and the T_d values are higher than one. This is a result of the better seismic performance of the damaged structures compared to the intact structure caused by the ductile behavior.

4.5 Comparison

The two probabilistic measures of the robustness are hard to compare directly, as the values are in different ranges. Moreover they does not express the same thing. The T_d measure only takes the ratio in annual probability of collapse into account. The value of β_R is the reliability of the intact structure, divided by the difference in reliability between the intact and damaged structure. If the difference between the values are small, the value of β_R is large, giving a robust structure. But if the reliability of the intact structure is large, as for the SCBF structure, it also makes β_R large. This also means that the reliability based robustness index in the CP limit state is in general larger than in the IO limit state, as the annual probability of collapse is in general smaller than the annual probability of yielding, as it occurs at smaller earthquakes.

The sensitivity analysis in section 4.3.4 shows that the T_d measure will not be influenced by the choice of σ_R , σ_{HU} , and σ_{RU} , as the values will affect P_{LS} for the intact and damaged structures with the same fraction. In fact the only values influencing T_d is a , b and k , as it can be seen from equation 4.11 and 4.5. This will not be the case for β_R that will be affected by the

other values as well.

Both robustness indices were calculated based on the annual probability of exceeding a limit state, but it might be interesting to examine the probability of exceeding a limit state during the lifetime of the structures, as this will influence the indices. Figure 4.10 shows the two indices, divided by the value calculated on basis of the annual probability, as function of the number of years taken into account.

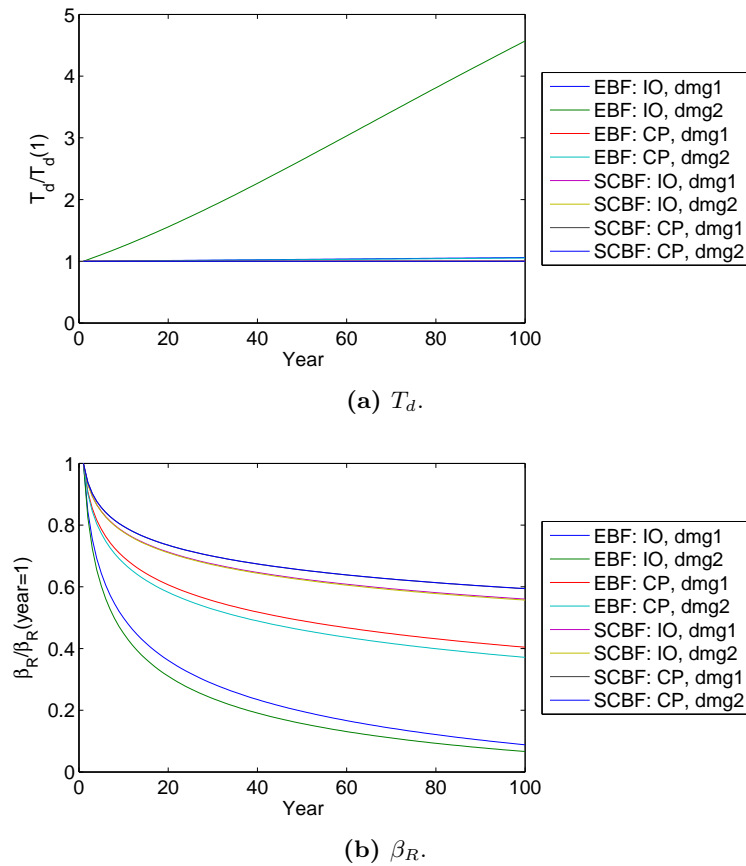


Figure 4.10: Sensitivity of T_d and β_R dependent of the number of years.

For the EBF in the IO limit for damage state 2, where the annual probability of exceeding the limit state is large cf. table 4.2, the T_d value is increased to approximately 450% calculated over 100 years compared to one year. But for all other cases, with smaller annual probability of exceeding a limit state, the variation over 100 years is maximum 6%.

The β_R value, on the contrary, drops to between 10% and 60% of the value for one year, again most for the cases with high annual probability of collapse.

4.6 Summary

In the probabilistic assessment of the robustness it was evaluated based on the annual probability of exceeding a limit state, where significant uncertainties were taken into account for both the capacity and demand.

The limit states were initially defined in terms of ISDA, found using a pushover analysis. Using the found relationship between the peak acceleration of the earthquakes and the resulting ISDA, the limits were expressed in terms of peak ground acceleration instead. The uncertainties connected to both steps were taken into account, and based on these values the fragility curves were found. They showed the the probability of exceeding a limit states for a given ground acceleration.

The next step was to take the relationship between the peak acceleration and the annual probability of the occurrence into account, to get the annual probability of exceeding a limit state. The epistemic uncertainties connected to the structural model and model of earthquake were taken into account, and the distribution function of the annual probability of exceeding a limit state was found.

The mean annual probability of exceeding a limit state was found for the three limit states for intact and damaged structures, and based on these values the damage tolerance factor, T_d , was found for each case. For the EBF damage state 1 was found to have a significantly larger T_d value than damage state 2. For the SCBF the values for the two damage states were higher than two, meaning that the annual probability of collapse is twice as high for an intact structure than for a damaged.

The reliability index was calculated based on the annual probabilities of collapse, and the redundancy indices, β_R , were calculated based on this. For the EBF the index was significantly larger for damage state 1 than for damage state 2 in the IO and CP limit, and for the SCBF both the values in the CP were negative as a result of the larger capacity for the damaged structures.

A sensitivity analysis showed that the T_d value was only influenced by the value of the shape factor k and the constants a and b giving the relationship between the peak acceleration and ISDA, as all other values gave the same change in percent for the intact and damaged structures. Further it was only sensitive to the number of years taken into account in one case, where the annual probability of exceeding the IO limit was very high.

On the contrary the β_R value are influenced by the choice of uncertainties, and it is influenced by the number of years taken into account as well.

Chapter 5

Risk analysis

In chapter 3 and 4 the robustness of the structures, cf. section 2.1, were assessed using a deterministic and a probabilistic approach. These measures tell something about the difference in behavior between an intact and damaged structure. This can be used in decision making if different designs are considered. These measures, however, do not take into account that the cost of the more robust structure will normally be larger than of a less robust structure, and the relative expected cost (consequence) of possible failure will be smaller for the more robust structure. The best choice of design will be the one with smallest expected total cost during the lifetime of the structure.

The total cost should be found for the total considered system. As sketched in figure 5.1 the total system exceeds the structure itself, as a collapse might influence other buildings, infrastructure, or the environment, if important tasks are located in or close to the building.

In the total cost everything should be included: building expenses, repair costs if the structure is damaged, and loss of human lives and societal consequences if the structure collapses. The total cost, C_T , can be found as:

$$C_T = C_I + R \quad (5.1)$$

where C_I is the building costs and R is the risk associated with consequences of failure.

The risk can be found as:

$$R = R_{dir} + R_{indir} = \sum_i \sum_j C_{dir,ij} P(D_j|E_i) P(E_i) + \sum_i \sum_j \sum_k C_{indir,ijk} P(S_k|D_j) P(D_j|E_i) P(E_i) \quad (5.2)$$

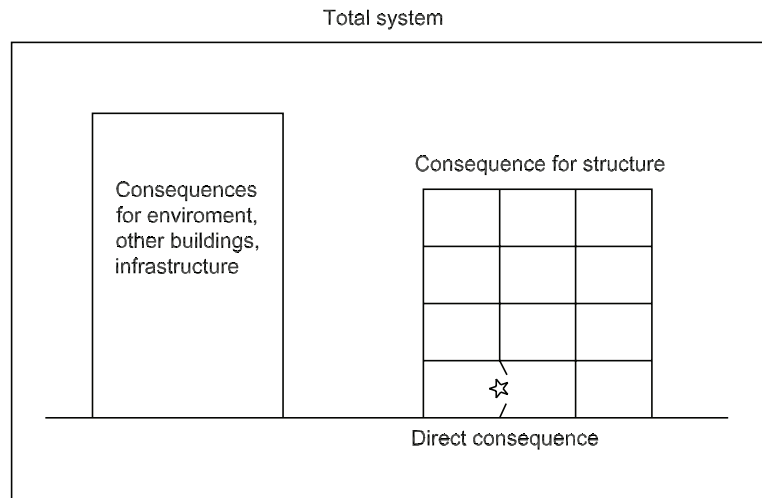


Figure 5.1: Definition of total system.

where $C_{indir,ikj}$ is the consequence (cost) of exceeding a limit state S_k given local damage D_j due to exposure E_i , and $C_{dir,ij}$ is the consequence (cost) of local damage. An event tree is shown in figure 5.2. As shown in figure 5.2 more limit states, given as s_k , can be taken into account in the analysis, eg the IO, SD, and CP limits, where the probability of occurrence is larger for the IO limit, but the consequences are larger for the CP limit.

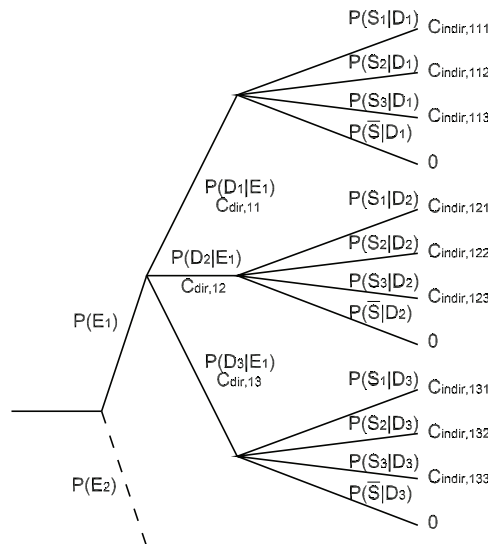


Figure 5.2: Event tree.

The exposures could be a design error, bad execution, impact or others, and for each exposure there is a probability of occurrence, $P(E_i)$. For each exposure there is a probability that the structure will be damaged, $P(D_j|E_i)$.

This local damage might have a consequence $C_{dir,ij}$, but there might also be a probability $P(S_k|D_j)$ that the local damage leads to the exceeding of a limit state on system level that will have the consequences $C_{indir,ijk}$. Examples of exposures and probabilities of damage given exposures are shown in table 5.1, where D_1 is the intact state where there is no local damage, and D_2 and D_3 are different damage states.

E	$P(E)$	$P(D_1 E)$	$P(D_2 E)$	$P(D_3 E)$
Large design error	0.001	0.4	0.35	0.25
Small design error	0.05	0.9	0.05	0.05
Large impact	0.005	0.2	0.3	0.5
Small impact	0.04	0.4	0.4	0.2

Table 5.1: Examples of exposures and probabilities of damage given exposures.

5.1 Analyzes

If different structural configurations are considered, the best choice will be the one where the total costs, C_T , is smaller. In the previous analyzes in this project, it has been assumed that a column might be damaged. If all columns were designed as key elements, the design would be more expensive, but the probability that one column is damaged is smaller, and the annual probability of collapse caused by an earthquake, will be smaller.

For a structure that is not designed for earthquake loads, an earthquake could be regarded as an exposure in the assessment of robustness. In this case however the earthquake is regarded as the most crucial load designed for, and it is taken into account with the factor $P(S_k|D_j)$. That corresponds to the annual probability of exceeding a limit state due to earthquakes that was found for both intact and damaged structures in chapter 4.

To compare the two designs similar analyzes should be performed for both structural models. Here it is assumed that the change in design only affects the probability of damage D_j given the exposure E_i , given as $P(D_j|E_i)$. If the intact state is regarded as a damage state as well, the sum $\sum_j P(D_j|E_i)$ is equal to one. The assumed values of the probability of each damage state given an exposure are shown in table 5.2 for two different designs. Design 2 is a more expensive design, where the probability of damage is smaller, and could be a case where the columns were designed as key elements.

With these values and the annual probabilities of exceeding a limit state, found in chapter 4, the expected total cost of the two different designs can be found, if the the probability of the exposure, the building costs, the

$P(D_j E)$	Design 1	Design 2
D_1 Intact	0.7	0.85
D_2 Damage 1	0.2	0.1
D_3 Damage 2	0.1	0.05

Table 5.2: Assumed probability of each damage state for two different designs.

consequence of damage, and the consequence of exceeding each of the limit states are known. As an example only the direct consequence of damage, C_{dir} , and collapse, C_{CP} , is considered. For the intact state, D_1 , C_{dir} is zero. In table 5.3 the probability of collapse (indirect consequence) given the damage and exposure is found using $P(CP|E) = P(CP|D_j)P(D_j|E)$ with the values in table 5.2 and the values found in chapter 4 for the EBF.

	$P(CP D_j)$	$P(CP E)$	
	Design 1 & 2 10^{-3}	Design 1 10^{-3}	Design 2 10^{-3}
D_1 Intact	0.126	0.0882	0.1071
D_2 Damage 1	0.172	0.0344	0.0172
D_3 Damage 2	1.171	0.1171	0.0585
$\sum P(CP E)$		0.2397	0.1829

Table 5.3: Probability of collapse given the damage, and probability of collapse given the exposure for the EBF.

For simplicity the probability of the exposure, $P(E)$, is set to one, and the total cost, C_T , is found as function of the consequence of collapse, C_{CP} . When only the difference in cost of the two designs, ΔC_I , is taken into account, and not the total value of C_I , the total cost can be found as:

$$C_T = \sum_{j=1}^3 (C_{dir} \cdot P(D_j|E) + C_{CP} \cdot P(CP|E)) + \Delta C_I \quad (5.3)$$

The values are shown in figure 5.3 for different values of the ratio between the consequence of collapse and the direct consequence, C_{CP}/C_{dir} , for two different designs, and the coordinates of the intersection points can be found in table 5.4.

This method can be used to find the best design out of more possibilities. For the shown example with $C_{CP}/C_{dir} = 10,000$ design 1 should be chosen if the ratio between the cost of collapse and the initial additional cost is less than approx 14,000, and design 2 should be chosen, if the fraction is more than 14,000. The slope of the lines are changed if other values of $P(E)$ and $P(D_j|E)$ are chosen.

C_{CP}/C_{dir}	$C_{CP}/\Delta C_I$	$C_T/\Delta C_I$
100,000	17,140	4.16
10,000	13,920	3.75
2,000	7,600	2.96
1,000	4,840	2.61

Table 5.4: Intersection points.

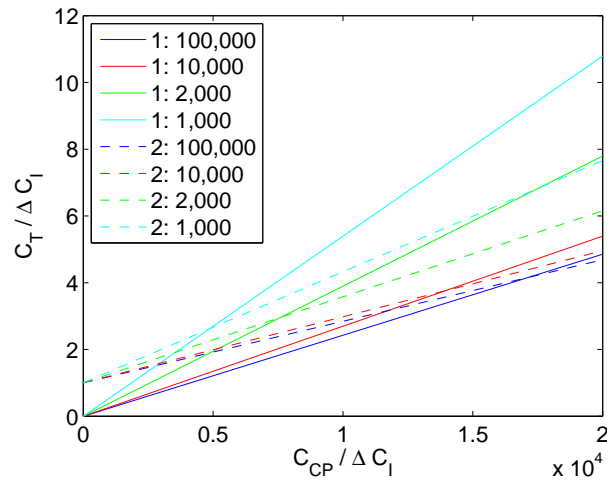


Figure 5.3: Expected total cost as function of the consequence of collapse for the EBF. Design 1 and 2 are marked with 1 and 2 respectively, and 100,000, 10,000, 2,000, and 1,000 are the values of C_{CP}/C_{dir} .

5.1.1 Robustness index

As an alternative the risk based robustness index I_{Rob} can be found:

$$I_{Rob} = \frac{R_{dir}}{R_{dir} + R_{indir}} \quad (5.4)$$

where R_{dir} is the direct risk associated with local damage and R_{indir} is the indirect risk associated with escalated damage [Baker et al. 2008]. The direct risk could be connected to the damage of a column, where the consequences are rather small, and the indirect risk could be connected to total collapse, where the consequences are larger. Thus the probability of collapse given the damage has to be decreased to make the robustness index larger (larger robustness).

For the two designs the the risk based robustness index is found as function of the ratio between the consequences of collapse and the direct consequences C_{CP}/C_{dir} , and is shown in figure 5.4.

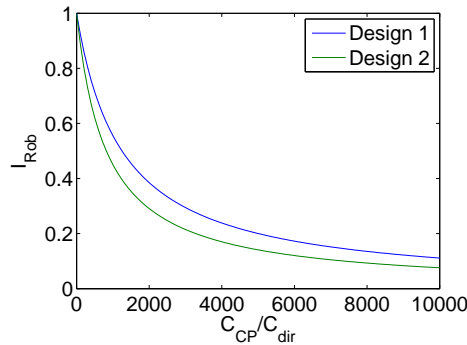


Figure 5.4: Robustness index.

In this case the risk based robustness index is larger for design 1, even though design 2 has a lower risk. But because both the direct and indirect risk is larger for design 1, because only the value of $P(D_j|E)$ is changed for design 2, this is possible. If the value of collapse given the damage, $P(S_k|D_j)$, was changed instead, the result would be different.

This example shows that the risk based robustness index is not always compatible with a full risk analysis, and in the given example the risk based robustness index is not a meaningful measure for the evaluation of the robustness of two different designs.

5.2 Summary

The risk analysis is the most complete way to assess the robustness, and to choose the best design out of more possibilities. The flaw of the method is closely connected to the advantage, as much information is needed to make the complete analysis. The results found in this chapter cannot be compared with the other methods because of limited knowledge of the values used in the analysis.

The analysis shows how the risk analysis can be used to assess the robustness, and to rank more designs due to the expected total cost of each. In this analysis the damage states are linked together in a total analysis, instead of being looked upon one by one.

The value of the risk based robustness index is highly dependent on the ratio between the consequence of collapse and the direct consequence of damage cf. figure 5.4. But as this analysis has shown, it can only be used meaningfully if two different designs have a different value of the probability of collapse given the damage $P(S_k|D_j)$. If a structure not designed for earthquake was compared to a structure designed for earthquake there would be a big difference in the value of $P(S_k|D_j)$, and the robustness index of the structure designed for earthquake loads would be larger.

For this analysis to make sense the damage has to be somehow caused by the earthquake or to be a hidden error eg in the design. If the damage was caused by an impact, independent of an earthquake, it would be repaired within a short time, and the probability than an earthquake would occur in that limited time is very small. For a hidden design error the local damage will not have a consequence until an earthquake happens, because it would have been noticed and repaired in that case. This is not taken into account in the given example, as the probability of an earthquake should have influence on the hidden error becoming a missing column, with the related consequences.

Chapter 6

Summary

In this project the robustness of two steel structures originally designed for earthquake loads in Seattle and Atlanta respectively has been assessed. Only the robustness in connection with horizontal loads was investigated in this analysis, and both deterministic, probabilistic and risk based analyzes were used.

The seismic resistance is for both structures ensured by braces in the facades, for the structure in Seattle by eccentrically braced frames (EBF) and in Atlanta by special concentrically braced frames (SCBF). For both structures a plane finite element model of one facade has been made, and nonlinear hinges have been assigned to reflect the post yield behavior of the elements. Nonlinear static pushover analyzes were used to find the global nonlinear behavior of the models, and different configurations were tested to investigate the sensitivity of the model. The SCBF was found to have a very limited ductile behavior, because equilibrium could not be found after the first failure of braces in compression. This might be caused by limitations in the program, which is made probable by the fact that onesome of the other tested models were able to find equilibrium. The performance based method in [ATC-40 1996] was used to find the performance of the structures using the pushover analyzes and the response spectra from the locations.

The robustness of the structures was examined by investigating the difference in capacity between an intact and damaged structure, where a column in the first floor was removed. Three limit states were investigated corresponding to first yield (IO), structural damage (SD) and collapse (CP). The drift limits were set based on the capacity curves, and the used definition of the SD limit was found not to be used meaningful in this kind of analysis, where damaged structures were investigated. The limit states were linked to values of the ground acceleration using a regression line through the found

points. The used approximation did not fit very well to the results from the pushover analysis, thus only two points nearest to the collapse state was used, to give the best result.

In general the damaged structures could resist a smaller static load than the intact structure, but when the resistance against seismic loads was examined it was found that the global ductility was very important for the capacity measured in terms of ground acceleration. Thus the SCBF was able to resist a larger ground acceleration in the damaged cases than the intact because of a more ductile behavior. For the EBF the intact structure performed best, but there was a big difference between the two investigated damage states. As a measure of the robustness the residual influence factor (*RIF*) used in the offshore industry was used, and it was found for the capacity measured in terms of both the load in force and in peak ground acceleration.

To investigate the influence of the properties of the material analyzes were performed, where the ductility and hardening of the plastic hinges were changed. Both a larger ductility and more hardening was found to give larger capacities, but smaller *RIF* values because the ductility and hardening helped more for an intact structure than a damaged. However for the damaged SCBF increased hardening seemed to hinder the global ductile behavior, and the capacity towards seismic loads became smaller.

Probabilistic seismic analyzes were performed, where both aleatoric and epistemic uncertainties were taken into account, and the annual probability of exceeding a limit state was found. The seismic demand was modeled by a function that only fitted the hazards curves provided by USGS in a limited range, and the fit was chosen in the point where the contribution to the probability of exceeding a limit state was largest.

Two different probabilistic measures of the robustness was used, one based on the probabilities of failure (T_d) and one based on the reliability indices (I_R). The first gave results in the same range as the *RIF* values, but were in general farther away from one. This is caused by the shape of the hazard curves. If the hazards curves had been linear the results would be equal to the *RIF* values. The size of the logarithmic standard deviations used for modeling of the uncertainties did not have any influence on this measure because a change would work for both the intact and damaged structures. Only the relationship between a given ground acceleration and the resulting drift had influence on the result.

The measure based on reliability indices (I_R) was in another range and was therefore harder to compare to the other. However it could be seen that they were not compatible as a general higher reliability gave higher redundancy index, where the general reliability level did not affect the T_d measure.

Further the uncertainties and the considered range of years affected the I_R measure.

Finally a risk based approach was used to assess the robustness, where the consequences were taken into account. The probability of the occurrence of damage and the exposure causing the damage were taken into account, thus the result was more accurate than the deterministic and probabilistic values, where it did not matter where the damage came from. In the risk based robustness index the ratio between the direct and total risk was found. The value was highly dependent on the ratio between the consequence of local damage and the consequence of collapse, and was found not always to be compatible with the result from the risk analysis.

Both the risk analysis and the different robustness indices can be used to find the best out of more designs. The risk analysis is the most complete analysis, but also the one than needs most information.

6.1 Conclusion

The aim of this project was to investigate whether structures designed for earthquake loads were robust too.

The common denominator in design for earthquake and robustness is the importance of ductile behavior. For earthquake design it is necessary to dissipate energy to decrease the force acting on the structure, and for robustness ductility is important to make use of alternate load paths.

The analyzes have shown that the damaged structures will often have a behavior that is different from that of the original structure, because the yielding mechanisms does not work the way they are designed to when members are missing. In one damage state for the EBF the behavior was more brittle, giving a low robustness index, and in the case of the SCBF the behavior was found to be more ductile, giving a larger capacity. The structural configuration is very important for the capacity of the damaged structure, because the structures are less sensitive if the damage of one column only affects one energy dissipating member, eg a shear link. This means that structures designed for seismic actions will not necessarily be robust towards seismic loads, as this depends on the structural configuration.

When the robustness is investigated towards earthquake loads at least a deterministic approach, where the capacity is measured in terms of ground acceleration, should be used. The probabilistic damage tolerance factor takes the shape of the hazard curve into account, and thereby gives a value closer related to the annual expected damage. The reliability based index

takes the total reliability into account, and the structure is not 'punished' for being safer to begin with.

A risk analysis gives the most complete assessment of the robustness, and the risk based robustness index should not be used uncritically as that may lead to wrong conclusions.

An increased capacity of the intact structure will make the structure more robust, and only the reliability based robustness index and the risk analysis takes this into account. Both risk based approaches takes the consequences into account, and only the risk analysis takes the effect of a decrease of the probability of the damage into account correct.

Increased ductility of the material was found to give a smaller deterministic robustness, but if the reliability based index or the risk analysis was used, it would most likely be seen to increase the robustness.

In general the ductility and redundancy will provide robustness against unforeseen vertical and horizontal loads, and human errors located in one element or connection. But for human errors distributed throughout the structure redundancy will not help.

Bibliography

- ASCE 7-05* [2005], American Society of Civil Engineers, New York.
Minimum design loads for buildings and other structures.
- ATC-40* [1996], Vol. 1, Applied Technology Council. Seismic Evaluation and Retrofit of Concrete Buildings.
- Baker, J. W., Schubert, M. & Faber, M. H. [2008], ‘On the assessment of robustness’, *Structural Safety* **30**(3), 253–267.
- Bazeos, N. [2009], ‘Comparison of three seismic design methods for plane steel frames’, *Soil Dynamics and Earthquake Engineering* **29**(3), 553–562.
- Bertero, R. D. & Bertero, V. V. [1999], ‘Redundancy in earthquake-resistant design’, *Journal of Structural Engineering* **125**(1), 81–88.
- Bommer, J. J. & Pinho, R. [2006], ‘Adapting earthquake actions in eurocode 8 for performance-based seismic design’, *Earthquake Engineering and Structural Dynamics* **35**(1), 39–55.
- Canasius, T. D. G., Sørensen, J. D. & Baker, J. W. [2007], ‘Robustness of structural systems’, *A new focus for the Joint Committee on Structural Safety (JCSS)* .
- Cornell, C. A., Jalayer, F., Hamburger, R. O. & Foutch, D. A. [2002], ‘Probabilistic basis for 2000 sac federal emergency management agency steel moment frame guidelines’, *Journal of Structural Engineering* **128**(4), 526–533.
- Dietsch, P. [2009], ‘The bad reichenhall ice-arena collapse’, *COST E55* .
- Ellingwood, B. R. [2001], ‘Earthquake risk assessment of building structures’, *Reliability Engineering and System Safety* **74**(3), 251–262.

- Ellingwood, B. R., Celik, O. C. & Kinali, K. [2007], 'Fragility assessment of building structural systems in mid-america', *Earthquake Engineering and Structural Dynamics* **36**(13), 1935–1952.
- Ellingwood, B. R. & Kinali, K. [2009], 'Quantifying and communicating uncertainty in seismic risk assessment', *Structural Safety* **31**(2), 179–187.
- Ellingwood, B. R., Smilowitz, R. & Dusenberry, D. O. [2007], *Best Practices for Reducing the Potential for Progressive Collapse in Buildings*, National Institute of Standards and Technology.
- EN 1990:2002 [2002], European Committee for Standardization. Eurocode - Basis of structural design.
- EN 1990 DK NA:2007 [2007], Erhvervs- og Byggestyrelsen. Nationalt Anneks til Eurocode 0: Projekteringsgrundlag for bærende konstruktioner.
- EN 1991-1-7:2006 [2006], European Committee for Standardization. Eurocode 1 - Actions on structures - Part 1-7: General actions - Accidental actions.
- EN 1998-1:2004 [2004], European Committee for Standardization. Eurocode 8 - Design of structures for earthquake resistance.
- Fajfar, P. [2000], 'A nonlinear analysis method for performance-based seismic design', *Earthquake Spectra* **16**(3), 573–592.
- FEMA 273 [1997], Federal Emergency Management Agency. NEHRP Guidelines for the Seismic Rehabilitation of Buildings.
- Frangopol, D. M. & Curley, J. P. [1987], 'Effects of damage and redundancy on structural reliability.', *Journal of structural engineering New York, N.Y.* **113**(7), 1533–1549.
- Khandelwal, K., El-Tawil, S. & Sadek, F. [2009], 'Progressive collapse analysis of seismically designed steel braced frames', *Journal of Constructional Steel Research* **65**(3), 699–708.
- Kinali, K. [2007], Seismic fragility assessment of steel frames in the central and eastern United States, PhD thesis, Department of Civil and Environmental Engineering, Atlanta (GA): Georgia Institute of Technology.
- Lind, N. C. [1995], 'A measure of vulnerability and damage tolerance', *Reliability Engineering and System Safety* **48**(1), 1–6.
- Munch-Andersen, J. [2009], 'Robustness versus human errors', *COST E55* .

- Nair, R. S. [2006], 'Preventing disproportionate collapse', *Journal of Performance of Constructed Facilities* **20**(4), 309–314.
- Newmark, N. M. & Hall, W. J. [1982], 'Earthquake spectra and design', *Earthquake Spectra and Design* .
- Nielsen, S. R. K. [2004], *Vibration Theory*, 3rd edn, Aalborg tekniske Universitetsforlag.
- Poursha, M., Khoshnoudian, F. & Moghadam, A. S. [2009], 'A consecutive modal pushover procedure for estimating the seismic demands of tall buildings', *Engineering Structures* **31**(2), 591–599.
- Robobat [2008], *Robot Millennium 20.1*, Autodesk Inc.
- Sørensen, J. D. & Christensen, H. H. [2006], 'Danish requirements for robustness of structures: Background and implementation', *Structural Engineering International: Journal of the International Association for Bridge and Structural Engineering (IABSE)* **16**(2), 172–177.
- Starossek, U. & Wolff, M. [2005], 'Design of collapse resistant structures', *JCSS and IABSE Workshop on Robustness of Structures* .
- Straub, D. & Faber, M. H. [2005], 'Risk based acceptance criteria for joints subject to fatigue deterioration', *Journal of Offshore Mechanics and Arctic Engineering* **127**(2), 150–157.
- USGS [2008], U.s. geological survey national seismic hazard maps.
http://earthquake.usgs.gov/research/hazmaps/products_data/2008/.
- Vrouwenvelder, T. & Sørensen, J. D. [2009], 'Robustness of structures', *EU COST action TU0601* .
- Wen, Y. K. & Song, S.-H. [2003], 'Structural reliability/redundancy under earthquakes', *Journal of Structural Engineering* **129**(1), 56–67.

Appendix

Appendix A

Time history analysis in Robot

The FEM program Robot by Robobat [Robobat 2008] has been chosen for this project, due to its applicability for time history analyzes and nonlinear analyzes. Further Robot is able to make time history analyzes, where the supports are subjected to an acceleration time history, or alternate a displacement or velocity time history. However it is not clear from the manual [Robobat 2008], whether it is possible to combine these options. The question was asked to Robot support that told that the use of elasto plastic elements was not recommended in a time history analysis, because of problems with convergence and very long calculation time. Instead they suggested the use of nonlinear hinges. Two test setups has been made to investigate, whether Robot is able to make the required analyzes which reliable results.

A.1 Time history of linear SDOF system

The first test setup was a simple SDOF system, with a vertical weightless cantilever beam with a point mass at the end, as shown in figure A.1. The natural vibration period is found to be 1.07 s.

The system is subjected to three different load cases with a horizontal forced displacement, forced velocity and forced acceleration time history of the support. The displacement time history was defined as:

$$d(t) = 0.2 \text{ m} \sin\left(\frac{2\pi}{0.8 \text{ s}}t\right) \quad (\text{A.1})$$

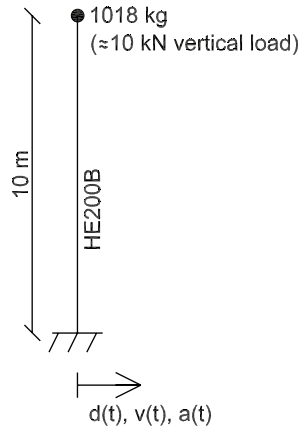


Figure A.1: Test setup for the linear SDOF system.

The velocity and acceleration time history was found by differentiation of equation A.1, thus the motions of the cases were equal, and the results should be that too. The damping was set to 5 %.

For each of the load cases the time history of the horizontal force, and the displacement, velocity, and acceleration of both nodes were found. The horizontal base shear force, shown in figure A.2, was almost equal in the three cases, but the mean from the acceleration time history was moved a bit away from the center. The maximum value of the force can be found analytical to be 15.7 kN [Nielsen 2004], which is close to the value found by Robot.

The displacement, velocity and acceleration of the support should in all cases be equal to the predefined values. However this is found only to be the case for the value that was set. Eg the velocity time history was correct in the case where the velocity was forced, but the others were not. For the node with the mass the results were correct for both the forced displacement and velocity, but in the case of forced acceleration, the mean of the displacement was an inclined line, thus the structure moved away with 1 m/second, as shown in figure A.3, which was clearly not intended.

The results questionize whether the time analysis with forced movement of the supports gives reliable results. However, the case with forced displacement and velocity gives good results, as long as the support nodes are not looked upon.

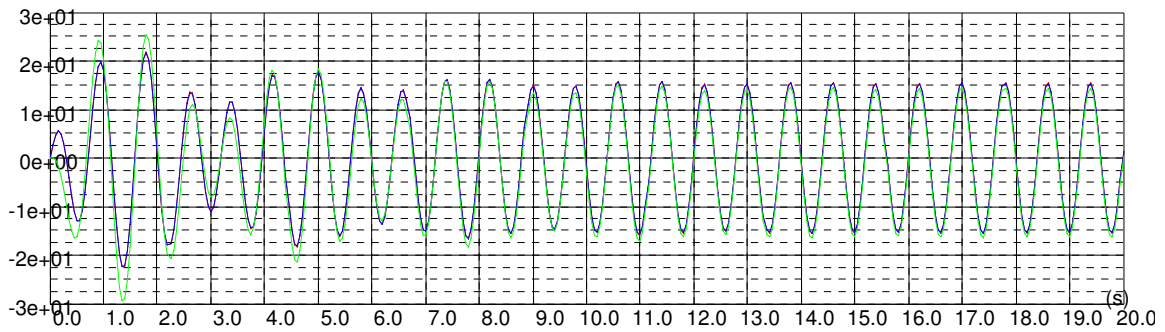


Figure A.2: Time history of the horizontal reaction [kN] of the linear SDOF system. Forced displacement (red), velocity (blue), acceleration (green). The red line is behind the blue line.

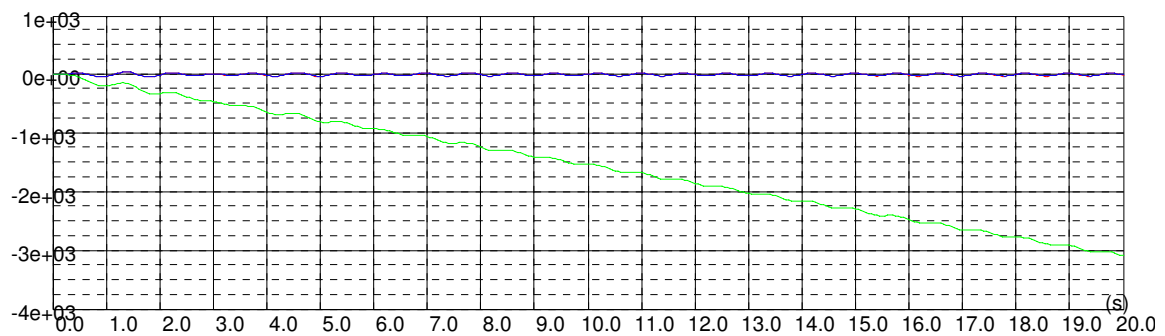


Figure A.3: Time history of the displacement [cm] of the linear SDOF system for forced displacement, velocity and acceleration. Forced displacement (red), velocity (blue), acceleration (green).

A.2 Time history of nonlinear SDOF system

To test whether the nonlinear solver gives reliable results for a time history analysis with forced movements of the support, the linear problem is solved using the implemented nonlinear solvers. It is possible to choose between *Newmark (acceleration)* and *Hilbert-Huges-Taylor*. Both solvers were used for both forced displacement, velocity and acceleration, but in all cases they either gave the result zero, did not converge, or in case of forced acceleration, had the same problem as the linear solver.

A.3 Conclusion on tests

Based on the investigations it can be concluded that the nonlinear time history analyzes with moving supports in Robot are not sufficient reliable to be used for the analyzes in this project. Alternatively an other program could be used, but due to limited time and resources it is chosen to use a simpler analysis type, the static pushover analysis.

Appendix B

Nonlinear static performance based analysis

This appendix describes the nonlinear performance based analysis procedure used in [ATC-40 1996]. The method is used to find the performance of a structure for a specific elastic response spectrum, when a static pushover analysis has been performed, and the capacity curve is found cf. section 1.1.1. There exist other methods for this task, eg the method proposed by [Fajfar 2000] and the method used in [EN 1998-1:2004 2004]. The method from [ATC-40 1996] is chosen because it is build into the finite element software Robot, and because the method provides a clear sight into how the hysteretic energy dissipation is taken into account, even though only a static analysis is performed.

B.1 Capacity curve

To get the capacity curve, is it necessary to complete a static pushover analysis. First a modal analysis is performed to find the mode shapes of the structure. Based on the mass distribution of the structure and the mode shape with largest mass participation, a set of lateral forces is applied to the structure. The force is increased in small steps until collapse is reached. Then a capacity curve with the base shear force as function of the horizontal roof displacement can be plotted. The procedure is shown in figure B.1.

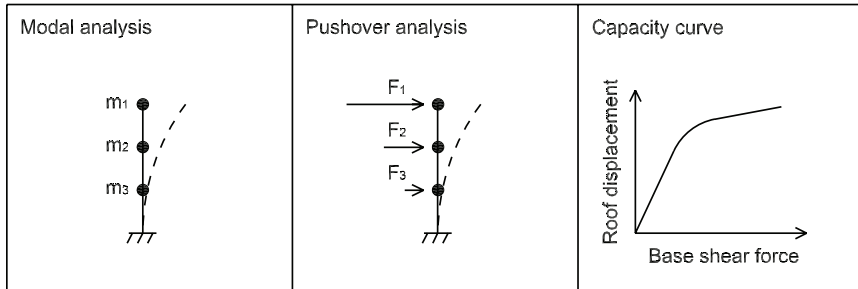


Figure B.1: Use of pushover analysis to make the capacity curve.

B.2 Performance point

The next task is to find the roof displacement and base shear force of the structure during the design earthquake that is the point where the capacity is equal to the seismic demand. This point is called the performance point, and has to be located on the capacity curve. Further it has to be located on the response spectrum, but not necessarily on the elastic spectrum. If the structure starts to yield during the earthquake, the response spectrum has to be reduced further due to the hysteretic dissipation of energy.

The procedure to find the performance point consists of the following steps that is described below:

1. Find the 5% damped elastic response spectrum for the site.
2. Transform the capacity curve into a capacity spectrum, and plot together with the response spectrum.
3. Select a trial performance point.
4. Find a bilinear representation of the capacity spectrum.
5. Calculate the spectral reduction factors using the bilinear representation of the capacity spectrum, and develop the reduced response spectrum.
6. Determine if the reduced response spectrum intersects the capacity spectrum in the trial performance point within acceptable limits.
 - (a) If yes: The found performance point and reduced demand spectrum is correct.
 - (b) If no: Choose a new trial performance point and go back to step 3.

The elastic response spectrum can be developed using the formulas in eg [EN 1998-1:2004 2004] or [ATC-40 1996]. Normally it is given as the peak spectral acceleration as function of the natural vibration period, but it has to be transferred to the acceleration-displacement response spectrum (ADRS).

This can be done using the relationship:

$$S_{di} = \frac{T_i^2}{4\pi^2} S_{ai} \quad (\text{B.1})$$

where S_{di} is the spectral displacement, S_{ai} is the spectral acceleration and T_i is the natural vibration period of the structure, all at point i . The two representations of the response spectrum are shown in figure B.2.

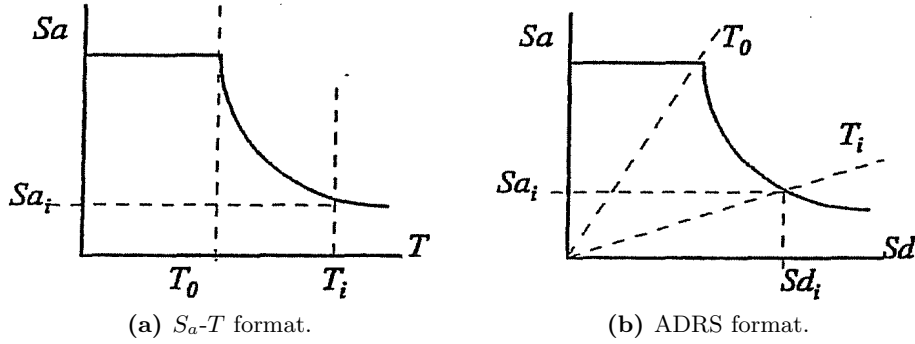


Figure B.2: Response spectrum in the two different representations. [ATC-40 1996]

The elastic response spectrum is based on the assumption that the structure is a SDOF system, and thus the capacity curve has to be transformed into a capacity spectrum for the corresponding SDOF system. This can be done using the results from the modal analysis, and the capacity spectrum can be plotted together with the elastic response spectrum in ADRS format, as shown in figure B.3. If the curves intersect in the elastic range of the capacity curve, there is no hysteretic damping, and the found intersection point is the capacity point. Else the response spectrum has to be reduced.

B.2.1 Hysteretic damping

The hysteretic damping is represented as an equivalent viscous damping. The total effective viscous damping, β_{eff} , can for 5% structural damping be calculated as:

$$\beta_{eff} = \beta_0 \kappa + 0.05 \quad (\text{B.2})$$

where β_0 is the damping due to hysteretic dissipation of energy for perfect hysteretic loops, and κ is a reduction factor that takes into account that the hysteretic loops are not perfect.

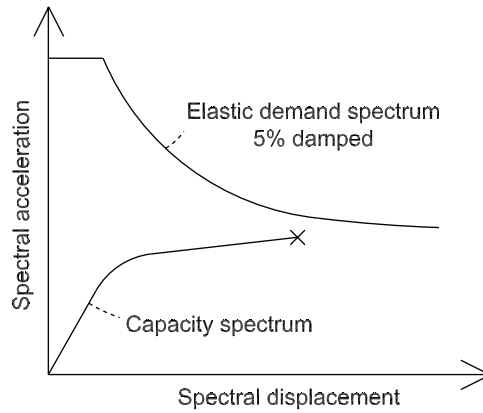


Figure B.3: Capacity spectrum and elastic demand spectrum.

The hysteretic damping can be calculated as:

$$\beta_0 = \frac{1}{4\pi} \frac{E_D}{E_{so}} \tag{B.3}$$

where E_D is the energy dissipated by damping and E_{so} is the maximum strain energy.

To calculate these energies the capacity spectrum is approximated with a bilinear representation of the capacity spectrum. The first line is drawn with the initial slope of the real curve, and the second line intersects the real curve at the trial performance point (d_{pi}, a_{pi}) , and is made with a slope so that the area over and under the curves are equal as shown in figure B.4.

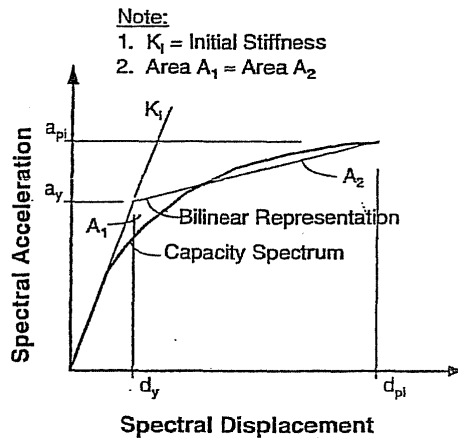


Figure B.4: Determination of the bilinear representation of the capacity spectrum. [ATC-40 1996]

With this representation the energy dissipated by damping and the maximum strain energy can be found as shown in figure B.5. Using this the

hysteretic damping, β_0 , can be calculated as:

$$\beta_0 = \frac{2}{\pi} \frac{a_y d_{pi} - d_y a_{pi}}{a_{pi} d_{pi}} \quad (\text{B.4})$$

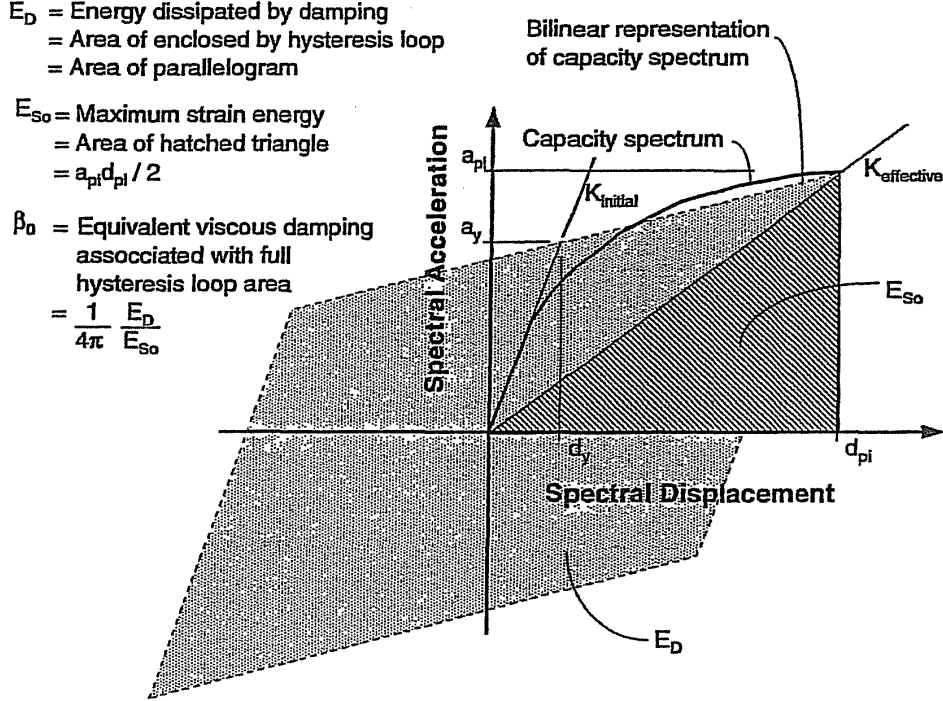


Figure B.5: Derivation of hysteretic damping. [ATC-40 1996]

The value of κ depends on the structural type. For a type A building, a new building in an area with high seismic activity, κ is:

$$\kappa = \begin{cases} 1 & \text{for } \beta_0 \leq 16.25 \\ 1.13 & \text{for } \beta_0 > 1.13 - \frac{0.51(a_y d_{pi} - d_y a_{pi})}{a_{pi} d_{pi}} \end{cases} \quad (\text{B.5})$$

The elastic 5% damped response spectrum then has to be reduced with the factors:

$$SR_A = \frac{3.21 - 0.68 \ln(\beta_{eff})}{2.12} \geq 0.33 \quad (\text{B.6})$$

$$SR_V = \frac{2.31 - 0.41 \ln(\beta_{eff})}{1.65} \geq 0.50 \quad (\text{B.7})$$

where SR_A is the reduction factor for the part of the curve with constant acceleration, and SR_V reduction factor for the part of the curve with constant velocity. The given limits counts for type A buildings. The reduced demand spectrum is shown in figure B.6.

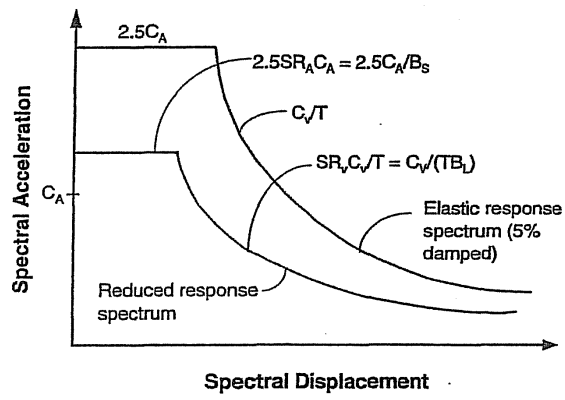


Figure B.6: Reduced demand spectrum with terms from ATC-40. [ATC-40 1996]

Appendix C

Programs

The enclosed CD contains MATLAB programs used for the calculations in this project. The major files are listed below and in addition a number of input files can be found on the cd.

main_deterministic.m Main file for deterministic analyzes

main_probabilistic.m Main file for probabilistic analyzes

pushover.m Function that calculates step nr. for the SD limit and performance points

isdaldef.m Function that calculates ISDA

powerreg.m Function that performs regression for ISDA- S_a relationship

hazard.m Function with data for seismic hazard curves

fragility.m Function that calculates the fragility curves and the annual probability of exceeding a limit state

hazardcurve.m Calculates fit to data from USGS

riskanalysis.m Calculations for the risk analysis

Irob.m Calculations for the risk based robustness index

sensitivitytears.m Calculates probabilistic indices for a number of years

